DECISION TREE CLASSIFICATION OF MULTI-TEMPORAL IMAGES FOR FIELD-BASED CROP MAPPING

A THESIS SUBMITTED TO
THE GRADUATE SCHOOL OF NATURAL AND APPLIED SCIENCES
OF
MIDDLE EAST TECHNICAL UNIVERSITY

BY

SEÇİL ŞENCAN

IN PARTIAL FULFILLMENT OF THE REQUIREMENTS
FOR
THE DEGREE OF MASTER OF SCIENCE
IN
GEODETIC AND GEOGRAPHICAL INFORMATION TECHNOLOGIES

AUGUST 2004

Approval of the Graduate School of Natural and Applied Sciences

Prof. Dr. Canan Özgen
Director

I certify that this thesis satisfies all the requirements as a thesis for the degree of Master of Science.

Assoc. Prof. Dr. Oğuz Işık
Head of Department

This is to certify that we have read this thesis and that in our opinion it is fully adequate, in scope and quality, as a thesis for the degree of Master of Science.

Assist. Prof.Dr. Mustafa Türker
Supervisor

Examining Committee Members

Prof. Dr. Vedat Toprak (METU, GEOE) ____________________

Assist. Prof. Dr. Mustafa Türker (METU, GGIT) ____________________

Assist. Prof. Dr. Ayşegül Aksoy (METU, ENVE) ____________________

Assist. Prof. Dr. M. Lütfi Süzen (METU, GEOE) ____________________

Dr. Hande Akçakoca (GAP) ____________________

I hereby declare that all information in this document has been obtained and presented in accordance with academic rules and ethical conduct. I also declare that, as required by these rules and conduct, I have fully cited and referenced all material and results that are not original to this work.

Name, Last name: Seçil ŞENCAN

Signature :

ABSTRACT

DECISION TREE CLASSIFICATION OF MULTI-TEMPORAL IMAGES FOR FIELD-BASED CROP MAPPING

Şencan, Seçil

M. Sc., Department of Geodetic and Geographic Information Technologies
Supervisor: Assist. Prof. Dr. Mustafa Türker

August 2004, 125 pages

A decision tree (DT) classification approach was used to identify summer (August) crop types in an agricultural area near Karacabey (Bursa), Turkey from multi-temporal images. For the analysis, Landsat 7 ETM+ images acquired in May, July, and August 2000 were used. In addition to the original bands, NDVI, PCA, and Tasselled Cap Transformation bands were also generated and included in the classification procedure. Initially, the images were classified on a per-pixel basis using the multi-temporal masking technique together with the DT approach. Then, the classified outputs were applied a field-based analysis and the class labels of the fields were directly entered into the Geographical Information System (GIS) database. The results were compared with the classified outputs of the three dates of imagery generated using a traditional maximum likelihood (ML) algorithm. It was observed that the proposed approach provided significantly higher overall accuracies for the May and August images, for which the number of classes were low. In May and July, the DT approach produced the classification accuracies of 91.10% and 66.15% while the ML classifier produced

84.38% and 63.55%, respectively. However, in August nearly the similar overall accuracies were obtained for the ML (70.82%) and DT (69.14%) approaches. It was also observed that the use of additional bands for the proposed technique improved the separability of the sugar beet, tomato, pea, pepper, and rice classes.

Keywords: Decision tree classification, multi-temporal masking, field-based analysis, crop mapping, Landsat 7 ETM+.

ÖZ

PARSEL BAZLI ÜRÜNÜN HARİTALANMASI İÇİN ÇOK ZAMANLI UYDU GÖRÜNTÜLERİNİN KARAR AĞACIYLA SINIFLANDIRILMASI

Şencan, Seçil

Yüksek Lisans, Jeodezi ve Coğrafi Bilgi Teknolojileri Bölümü
Tez Danışmanı: Yrd. Doç. Dr. Mustafa Türker

Ağustos 2004, 125 sayfa

Karacabey (Bursa), Türkiye, yakınlarındaki tarımsal alanlarda Ağustos ayına ait tarım ürünlerini sınıflandırmak için karar ağacı sınıflandırma tekniği ile beraber çok zamanlı uydu görüntüleri kullanılmıştır. Analizler için Mayıs, Temmuz ve Ağustos 2000'de elde edilen Landsat 7 ETM+ görüntülerinden yararlanılmıştır. Orijinal bantlara ek olarak NDVI, PCA ve Tasselled Cap Transformation bantları oluşturulmuş ve sınıflandırma işlemine dahil edilmiştir. Öncelikle, karar ağacı sınıflandırma yaklaşımı ile beraber çok zamanlı maskeleme tekniği kullanılarak görüntüler piksel bazlı olarak sınıflandırılmıştır. Elde edilen görüntülere parsel bazlı analiz uygulanarak parsellerdeki ürün bilgileri doğrudan Coğrafi Bilgi Sistemi (CBS) veritabanına girilmiştir. Sınıflandırma sonuçları, üç adet görüntünün geleneksel en büyük olasılık algoritması kullanılarak elde edilen sınıflandırma sonuçları ile karşılaştırılmıştır. Önerilen yaklaşımla elde edilen toplam doğruluğun sınıf sayıları az olan Mayıs ve Ağustos görüntüleri için oldukça yüksek olduğu gözlenmiştir. Mayıs ve Temmuz aylarında karar ağacı yöntemi ile 91.10% ve 66.15%, en büyük olasılık sınıflandırma yöntemi ile ise

84.38% ve 63.55% doğruluk değerleri elde edilmiştir. Bununla beraber, Ağustos ayında en büyük olasılık (70.82%) ve karar ağacı sınıflandırma (69.14%) yöntemleri için yaklaşık olarak aynı toplam doğruluk sonuçları elde edilmiştir. Ek olarak kullanılan bantların karar ağacı sınıflandırma yönteminde şeker pancarı, domates, bezelye, biber ve pirinç sınıflarının görüntü üzerinden ayrılabilirliğini arttırdığı gözlemlenmiştir.

Anahtar Kelimeler: Karar ağacı sınıflandırması, çok zamanlı maskeleme, parsel bazlı analiz, ürün haritalama, Landsat 7 ETM+.

ACKNOWLEDGEMENTS

I would like to thank my supervisor, Assist. Prof. Dr. Mustafa Türker, for his support and assistance during this thesis work.

I would like to thank the jury members, Prof. Dr. Vedat Toprak, Assist. Prof. Dr. Ayşegül Aksoy, Assist. Prof. Dr. M. Lütfi Süzen and Dr. Hande Akçakoca for their valuable comments.

It was a great honour to meet Prof. Dr. R. Sezer Aygün who gave her support and encouragement sparingly during all that hard times and inspired me with the motivation to finish this thesis study.

My family deserves a great deal of gratitude for their endless affection and emotional support even at times when they needed the most.

This part of my thanks goes to friends who gave their support during this study.

TABLE OF CONTENTS

LIST OF TABLES

LIST OF FIGURES

CHAPTER 1

INTRODUCTION

Observations of the earth surface began with aerial photography and continued with the development of earth-orbiting satellites in 1960s. With the development of digital electronic imaging systems, image data started to be transferred back to earth. Image processing and analysis techniques have been and will be widely used on these data in order to sharpen, rectify, and classify images, and to overlay images taken at different times.

Remotely sensed images are useful data sources for several earth related applications such as environmental modelling and monitoring, and the updating of geographical databases. Today, most natural resource mapping and measurements are carried out using remote sensing techniques such as, land use/land cover and soil mapping, elevation and crop condition measurements. To transform remotely sensed data into thematic information, one of the most widely used techniques is multispectral classification. Image classification can be performed using various algorithms including 1) hard classification using supervised or unsupervised approaches, 2) classification using fuzzy logic and/or 3) hybrid approaches that involve the use of ancillary information (Jensen, 1996). In supervised classification, various algorithms can be used to assign an unknown pixel to a class. These algorithms can be divided into two general subgroups according to the assumption of whether each class is normally distributed or not (Jensen, 1996):

1. Parametric (e.g., Maximum Likelihood Classification), and
2. Non-parametric (e.g., Decision Tree Classification).

Of the parametric classification techniques, the Maximum Likelihood Classifier (MLC) performed on an uni-temporal image is very widely used for extracting thematic information from remotely sensed images and often generates good results if the images contain spectrally distinct classes. However, where the classes display similar reflectance characteristics, using an uni-temporal image may lead to less reliable classification results. The reliability of information extraction can be improved if multiple images of the same area taken in different periods of time are included in the classification procedure. The change in the appearance of a feature leads to change in the spectral characteristics of features that make near-similar features easily discernable over time such as wheat and maize. On the other hand, because of the noise in the data, atmospheric effects, mixed edge pixels and variation within the land cover type groups of pixels representing the same land cover type will not in all case have the same spectral information. In such a case, if the contextual information is included in the classification, then the classification results could be improved. Thus, through the integration of remotely sensed imagery and digital vector data the problems encountered while performing the per-pixel classification can be minimized. With this integration, the attributes of classified objects can also be easily updated by directly entering field-based analysis results into GIS database.

For some land cover classification studies, using only the multi-temporal data set may not be enough to discriminate some of the land cover types. Therefore, for such cases it becomes quite necessary to use high-level image processing techniques. There are several image processing techniques but three of the widely used are Normalized Differences Vegetation Index (NDVI), Principal Components Analysis (PCA), and Tasselled Cap Transformation.

NDVI is one of the first successful vegetation indices developed by Rouse et al. in 1973. It is used for the measurement of vegetative amount and condition based on an analysis of remote sensing spectral measurements, i.e., band rationing (Jensen, 1996).

PCA is a technique used to reproject a correlated set of multispectral data onto a new set of statistically independent orthogonal axes. Using this mathematical transformation the duplication in the multispectral data can be reduced as well as the information content of a number of bands of the original image can be compressed into fewer bands which are called principal components. Hence, comprehension and analysis of these fewer bands would be simpler and more efficient than that of the original bands (Jensen, 1996, Walsh et al, 1990, Mather, 1989, and CCRS).

The Tasselled Cap Transformation is an another vegetation index which is used for compressing spectral data into a few bands associated with physical scene characteristics. It was originally constructed by Kauth and Thomas in 1976 for understanding the development of crops in spectral space. With this tranformation the axes of new coordinate system represent the specific concepts, such as called brightness and greenness, in which the soil line and the region of vegetation are more clearly described (Jensen, 1996, Huang, 2002, and Mather, 1989).

1.1 STUDY OBJECTIVES

The objectives of this study are as follows:

- To develop a Decision Tree Classification methodology for the identification of summer (August) crops using multi-temporal remotely sensed data,
- To perform post-classification field-based image analysis in order to increase the classification accuracy, and
- To compare the results of the proposed decision tree classification with the results of the conventional Maximum Likelihood Classification.

1.2 THE SOFTWARE USED

In order to perform the pre-processing and image analysis operations, several software were used. The validation of vector attributes was carried out using MS

Excel and ArcGIS 8.2 programs through constructing spreadsheets in order to partially print out the database or creating the thematic maps. MS Excel was also used for constructing the coincidence spectral plots and the error matrices.

The pre-processing of image data prior to analyses, the extraction of features, the selection of training areas, the multi-temporal per-pixel classification, and the single stage per-pixel classification were performed using PCI Geomatica (v 8.2.3) software. On the other hand, all field-based analysis operations were carried out using SPANS GIS software, which is an advanced GIS module of PCI Geomatica.

1.3 THE ORGANIZATION OF THE THESIS

The main sections of this thesis are as follows:

Chapter 2 provides a background information about per-pixel classification, image classification using ancillary data, and per-field classification as well as image transformation algorithms NDVI, PCA, and Tasselled Cap Transformation.

Chapter 3 introduces the study area and data, describes the processes applied to the images and the vector data, and addresses the applied classification methods. An accuracy assessment for field-based classification results was also included in the chapter.

Chapter 4 presents the results and the discussion of the results.

Chapter 5 provides the conclusions of the proposed methodology and the recommendations for the future studies.

CHAPTER 2

BACKGROUND STUDY

In this chapter, a brief theoretical information and the previous studies about image classification methods and image transformation algorithms are given. The image transformation algorithms provided include NDVI, PCA, and Tasselled Cap Transformation. Regarding the image classification methods, per-pixel maximum likelihood, per-pixel decision tree, the use of ancillary data in image classification, and per-field classification techniques are explained.

2.1 IMAGE CLASSIFICATION

Images are useful data sources for geographical analysis. However, they are meaningless if the spectral data composing the image are not converted into thematic information. This conversion can be managed using several pattern recognition techniques. These techniques can be grouped into two categories: (i) pixel-based and (ii) field-based.

2.1.1 PER-PIXEL CLASSIFICATION

Per-pixel image classification is based on the individual pixel values. Two broad categories can be defined for classifying images in a pixel-based approach, that are unsupervised and supervised techniques. In an unsupervised classification, identities of land cover types present in the image are generally not known a priori because of lacking or not well defined ground reference data. Hence, to group spectral classes, clustering algorithms are used. Then, the analyst combines and matches the spectral clusters to information classes of interest. K-means and ISODATA are widely used unsupervised algorithms for classifying the images. The main difference between the two classifiers is that while k-means initially defines the locations of cluster means randomly, ISODATA determines them using the mean and the standard deviation of each band. The basic algorithm used by these classifiers can be described as follows:

Initially, the locations of the cluster means are determined by the algorithm. Then, each pixel is assigned to the cluster whose mean is closest to the pixel. Thereafter, locations of the cluster means are recalculated based on the pixels that are assigned to the clusters in the previous iteration. Then, pixels are reassigned to clusters using recalculated means. The whole process is repeated until the change in locations of the class means between iterations becomes insignificant.

In a supervised classification, the analyst collects homogenous representative samples that are called training samples for each of the information classes. Then, the statistics derived from these samples such as the means, standard deviations, and the co-variance matrices are computed to train the classification algorithm in order to classify the image. There are various supervised classification algorithms including the maximum likelihood, minimum distance to means, and parallelepiped classifiers. Of these techniques, the maximum likelihood classifier is the most popular and most widely used classification algorithm.

2.1.1.1 MAXIMUM LIKELIHOOD CLASSIFICATION

The maximum likelihood (MLC) uses the probability function to allocate each pixel to an information class. It assumes that the training data for each class is normally distributed, meaning that it represents only one class. Another assumption with this classifier is that each class has an equal probability of occurring. However, this assumption is not always the real case, since in most remote sensing applications some classes can be observed more often than the others.

When classifying an image using a maximum likelihood decision rule the following two main steps are carried out:

- calculation of the probability of a pixel belonging to each of a predefined set of classes and,
- assignment of the pixel to the class for which the probability is the highest.

The algorithm works as follows:

A set of pixels belonging to a given class can be defined by an ellipse which represents contour of class membership probability. The maximum likelihood classifier delineates these “equi-probability contours” with Mahalanobis distance equation using the mean vector (m_k) and the covariance matrix (Cov_k) parameters of each training class (k). Then, the algorithm calculates the probability of the pixel belonging to each of them, using Equation 2.1 (Chan et al.,2001), and allocates the pixel into a class k if and only if $Prob_k \geq Prob_i$, where i=1, 2, 3, ..,m classes.

$$Prob_k = [\ -0.5\log_e (\det (Cov_k))\ ] - [\ 0.5(X-m_k)^T (Cov_k^{-1}) (X-m_k)\ ] \qquad \text{(Equation 2.1)}$$

In this notation, det and ^{T} indicate the determinant of the matrix and the matrix transpose, respectively, X denotes the vector of the unknown pixel, and (Cov_k^{-1}) refers to the inverse of the covariance matrix of class k.

This classification method has been used for more than a decade to classify the remotely sensed images like other conventional classification techniques. In such a statistical classifer, for a fixed sample size, the addition of spectral bands causes an increase of the estimated number of parameters. Consequently, for each estimate, the confidence limits become wider and once a certain number of dimensions is reached the effectiveness of the classifier begins to decrease (Tso and Mather, 2001).

2.1.1.2 DECISION TREE CLASSIFICATION

The decision tree is one of the algorithms proposed to compensate the incapabilities of traditional approaches such as maximum likelihood and parallelepiped classifiers in resolving inter-class confusions. It is based on a set of tests applied at each node in the tree to recursively split a data set into smaller subgroups until there is no subdivision. The tree is made up of a root node–the whole data, a set of internal nodes–splits, and a set of terminal nodes–leaves, representing the label for the pixel being classified. According to the algorithms used to estimate the internal nodes, the classifier is described as homogeneous or hybrid.

Based on the homogeneous model two types of decision trees can be examined: univariate and multivariate decision trees (Friedl and Brodley, 1997). If the whole data is to be partitioned using a single feature of the data, at each node, the classifier is called univariate decision tree. However, if more than one feature of the input data is used at each node to split the whole data, the decision tree is referred to as multivariate tree. An example for multivariate tree would be using a partitioning value combined with NDVI and surface temperatures at each node.

What makes different hybrid decision trees from the homogeneous model is that different classification algorithms may be used in different subtrees of a larger tree, such as decision trees, linear discriminant functions, and k nearest-neighbour classifier.

Lauver and Whistler (1993) applied a hierarchical classification strategy to identify native grasslands and rare species habitat with a single Landsat TM scene. They did not recommend this classification strategy for detailed mapping of natural areas. On the other hand, when compared with their experience using aerial photographs and aerial surveys to generate maps of potential natural areas, this method was found to be more accurate and faster.

Continously changing life forms of the plants make their spectral discrimination in most cases difficult over a single remotely sensed image. However, the use of multi-temporal remotely sensed data can improve the discrimination of these land cover types by using their changing spectral responses over a period of time.

There are several scientific research studies using the multi-temporal data based on different classification algorithms.

Friedl and Brodley (1997) evaluated univariate, multivariate, and hybrid decision models on multi-temporal AVHRR and a single-date Landsat TM data sets. They concluded that hybrid decision trees gave higher overall classification accuracies when compared to other decision trees, maximum likelihood, and linear discriminant function classifiers.

CART (Classification and Regression Tree) model is a well known example of a univariate decision tree approach (Friedl and Brodley, 1997). Lawrence and Wright (2001) used CART analysis to develop a means for creating a rule-based classification. As the input data, two pairs of Landsat TM scenes and the first three components of Tasselled Cap Transformation (brightness, greenness, and wetness) derived for each date were utilized. With this automated statistical analysis, they obtained 96 percent overall accuracy at level 1 classification, 79 percent at level 2, and 65 percent at level 3 classification.

Schriever and Congalton (1995) compared classification accuracies for three temporal data sets (autumn, spring, and summer). They concluded that time of the year significantly affects the cover-type classification accuracy. They also stated that various techniques such as the use of combined and individual multi-temporal data sets for generating additional vegetation indices and band ratios, the utilization of ancillary data should help improve the classification accuracy.

Wolter et al. (1995) developed a layered multi-temporal approach for forest cover classification in the Northern Lake States using Landsat data. Among the 22 forest types classified, 13 were separated with the aid of the multi-temporal analysis and 80.1 percent forest classification accuracy was achieved.

Oetter et al. (2000) utilized multiseasonal Tasselled Cap imageries in a hierarchical image processing with either supervised or unsupervised classifiers to map an agricultural setting and obtained 26 percent error for the final map.

Murakami et al. (2001) generated Annual Normalized Difference Vegetation Index (NDVI) profiles to characterize seasonal spectral changes of six crop types by using multi-temporal SPOT/HRV dataset. They were able to determine the optimal dates of coverage by using this dataset. They concluded that based on the results, observations can be requested during specific time intervals considering local crop calendars and environmental conditions.

Lanjeri et al. (2001) used multi-temporal Landsat 5 TM images with the maximum likelihood classification method and masking techniques for mapping of vineyard areas and determining the relationship between the spectral signature and agronomical parameters (biomass, height, and coverage). The validation of results was carried out by comparing the percentage of the classes in the classification image to those proposed by the ground truth maps. The 14 percent difference between the ground truth and the classification data was attributed to the spectral confusion between certain classes. Besides, good correlation coefficients were obtained between the NDVI and biomass ($r=0.86$), height ($r=0.90$), and the vegetation cover surface ($r=0.82$).

Beltrán and Belmonte (2001) applied a synergistic combination of maximum likelihood algorithms, decision-tree criteria, and contextual classifiers to identify irrigated crops with multi-temporal Landsat TM images. They obtained over 90 percent classification accuracy and concluded that the context classifier was a useful and sufficient tool to improve surface quantification.

Guerschman et al. (2003) investigated that how many Landsat TM images from the same growing season were required for accurate classification of land cover types in the south-western portion of the Argentine Pampas, and given a fixed number of dates, what combination of dates gave the best results. They also tested the effect of using only the NDVI images on the classification accuracy and the use of a majority filter over the classified image. It was concluded that at least two Landsat TM images embracing the shift between winter and summer crops (i.e. one spring and one summer image) were required to obtain satisfactory classification results. When the NDVI was utilized instead of the avaliable Landsat TM bands 3, 4 and 5, the biological interpretability of the results was observed as increased while the accuracy was observed as decreased. Finally, it was shown that the use of a majority filter not only improved the visual quality of classified output, but also enhanced the classification accuracy.

McCauley and Goetz (2004) tested a method for mapping residential density at the parcel level and to distinguish these parcels from agriculture and commercial/industrial parcels using decision tree classifer in Montgomery County, Maryland, USA. For analysis, two dates Landsat TM data and additional derived images namely NDVI, an NDVI difference, the ratio of band 5 to band 1, brightness, greenness and wetness were utilized. As a result, the low-density residential areas showed greater classification errors due to the range of land cover types within this land use and their associated spatial variability. To decrease these errors they emphasized the importance of training data selection mode and suggested the incorporation of methods that account for the presence and amount of impervious surfaces.

Although the entities shown in remotely sensed imagery are based not only on local tone and color, but also on size, shape, texture, pattern, and context, these elements are not involved in per-pixel image classification. The statistical classifiers, therefore, often do not give satisfactory results. The solution could be to extend the classification procedure by using ancillary data, which is referred to data other than remotely sensed imagery. Ancillary data are primarily either map-based such as elevation and soil type information or image-based that is the classification results of another image of the same spatial area. Additionally, any type of nonspatial information can also be referred to ancillary data.

2.1.2 THE USE OF ANCILLARY DATA IN IMAGE CLASSIFICATION

The use of ancillary data may be of a value in discriminating spectrally confused classes. Therefore, they are preferred to be used in digital image classification process. However, to involve ancillary data in the classification procedure, the software used must provide a certain level of integration between remote sensing and GIS for performing integrated analysis of raster imagery, vector graphics, and attributes. The ancillary data can be incorporated into image analysis before, during, or after classification through geographical stratification, classifier operations, and/or post-classification sorting. Hutchinson (1982) discussed the advantages and disadvantages of these techniques for combining Landsat and ancillary data. Archibald (1987) discussed both the display and database integration functions required to develop an operational interface for forestry related applications. Ehlers et al. (1989) gave information about some of the many preliminary efforts made for the integration of remote sensing and GIS. They defined this integration at three stages (i) “separate but equal”, (ii) “seamless integration”, and (iii) “total integration”. Ehlers et al. (1991) identified the key impediments for integration of remote sensing and GIS, that are based on data structures used to acquire, access, and store the data. In addition, they also examined the functions of spatial data archives.

White et al. (1995) modified an unsupervised spectral classification of Landsat TM data by using topographic data in a GIS to define species level composition of forests where accessibility is limited but information regarding to the area is necessary. They generated genus-level maps from unsupervised classifications of Landsat TM data at an accuracy level of 73 percent. It was also demonstrated that species-level maps can be created by post-stratification of the spectral classification with topographic data in a GIS at an accuracy level of 58 percent.

Congalton et al. (1998) described a process for integrating remote sensing and spatial data analysis to accurately map and monitor agricultural crops and other land cover types. The maps generated with 93 percent overall accuracy were then used as input data into the water consumption model. Seong and Usery (2001) classified multi-temporal AVHRR NDVI data using fuzzy classification methods with the invariant pixel approach and latitudinal image stratification. They showed that the stratification method could be used to decrease the spatial variation of phenological characteristics of vegetation.

Wayman et al. (2001) developed a hybrid classifier called Iterative Guided Spectral Class Rejection (IGSCR) in order to estimate the forest areas using Landsat TM images. They found that estimations derived from images were not significantly different from the aerial photographs. However, they concluded that the new classifier was fast, objective, repeatable across users, regions, and time. They also stated that when reference polygons consisting of recent harvest areas were included in the training data set, the recent forest clear-cuts were more accurately classified.

Bailey et al. (2001) used remote sensing and GIS data products to estimate and monitor wild rice production. Derived products were stored to utilize them for future wild rice management studies.

Ma et al. (2001) introduced a two-stage classification procedure developed for mapping land cover types across large geographic areas from Landsat TM imagery. The classification is based on an unsupervised classification in the first stage and a supervised classification in the second which is taking place in a GIS environment. In the second stage, after spectral and biophysical attributes are calculated for each raster polygon in the image, they are labelled with land cover types.

McIver and Friedl (2002) proposed a method for incorporating prior probabilities in remote-sensing-based land cover classification using a decision tree classification algorithm. The methodology was assessed using both Landsat TM and AVHRR data. It was concluded that the proposed approach successfully improved classification results at both fine and coarse spatial resolutions. In particular, the method was found to be useful for improving discrimination between agriculture and natural vegetation in coarse-resolution land cover maps.

The reliability of image classification can be further improved by including a priori knowledge about the contextual relationships of the pixels in the classification process. GIS's now hold vast amount of information that can be used in the analysis of remotely sensed images. In a GIS, the agricultural field boundaries are represented as polygons. The field boundary network integrated with the remotely sensed data divides the image into homogeneous fields each of which can be analyzed separately. Therefore, the per-pixel image classification can be replaced by the per-field classification.

2.1.3 PER-FIELD CLASSIFICATION

Per-field image classification techniques have been used to generate land cover information for more than a decade. They are achieved through the integration of remotely sensed imagery and digital vector data. The classification is usually performed by calculating the modal land cover class within each field and applying this class to the entire field. The success of a per-field classification depends on several factors; the relationship between the spectral and spatial properties of the imagery, the size and shape of the fields, and the land cover classes used (Aplin et al., 1999).

Janssen et al. (1991) described and tested the object-based classification using a Landsat TM image. Three agricultural areas in the Netherlands were used for the analysis. The object-based classification was applied to these fields at two moments: (i) pre-classification and (ii) post-classification. They found that the object-based classification, in particular, post-object classification provided approximately 20 percent better results when compared to per-pixel maximum likelihood classification.

A map-guided approach was applied for identifying the forest stands damaged by the spruce budworm on Landsat TM images by Chalifoux et al. (1998). For coniferous and mixed stands 95 and 77 percent accuracies respectively were achieved. They concluded that this technique had the advantages over the other standard methods using the individual pixel value.

Aplin et al. (1999) introduced a set of techniques developed for classifying land cover on a per-parcel basis by integrating fine spatial resolution simulated image data with digital vector data. They achieved increased classification accuracy.

Özen (2000) applied per-field classification approach to two different agricultural areas using Landsat 5 TM and IRS 1-C LISS III images. She applied both the per-pixel maximum likelihood and the decision tree classifiers. She reported that the decision tree classifier gave higher accuracy than the maximum likelihood classifier. The classified outputs were also analyzed in a field-based manner. For both classifiers, the accuracies of per-field approaches were found to be higher than that of per-pixel techniques.

Aplin and Atkinson (2001) developed a new method for land cover classification at the sub-pixel scale for subsequent per-field classification. To perform this method three stages were determined. Initially, by using vector field boundaries image pixels were segmented. Then, the pixel segments were labelled with a land cover class. Finally, the modal land cover classes were assigned to fields rather than pixels. They stated that significantly higher classification accuracy was achieved when compared to corresponding hard per-pixel classification and per-field classification based on hard per-pixel classified imagery.

2.2 IMAGE TRANSFORMATIONS

Different feature extraction algorithms were developed to highlight the information content of a raw image. By using these algorithms, multiple bands of data whether from a single multispectral image or from multi-temporal images can be transformed into new images. Three of the widely used feature extraction algorithms are Normalized Difference Vegetation Index (NDVI), Principal Component Analysis (PCA), and Tasselled Cap Transformation.

2.2.1 NORMALIZED DIFFERENCE VEGETATION INDEX (NDVI)

NDVI is a spectral ratio between the red and near infrared portions of the electromagnetic spectrum. It was developed for monitoring vegetation conditions. The reasons why these two bands are used for this rationing are (Chesapeake Bay & Mid-Atlantic from Space):

- they are mostly affected by the condition and the density of green vegetation, and
- they have maximum contrast between vegetation and soil.

Todd and Hoffer (1998) evaluated the spectral indices NDVI and GVI (Greenness Vegetation Index) for characterizing variation in green vegetation biomass across small regions with heterogeneous soil background characteristics. They stated that GVI was less variable than NDVI in predicting green vegetation cover when soil backgrounds varied by type and moisture content.

2.2.2 PRINCIPAL COMPONENT ANALYSIS (PCA)

PCA generates the new images (components or axes) that are linear combinations of the original images. These new images have no mathematical correlation with one another and the axes are orthogonal to each other (CCRS, Chavez and Kwarteng, 1989). The process of this technique can be explained with three stages (Tso and Mather, 2001):

- calculation of the variance-covariance (or correlation) matrix of multiband images,
- extraction of the eigenvalues and eigenvectors of the matrix, and
- transformation of the feature space coordinates utilizing the extracted eigenvectors.

PCA is mainly used to reduce the number of images that are needed for analysis. However, two problems can be encountered with the resultant components that are generated by applying the “standard” PCA method, in which all the available bands are used as input simultaneously. One of the problems is information of interest might be mathematically mapped to one of the unused components. The other is that visually interpreting a color composite made from standard PCA results can be difficult. These two problems can be minimized by using the “selective” PCA method where only the subset of these bands are utilized. Chavez and Kwarteng (1989) described how selective PCA can be used to minimize the problems encountered with standard PCA and showed that how this PCA can be used to map the spectral contrast between different spectral bands.

Ricotta et al. (1999) examined the implications of PCA on the spatial structure and content of multispectral remote sensing images using a Landsat TM image of northern Sardinia, Italy. The results showed that the resulting principal components exhibited noticeably different spatial structure and content from one another and from the original images. Therefore, they said that extreme care must be given when applying PCA to remote sensing images and interpreting the results.

The parameters of PCA transformation are determined by the statistical relationships among the spectral bands of the image being analyzed. Therefore, the parameters of this transformation vary from one multispectral image set to another. On the contrary, the parameters of the Tasselled Cap Transformation are defined a priori. Thus, the parameters are not affected by variations in crop cover and stage of growth from image to image (Mather, 1989).

2.2.3 TASSELLED CAP TRANSFORMATION

The Tasselled Cap is an empirically-based transformation which was developed by Kauth and Thomas in 1976, for Landsat MSS images. By rotating and scaling the four dimensional space axes of Landsat MSS bands, new four dimensional axes are constructed. This new coordinate system axes are defined as “brightness”, “greenness”, “yellowness”, and “nonesuch” (Mather, 1989).

Crist and Cicone, in 1984, modified this Tasselled Cap Transformation to deal with six band Landsat TM images (excluding the thermal infrared band). They transformed the six dimensional TM space axes into three new coordinate axes called “brightness”, “greenness”, and “wetness” (Tso and Mather, 2001).

The first two TM Tasselled Cap axes are similar to the first two MSS Tasselled Cap axes. The first transformed axis, “brightness”, is associated with variations in the soil background reflectance, while the second axis, “greenness”, is correlated with variations in the vigour of green vegetation. The third axis, “wetness”, is related to soil features, including moisture status (Tso and Mather, 2001, Mather, 1989, and Jensen, 1996).

Essentially, the transformations developed for Landsat TM are based on a digital number (DN) (Crist and Cicone, 1984) and a reflectance factor (Crist, 1985). For simplicity, Huang et al. (2002) referred to these Tasselled Cap Transformations as DN based and reflectance factor based transformations, respectively. And, they developed at-satellite reflectance based Tasselled Cap Transformation based on Landsat 7 ETM+ images for regional applications where atmospheric correction is not feasible. There are two reasons behind developing this transformation for large area applications. The first reason is that in order to apply the reflectance factor based transformation to images, it requires the images to be corrected for atmospheric effects due to this transformation was developed based on ground measurements with little atmospheric effects. However, many users are often not prefer to correct atmospheric effects due to lack of or uncertainities in the ground and atmospheric data which are used in atmospheric correction equations. The second reason is that in multi-scene applications, DN values changing by the sun illumination geometry strongly affect the tasselled cap value that is derived with DN based transformation.

CHAPTER 3

THE METHODOLOGY

In this chapter, initially the general steps of the proposed decision tree classification methodology and the maximum likelihood classification approach that was used to test the utility of the proposed classification method are presented. Then, the study area and data are described. Finally, the processes mentioned in the general steps are explained in detail.

3.1 GENERAL STEPS

The main objective of this study was to perform a decision tree classification of multi-temporal remotely sensed data for field-based crop identification. To achieve this objective, the following main processing steps were carried out:

1. Pre-processing of the images and vector data,
2. Feature extraction (NDVI, PCA, and Tasselled CapTransformation)
3. Per-pixel classifications of the images,
4. Field-based analyses of the pixel-based classified data,
5. Assessment of the results.

The pre-processing step consists of the following processes applied to both raster data of each date of imagery and vector data. These include checking the correctness of the relational attribute data and the exclusion of irrelevant areas and boundaries of the agricultural fields using integrated vector and raster data.

After the pre-processing, NDVI, PCA, and Tasselled Cap were generated for each image. Then, using integrated raster and vector data with the related GIS database training areas were selected and the class signatures were computed for each original and derived bands (Figure 3.1). After then, the images were classified using the proposed per-pixel decision tree approach. As mentioned earlier, the decision tree is the layered classification procedure that sequentially partitions a data set according to a set of defined rules.

Then, the field-based analysis operations were performed on the outputs of the per-pixel decision tree classifier. During the field-based analysis, the crop fields were labelled using the highly observed pixel information based on the frequency of the pixels. At this stage, the results obtained from the field-based analysis procedures were entered into the GIS database.

In order to compare the results of the proposed decision tree classifier, the maximum likelihood classifier was applied on each image. The maximum likelihood classifier uses the probability density function in order to perform the classification at a single stage whereas the decision tree uses the strict decision boundaries to perform the classification at a multi-stage. The main processing steps for the maximum likelihood approach are the same with the proposed method. However, while applying the maximum likelihood classifier no pre-processing was performed since the same vector and raster data prepared for the proposed methodology were utilized. It should be noted that for the maximum likelihood classification only the original bands of the Landsat ETM+ data were utilized. After performing the per-pixel maximum likelihood classification, the per-field analysis operations were applied on the per-pixel classified output images and the GIS database was directly updated by entering the results obtained from the field-based analyses.

In order to assess the utility of the proposed methodology, for each date of the imagery, an accuracy assessment was carried out for both classifiers and provided in the form of error matrices. The same samples were used for training and accuracy assessment purposes for both classifiers. Figure 3.1 and Figure 3.2 depict the schematic diagrams of the decision tree classification and the maximum likelihood classification processes, respectively.

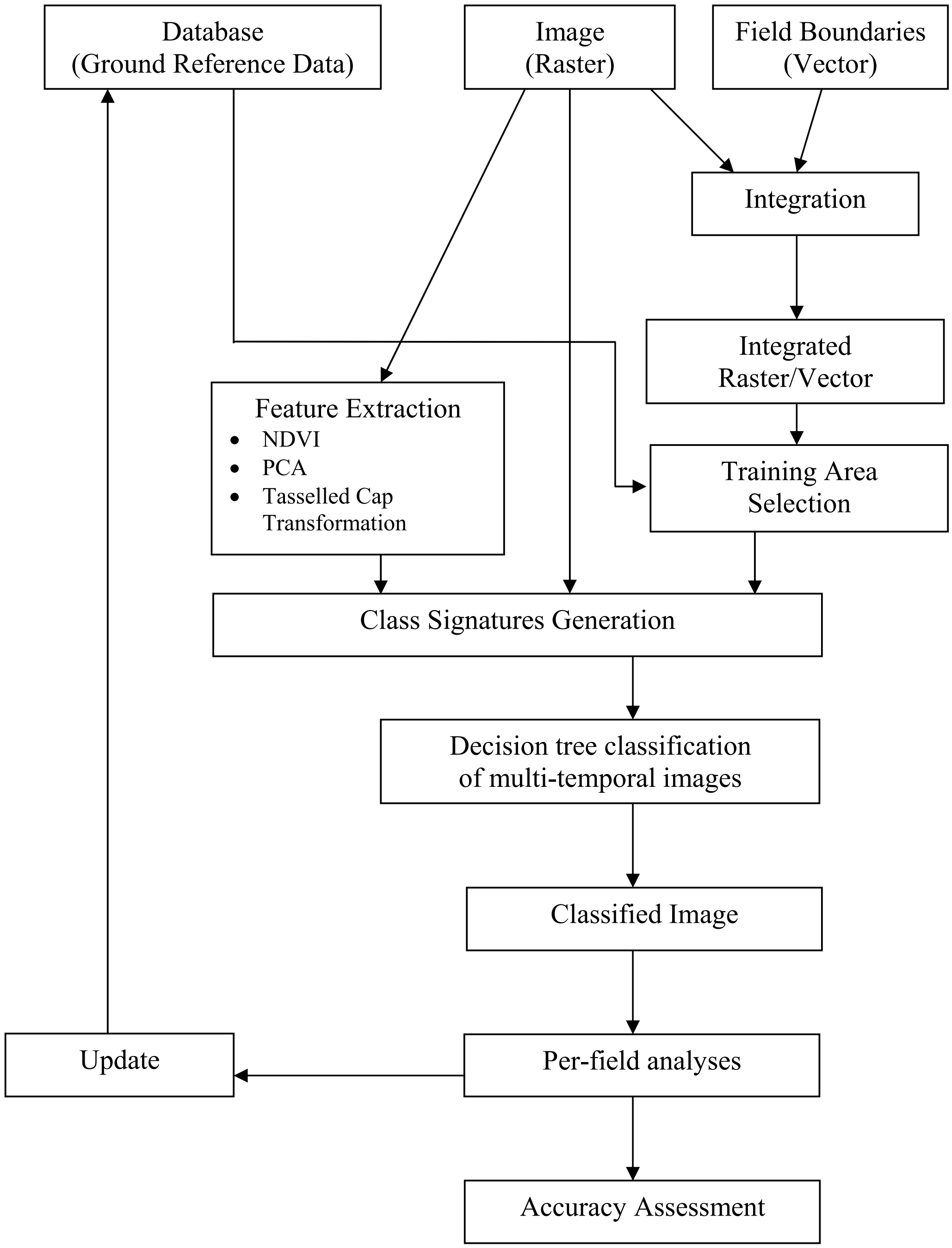

Figure 3.1 The schematic diagram of the decision tree classification

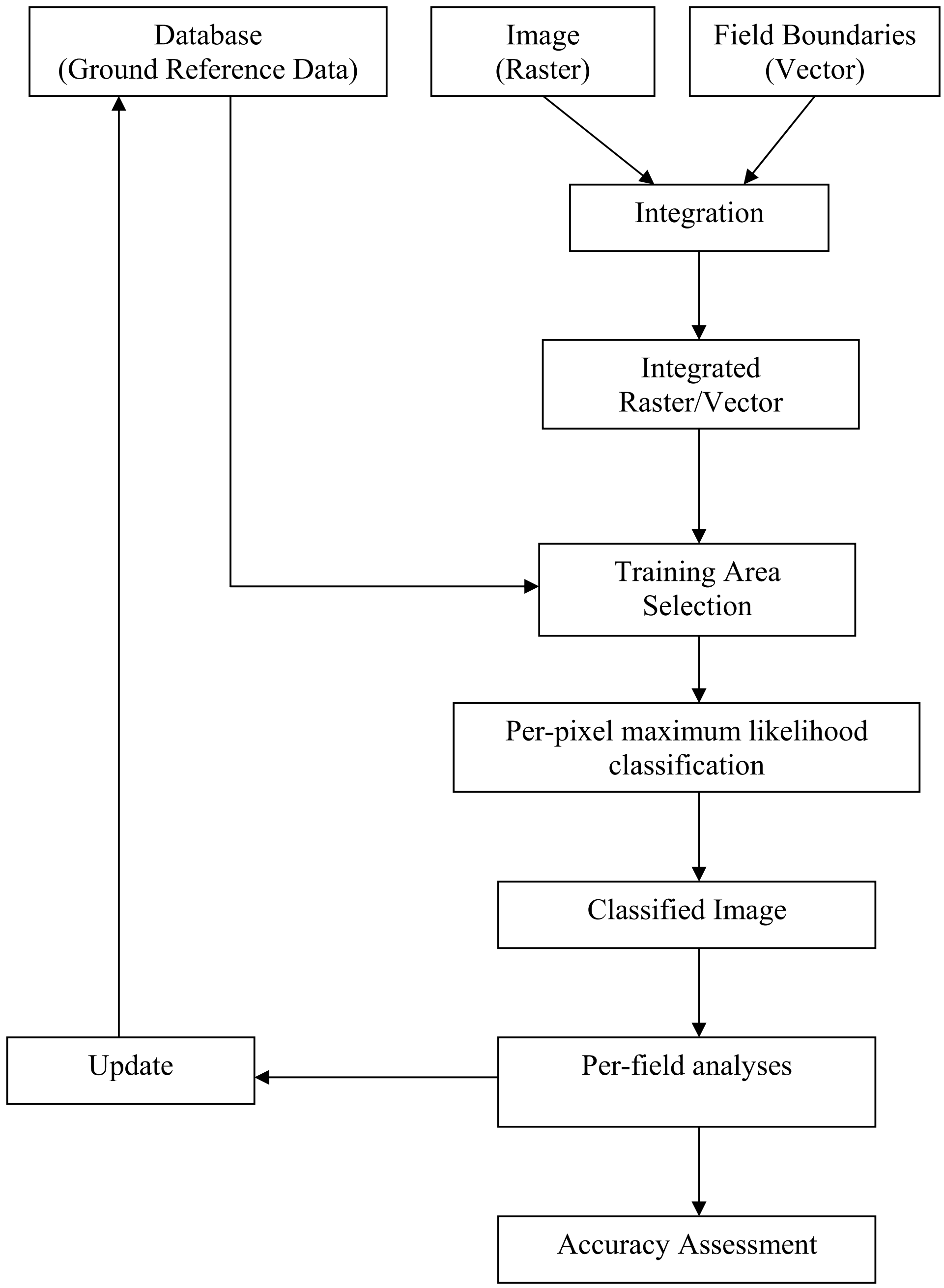

Figure 3.2 The schematic diagram of the maximum likelihood classification

3.2 DESCRIPTION OF THE STUDY AREA AND DATA

The study area occupies an agricultural land about 74 km^2 in Karacabey, Bursa located in Northwest of Turkey. The villages fall within this agricultural site are Akhisar, Eskisarıbey, Hotanlı, İsmetpaşa, Küçükkaraağaç, Ortasarıbey, Sultaniye, Yenisarıbey, and Yolağazı (Figure 3.3). Because of the appropriate climate properties, gentle topographic relief and growing conditions (rich and loamy type soil), this area is covered by the agricultural land cover types. The land cover types in the region include arable crops, namely, corn, wheat, tomato, sugar beet, pepper, rice, watermelon, pea, and cauliflower. Besides, several pasture, clover, and non-vegetated fields also exist. Size of the agricultural fields varies from 0.0074 to 48 hectares. Although a land consolidation work was conducted in the area, large number of the fields are observed as small in size. The percentages of coverages of the fields are given in Table 3.1.

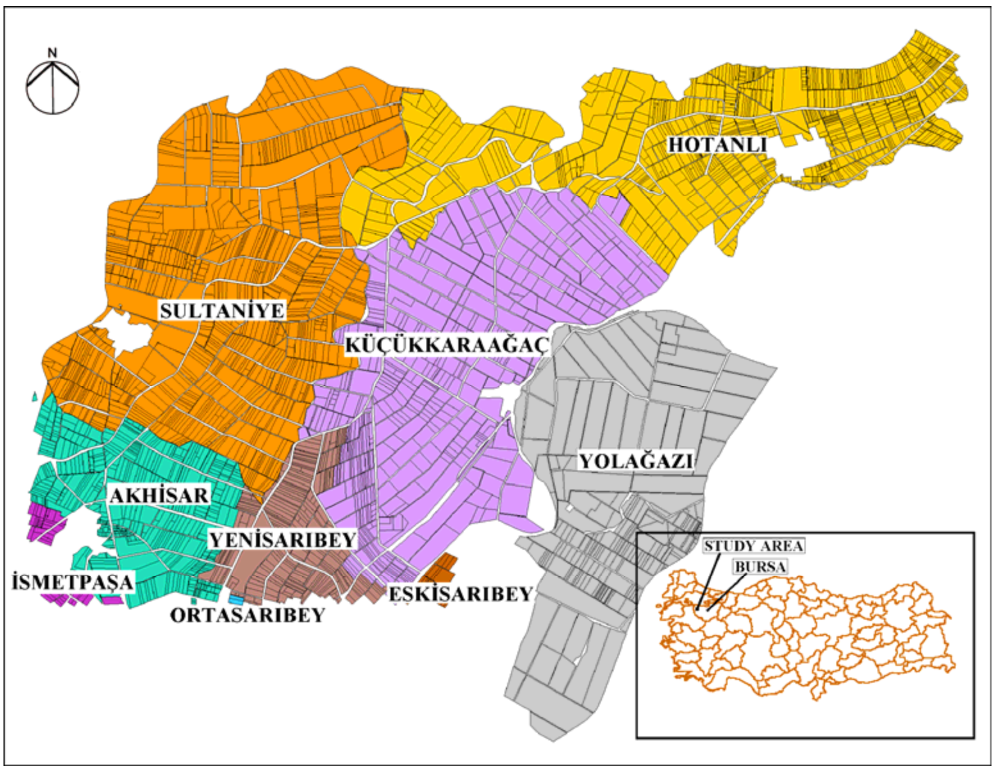

Figure 3.3 The study area (Scale ~1: 135 000)

Table 3.1 The percentages of coverages of the fields within the study area

Number of Fields	Field Size (ha)	Percentage (%)
735	0.0074 - 0.4995	21.61
808	0.5000 - 0.9994	23.76
1614	1.0022 -5.9836	47.46
129	6.0168 - 9.9811	3.79
81	10.0042 - 19.9010	2.38
23	20.4934 - 29.9463	0.68
11	31.6342 - 47.9745	0.32

To carry out the proposed classification approach, a multi-temporal cloud-free Landsat 7 ETM+ data set consisting of three image dates (August 19, July 2, and May 15) from the year 2000 was used. These dates are suitable for monitoring the vegetation in the area for they coincide with different phenological cycles of several crop types present in the study area. The spectral characteristics of the ETM+ sensor of Landsat 7 are summarized in Table 3.2. The image obtained from this sensor has six 30 m multispectral bands, one 60 m thermal infrared band and one 15 m panchromatic band.

Table 3.2 Description of the spectral bands of Landsat 7 ETM+ image

Band No	Band Width (μm)	Ground Resolution(m)	Band Wavelength
1	450-520	30	Visible (Blue)
2	520-600	30	Visible (Green)
3	630-690	30	Visible (Red)
4	760-900	30	Near-Infrared
5	1550-1750	30	Middle-Infrared
6	10420-12500	60	Thermal-Infrared
7	2080-2350	30	Near-Infrared
8	520-900	15	Panchromatic

For classifying the images, six multispectral bands numbered as 1, 2, 3, 4, 5, and 7 were used. The size of the utilized image area is 600 pixels by 450 lines for the multispectral bands and 1200 pixels by 900 lines for the panchromatic band. To perform field-based analysis, the agricultural field boundaries stored as vector polygons in PCI GEOMATICA were used. The agricultural field boundaries obtained from the regional cadastral office in hard-copy form were converted into digital form for a previous study conducted in the department. In addition, the relational attribute database was also constructed during this study using the data collected from the farmers and the land cover survey in the area. A detailed description about these processes can be found in Arıkan (2003).

The attributes of digital vector data include descriptive (*ID*, *Region*, *PNO*, *SPNO*) and reference data (*Refcrop, Prevcrop, Notes*) (Figure 3.6). An *ID* is a unique identification code given to each polygon in order to link a field to GIS database. *Region* indicates 2 or 3 letter abbreviation of the village name that the parcel belongs to. *PNO* and *SPNO* are lot and parcel numbers respectively as indicated in the cadastral maps. The attribute *Refcrop* indicates cultivated crop type within the field in August, July and May, whereas *Prevcrop* indicates onion and pea crop types within the field in July and/or May. The other previous crop types were concluded from the phenological cycles of crops and from the farmer cropping traditions in the study area. In *Notes* attribute column additional observations about the fields are given.

General information about the crop types planted in the study area is as follows: In the area of interest, the planting of sugar beet is regulated by the government in order to produce healthy and good quality crop supply. According to the regulations, sugar beet is allowed to be planted in every three or four years. In year 2000, cauliflower was planted only in the fields of Hotanlı village. This crop type is planted in place of pea, onion, wheat, and early tomato.

The information, at hand, about the crop calendar of the corn, tomato, pepper, cauliflower, onion, and pea classes, is illustrated in the Figure 3.4. In the graphical representation, white-coloured rectangular boxes represent sowing or planting dates, grey-coloured rectangular boxes illustrate harvesting dates, and the vertical lined rectangular boxes indicate that the end of the planting or harvesting dates are not known exactly.

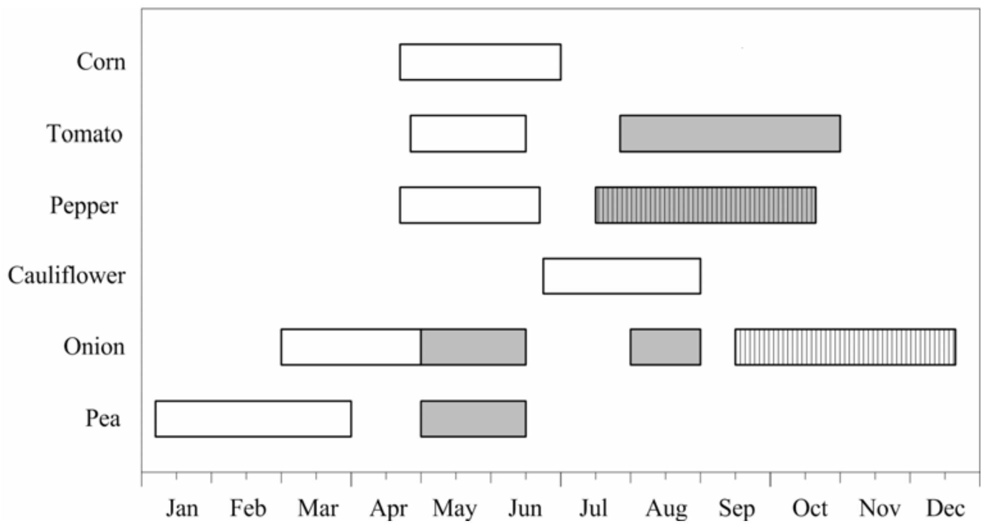

Figure 3.4 Crop calendar of the corn, tomato, pepper, cauliflower, onion, and pea classes

To facilitate the integration of vector and remotely sensed data, both data must be in the same coordinate system. The projection and the datum georeferencing parameters of utilized data are UTM Zone 35 and WGS 84, respectively (Arıkan, 2003).

3.3 PRE-PROCESSING

Improper data have impact on the accuracy of subsequent image analysis operations. The error propagated throughout data analysis operations can degrade the quality of the results. Therefore, it is generally necessary to pre-process data prior to actually analyzing it. The type of pre-processing changes according to the type of data (raster imagery, vector, etc.) and to the purpose that the data will be used for. For instance, a detailed mapping of the particular vegetation types requires geometric correction of remotely sensed data whereas only determining the presence or absence of a particular land-use type rather than its precise location does not require correction for geometric distortion (Mather, 1989). The pre-processings were applied both to vector and raster data.

3.3.1 PRE-PROCESSING OF VECTOR DATA

The vector data are composed of graphical data (Figure 3.5) and relational attribute data (Figure 3.6). The graphical data that represent the agricultural field boundaries were available in digital form. In addition, the relational attribute data consisting of seven types of attribute data were also available. The attribute information was to be used for training area selection and for the accuracy assessment. Therefore, the attribute data were carefully checked prior to image classification to find out if they contained any errors.

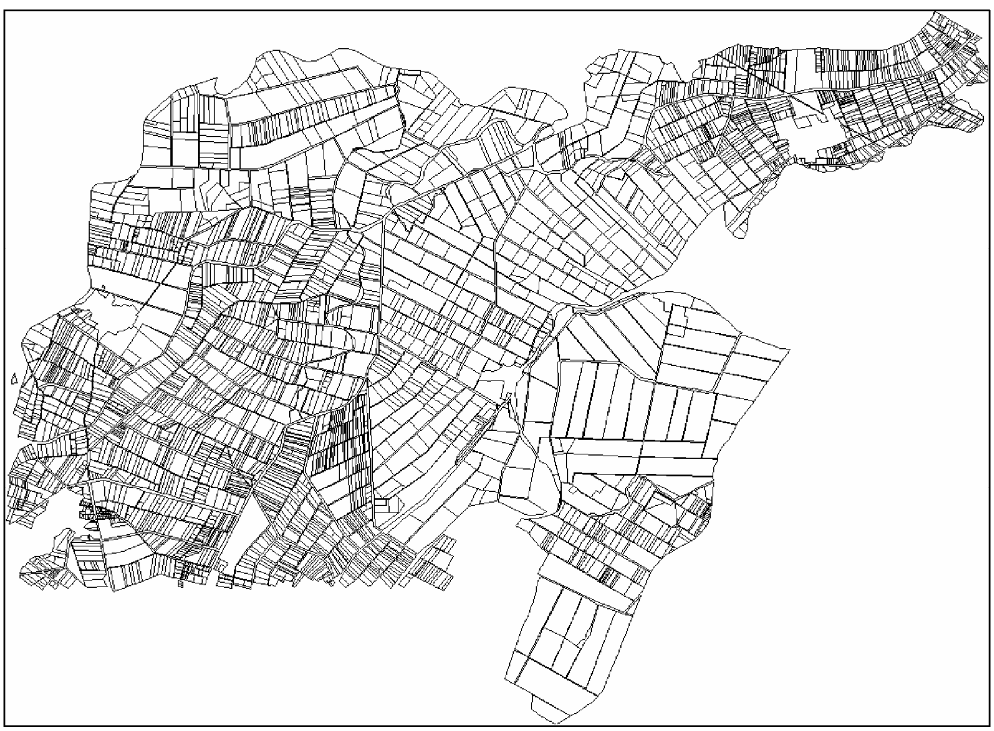

Figure 3.5 The vector field boundaries

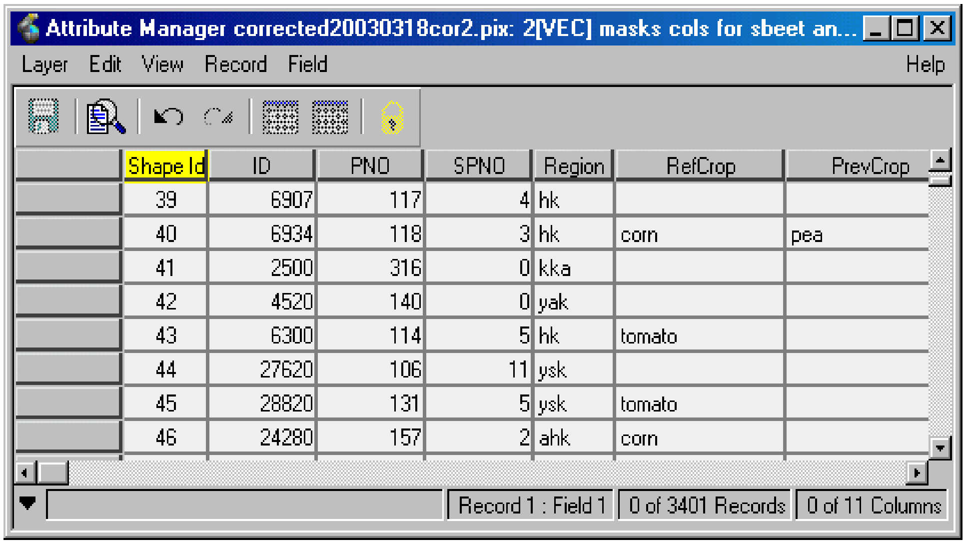

Figure 3.6 The attribute data

This checking process was conducted in two steps. In the first step, the descriptive data abbreviated as *ID*, *Region*, *PNO*, and *SPNO* were checked by comparing their printouts with the map sheets containing the village land consolidation boundaries, parcel boundaries, parcel numbers, and the land cover information. These maps consist of nine 1:5000-scale standard cadastral maps, two 1:5000-scale, and one 1:7500-scale land consolidation map sheets (Table 3.3).

Table 3.3 The cadastral maps used for the validation process

Map Data	Number	Scale	Date
Standard Cadastral Map	9	1:5000	2000
Cadastral Map of Küçükkaraağaç Village	1	1:5000	2000
Cadastral Map of Yolağazı Village	1	1:5000	2000
Cadastral Map of Hotanlı Village	1	1:7500	2000

In the second step, the reference crop and the previous crop attribute data entered earlier in GIS database were checked by comparing them with the reference data marked on 12 original map sheets. To carry out this comparison, thematic maps were created for the reference crop and the previous crop attribute data using ArcMap facility of ArcGIS software (Figure 3.7 and Figure 3.8). The selected area of study consists of 3401 agricultural fields. It was therefore difficult to visually interpret the created maps in one paper presentation. Hence, the study area was divided into four parts containing about the same number of fields in each map. The number of fields in each village is given in Table 3.4. Then, the created eight A3 size thematic maps were examined for correctness by comparing them with the original map sheets. The necessary editings were made both in the descriptive and the reference data stored in the GIS database.

Table 3.4 The number of the agricultural fields in each village

Name of the Village	**Number of the Agricultural Fields**
Akhisar	483
Eskisarıbey	19
Hotanlı	856
İsmetpaşa	58
Küçükkaraağaç	396
Ortasarıbey	1
Sultaniye	734
Yenisarıbey	238
Yolağazı	192

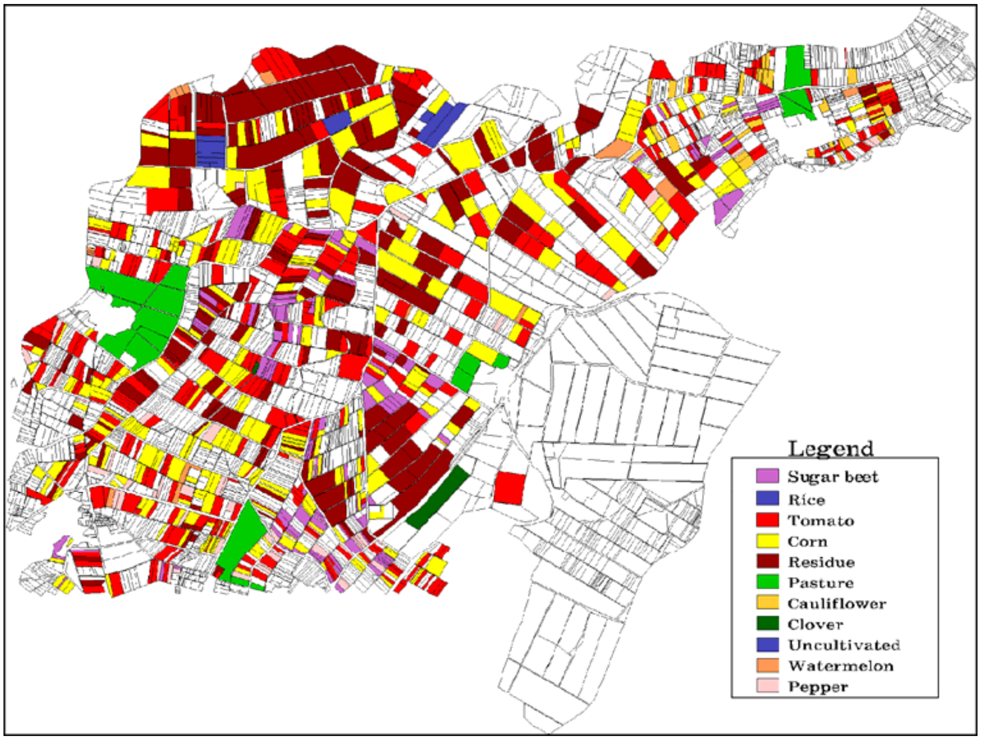

Figure 3.7 The distribution of the reference land cover types

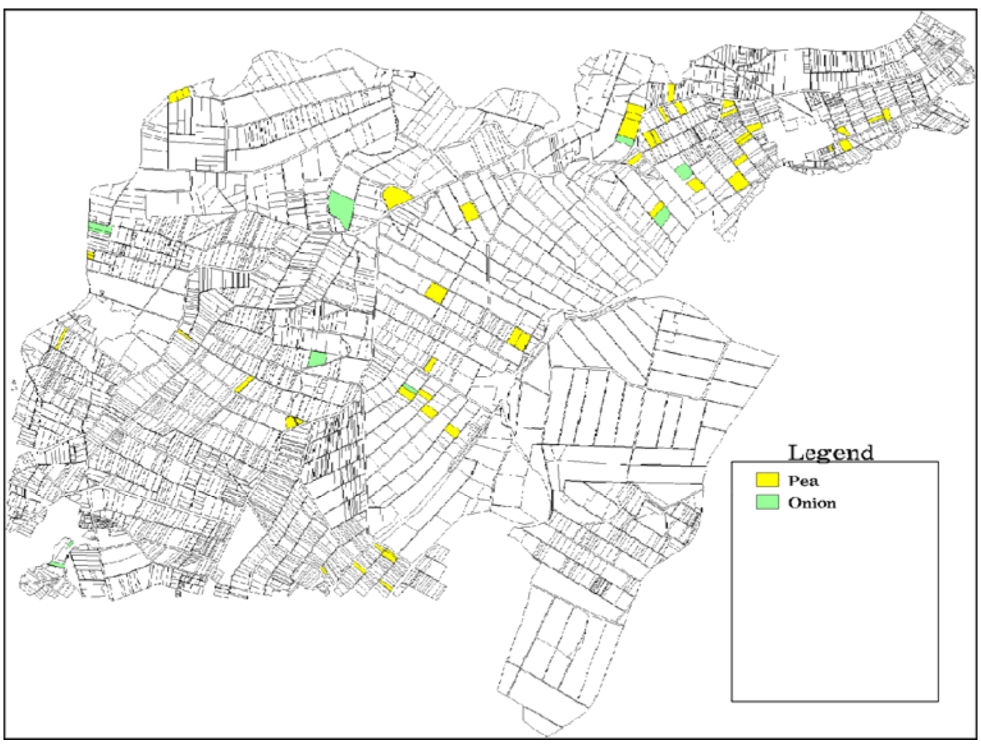

Figure 3.8 The distribution of the previous land cover types

3.3.2 PRE-PROCESSING OF REMOTE SENSING DATA

The remote sensing data of the study area is composed of the merged 15 m spatial resolution panchromatic and 30 m spatial resolution multispectral bands (Arıkan, 2003). In this data, the spectral characteristics of each multispectral band were preserved while providing the 15 m spatial resolution. The dimensions of the merged and geometrically corrected images were 1200 pixels by 900 lines and containing scenes outside the study area (Figure 3.9).

Figure 3.9 The visible bands (3-2-1) of August image overlayed with the agricultural field boundaries

The root mean square (RMS) error of the geometric correction for the August, July and May images were computed to be 0.58, 0.67 and 0.52 pixels, respectively, using the RMS values in X and Y directions reported in Arıkan, 2003. The image scenes that are not in the area of interest and the mixed pixels falling on the boundaries of the fields, which are known to cause the misclassification of the fields, were excluded by masking them out from each band of the images. To accomplish this process, initially the mask was generated for the areas to be used in the analyses by utilizing the vector data layer. Then, the outer part of this mask was excluded from each band of the images. The mask was generated with the polygon gridding function of PCI. First, using the function “POLYGON” the whole polygons (both edge and interior) were gridded. Then, using another function “EDGE ONLY” was applied to vector data layer in order to grid only the polygon edges. Finally, the bitmap information obtained using the second function was subtracted from the bitmap information obtained using the first function. Hence, the mask displaying the coverage of the study area was created (Figure 3.10). Figure 3.11 illustrates the August image after the masking procedure was applied.

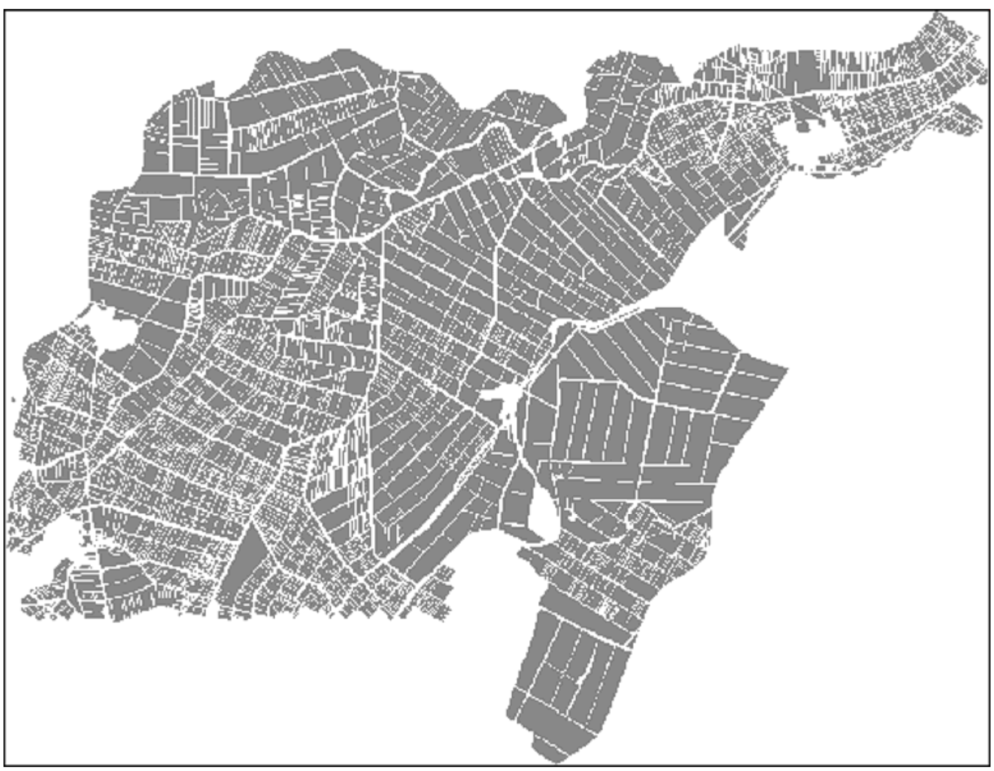

Figure 3.10 The raster mask generated using the vector polygon layer

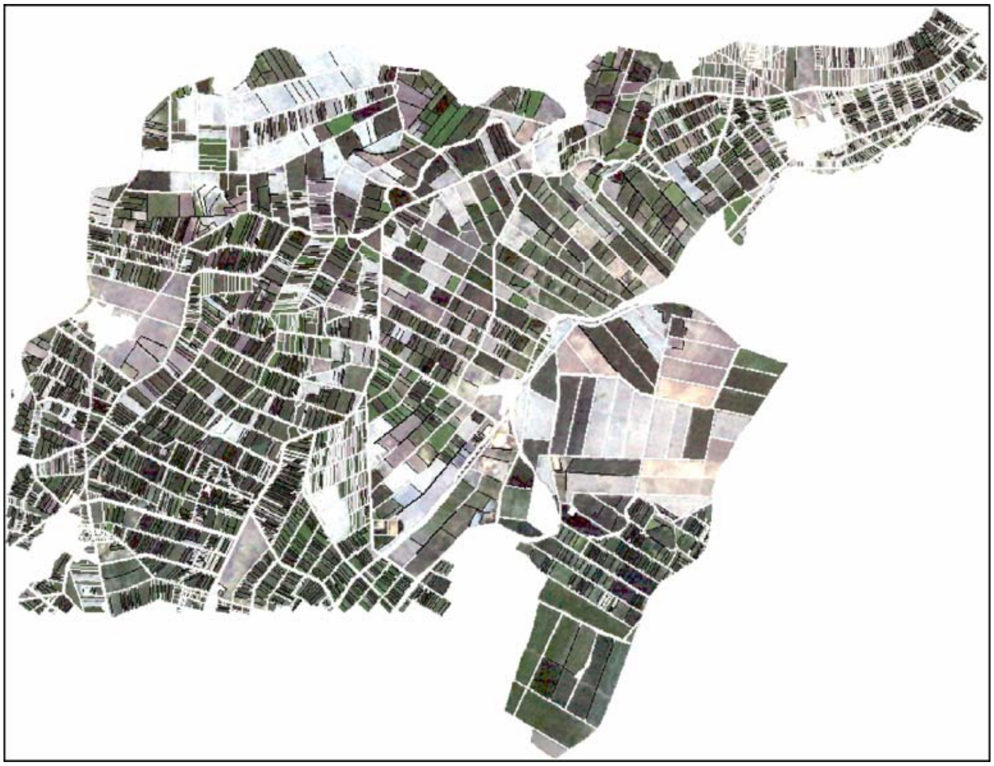

Figure 3.11 The August image after the masking procedure was applied

After performing the masking operation, several fields that contain a few pixels only have became extinct since they contained no pixels inside. As a result, the number of the fields have dropped from 3401 to 3240 for the August image, to 3245 for the July image and to 3238 for the May image. As can be seen, the number of the fields are not the same for the images. The reason for this is that, for each image, the geometric correction performed using the digital vector data provided different RMS error values. Therefore, due to different geometry of the images, the number of the fields which contain no pixel differ for each image date.

3.4 IMAGE CLASSIFICATION

The main steps of the classification process include the selection of training areas, the extraction of new bands (NDVI, PCA, and Tasselled Cap

Transformation), the computation of class signatures, per-pixel classification of multi-temporal images using a decision tree approach, and the per-field analysis of the classified outputs in the integration of remote sensing and GIS. In addition, to assess the utility of the proposed methodology, the per-field analysis was also applied on the output of the traditional per-pixel maximum likelihood classified images.

3.4.1 TRAINING AREA SELECTION

In order to classify an image using a supervised classification technique, initially the relevant and adequate sample data are collected for each class of interest. The training stage is important because the statistical estimates derived from the training samples are used to identify the pixels making up the image. Therefore, it is required to pay attention to some necessary criteria when selecting the training areas. These mainly include:

- collecting the samples throughout the image by taking into account the distribution of the classes over the area,
- collecting sufficient number of samples to ensure that each class is properly represented, and
- delineating samples from relatively homogeneous parts of the classes of interest in order to generate informationally unique training statistics.

To select the training samples, the raster imagery and vector data were overlaid through the integrated display of raster image and vector map interface function of the PCI GEOMATICA software. Then, the vector attribute data were used to query each class of interest and to highlight it on the graphical display. Approximately, one third of the reference data were used for selecting the training sample pixels. While determining the fields for the collection of training samples, the color composites of the bands 4, 5, 3 and 3, 2, 1 were used to visually inspect both the spectral classes and the homogeneous areas for each spectral class. For each information class, the training samples were collected from either one or several spectral classes. Figure 3.12 illustrates the training area collection inside the agricultural fields in the integration of remote sensing and GIS.

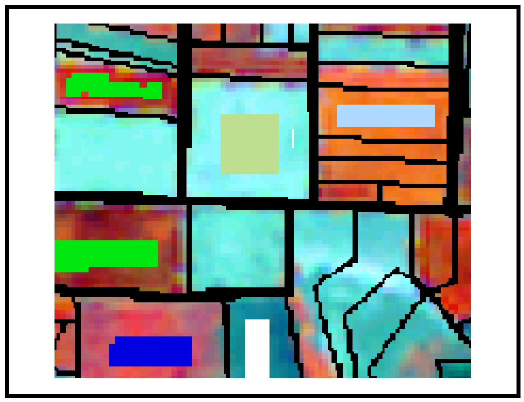

Figure 3.12 A part of the image illustrating the training sample collection inside the agricultural fields

The number of information classes determined for August, July, and May were 11, 12, and 7, respectively. In the August image, the classes include corn, tomato, sugar beet, pepper, rice, watermelon, cauliflower, pasture, clover, uncultivated, and residue. In the July image, the classes consist of the same classes as the August image as well as onion. The May classes are wheat, rice, pea, pasture, clover, newly seeded crop, and onion. For each class, training samples ranging from 123 to 1997, from 105 to 2380, and from 144 to 1289 pixels were selected from the August, July, and May images, respectively. In order to make the spectral classes more interpretable, they were numbered sequentially for the subsequent analyses (Table 3.5).

Table 3.5 The spectral classes and the class numbers assigned for each class

AUGUST	JULY	MAY
corn: 1	corn-1: 1	newly seeded-1: 1
residue-1: 2	corn-2: 2	newly seeded-2: 2
residue-2: 3	corn-3: 3	wheat: 3
tomato-1: 4	corn-4: 4	clover: 4
tomato-2: 5	residue-1: 5	pasture-1: 5
tomato-3: 6	residue-2: 6	pasture-2: 6
sugarbeet: 7	tomato-1: 7	rice-1: 7
clover: 8	tomato-2: 8	rice-2: 8
pasture: 9	tomato-3: 9	pea-1: 9
pepper: 10	tomato-4: 10	pea-2: 10
watermelon: 11	sugar beet: 11	onion-1: 11
uncultivated: 12	clover: 12	onion-2: 12
rice: 13	pasture: 13	
cauliflower-1: 14	pepper-1: 14	
	pepper-2: 15	
	watermelon: 16	
	uncultivated: 17	
	rice-1: 18	
	rice-2: 19	
	cauliflower-1: 20	
	cauliflower-2: 21	
	onion-1: 22	
	onion-2: 23	

To examine the quality of the training areas and the class signatures, Jeffreys-Matusita (J-M) distance values were calculated. The J-M distance (Equation 3.1) is a measure used to examine how well each class is separated from each of the other classes. It is calculated as follows (Bruzzone and Serpico, 2000):

$JM_{ij} = \{ \int_x [\sqrt{p(x/w_i)} - \sqrt{p(x/w_j)}]^2 dx\}^{½}$ (Equation 3.1)

where $p(x/w_i)$ refers to the conditional probability density functions for the feature vector x, given the class w_i ($i = 1, 2, \ldots, c$) and class w_j ($j = 1, 2, \ldots, c$).

The values are real values changing from 0.0 to 2.0. The value 0.0 indicates that there is a complete overlap between the signatures of two classes. On the contrary, 2.0 indicates a complete separation between the two classes. To define the degree of separation, the suggested possible ranges are given in Table 3.6 (PCI Geomatica, 1997).

Table 3.6 The J-M distance ranges

Ranges	Degree of separation
0.0 – 1.0	very poor separability
1.0 – 1.9	poor separability
1.9 – 2.0	good separability

While selecting the training cells the J-M distance values were utilized. For each class, those training pixels that decreased the J-M value to the range of 0.0-1.0 or 1.0-1.9 were eliminated from the training samples. Instead, those training pixels that increased the separability value were chosen. However, it should be noted that for some of the classes, it was not possible to find the pixels that have J-M distance value in the range of 1.0-1.9 or 1.9-2.0. Therefore, the training pixels for these classes depicted lower separability. For example, this was the case for pepper-1 and cauliflower-2 in the July image. They showed a very poor separability with a J-M distance of 0.798. The J-M distance values computed for the training data sets of the August, July, and May images on the original bands 1, 2, 3, 4, 5, and 7 are given in Table A.1, Table A.2, and Table A.3 in Appendix A, respectively.

Once the training statistics were collected, the corresponding coincidence spectral plots were drawn at $\pm 2\sigma$ and $\pm 3\sigma$, for each band, using MS Excel. These plots are useful to understand the spectral distribution of the data being analyzed since they are graphical representations. On these plots, the mean and the variance of the distribution of each class for each band were displayed. This provided a visual analysis of the degree of between-class separability one band at a time. Using these plots, the bands most effectively discriminating each class from all others were defined. In a decision tree classification it is required to find out the optimum band or the band combinations to separate the classes. Therefore, this analysis was performed for each of the original and the derived bands (refer to 3.4.2). Figure 3.14, Figure 3.15, and Figure 3.16 illustrate a part of the coincidence spectral plots drawn at $\pm 2\sigma$ for the August, July, and May images, respectively.

3.4.2 FEATURE EXTRACTION

The NDVI and the Tasselled Cap Transformation bands are known to sensitive to vegetation and to the factors affecting the vegetation’s existence (soil, moisture). Therefore, these additional bands were generated to be utilized for the proposed classification procedure. In addition, the principal components were also generated to be included in the classification operation.

3.4.2.1 NDVI

NDVI is probably the most widely used vegetation index used to quantify the vegetation cover. It is a spectral ratio between the measured reflectivity in the red and the near infrared portions of the electromagnetic spectrum. The values produced with this ratio (NDVI= B4-B3 / B4+B3) changes in the range of -1.0 to 1.0. The ratio values greater than zero indicate the vegetation areas, whereas the negative values indicate the non-vegetation areas. In this study, the NDVI bands were generated for the August, July, and May images. Figure 3.13 illustrates an NDVI band generated for the August image.

To make the derived NDVI values compatible with the training statistics (mean values, standard deviations) of other bands, they were scaled to 0-255 range. This made it easy to interpret the coincidence spectral plots that were constructed using the training statistics.

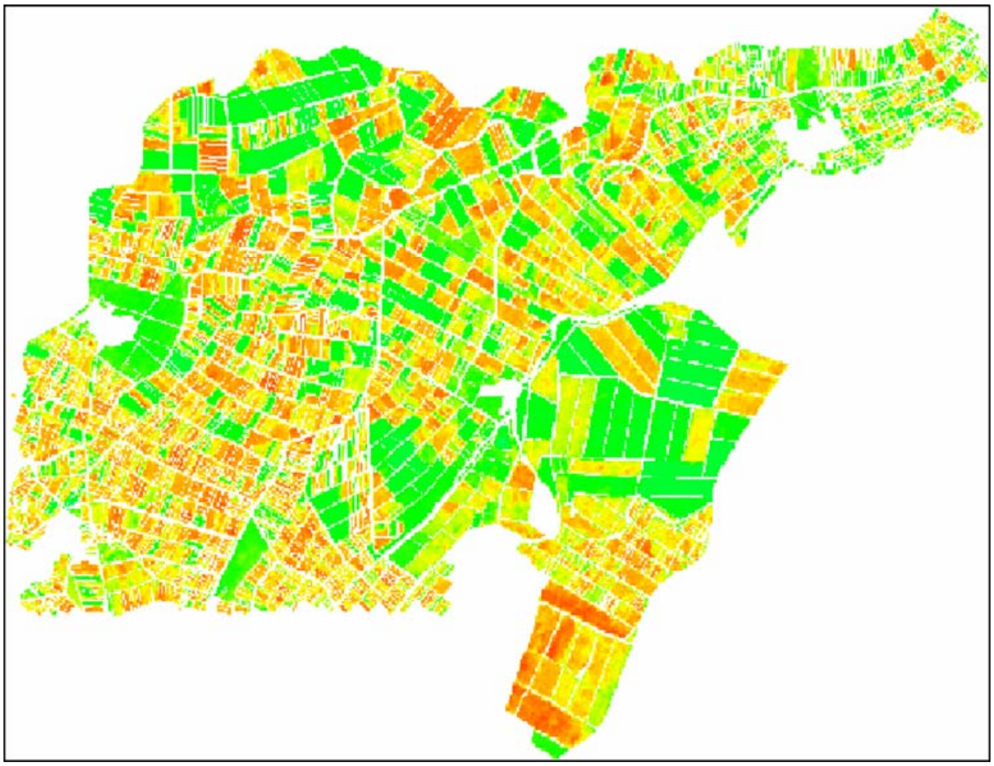

Figure 3.13 An NDVI band generated for the August image

3.4.2.2 PCA

The vegetated areas show positive correlations among the visible bands or negative correlations between the near infrared and the visible red bands (Mather, 1989). To reduce this correlation and thus repetition of the information between bands, PCA can be used. With this analysis, while the number of bands being processed is reduced, the computational efficiency is managed without missing much information when used in an image classification (Lillesand and Kiefer, 1994). In this study, the new principal component bands were created using the PCA algorithm of the PCI GEOMATICA software for determining if these new bands can be used in discriminating some of the classes better than the original bands in the decision tree classifier. For each image date, the variances that indicate the information content within each principal component bands are given in Table 3.7.

Table 3.7 The variances obtained for the principal component bands of the August, July, and May images

Eigenchannel	**August Variance(%)**	**July Variance(%)**	**May Variance(%)**
1	89.49	78.24	84.07
2	7.15	14.58	13.68
3	2.24	4.89	1.52
4	0.88	1.89	0.50
5	0.16	0.30	0.14
6	0.08	0.09	0.08

In the present study, the first 3 components of the May image and the first 4 components of the July and August images account for 99.27%, 99.60%, and 99.76% respectively of the total variance of the original data sets. Therefore, the first 3 principal components (PCs) of the May image and the first 4 PCs of the July and August images were used in the classification procedure.

3.4.2.3 TASSELLED CAP TRANSFORMATION

In addition to normalized difference vegetation index and the principal components analysis mentioned above, the Tasselled Cap Transformation was also carried out to obtain the “Brightness”, “Greenness”, and “Wetness” bands to be included in the decision tree classification procedure.

In order to apply at-satellite based Tasselled Cap Transformation, at-satellite reflectance images should be used. Hence, at-satellite reflectance images of the three image dates were obtained by converting the radiometric measurement of the raw digital images (DN's) to at-sensor reflectance.

The variation in a digital image is represented by three principal ways (University of Idaho, Remote Sensing Lecture Notes):

1. Digital numbers (8 bit – 0-255),
2. Radiance (energy value – watts), and
3. Reflectance (percentage – incident).

Radiance is the actual energy recorded by the detectors of the sensor. This is called at-sensor radiance and stored as DN's. To convert the DN's back to at-sensor spectral radiance, for each band, it is required to know the information about the sensor constants (gain and offsets) (Table 3.8).

Table 3.8 The gain and offset values of the May 15, July 2, and August 19, 2000 Landsat 7 ETM+ Images

BAND	GAIN	OFFSETS
1	-6.200000000000000	0.775686274509804
2	-6.400000000000000	0.795686274509804
3	-5.000000000000000	0.619215686274510
4	-5.100000000000000	0.965490196078431
5	-1.000000000000000	0.125725490196078
7	-0.350000000000000	0.043725490196078

The equation used to generate the radiance values from DN values is:

L_λ = "gain" * QCAL + "offset" (Equation 3.2) which is also expressed as:

$$L_\lambda = ((LMAX_\lambda - LMIN_\lambda) / (QCALMAX - QCALMIN)) * (QCAL - QCALMIN) + LMIN_\lambda \quad \text{(Equation 3.3)}$$

Where:

L_λ= Spectral Radiance at the sensor's aperture in watts/(meter squared * ster * µm)

"gain"= Rescaled gain (the data product "gain" contained in the level 1 product header or ancillary data record) in watts/(meter squared * ster * µm)

"offset"= Rescaled bias (the data product "offset" contained in the level 1 product header or ancillary data record) in watts/(meter squared * ster * µm)

QCAL = the quantized calibrated pixel value in DN

$LMIN_\lambda$= the spectral radiance that is scaled to QCALMIN in watts/(meter squared * ster * µm)

$LMAX_\lambda$= the spectral radiance that is scaled to QCALMAX in watts/(meter squared * ster * µm)

QCALMIN= the minimum quantized calibrated pixel value (corresponding to $LMIN_\lambda$) in DN

= 1 (LPGS Products)

= 0 (NLAPS Products)

QCALMAX= the maximum quantized calibrated pixel value (corresponding to $LMAX_\lambda$) in DN

= 255

While converting the DNs to radiance values, Equation 3.2 was used because it is the simplified form of Equation 3.3.

In order to reduce between-scene variability in relatively clear Landsat images, combined surface and atmospheric reflectance values of the earth is computed by using at-sensor radiance values (Landsat 7 Science Data Users Handbook). This is accomplished by computing the following formula for every pixel of each band of the images displaying variation with at-sensor radiance values:

$$\rho_p = \pi * L_\lambda * d^2 / ESUN_\lambda * \cos\theta_s \qquad \text{(Equation 3.4)}$$

Where:

ρ_p = Unitless planetary reflectance

L_λ = Spectral radiance at the sensor's aperture

d= interpolated from values listed in Table 3.9 (Landsat 7 Science Data Users Handbook).

$ESUN_\lambda$= Mean solar exoatmospheric irradiances from Table 3.10 (Landsat 7 Science Data Users Handbook).

θ_s= Solar zenith angle in degrees

Table 3.9 Earth-Sun Distance in Astronomical Units

Julian Day	**Distance**	**Julian Day**	**Distance**	**Julian Day**	**Distance**	**Julian Day**	**Distance**
1	0.9832	106	1.0033	213	1.0149	319	0.9892
15	0.9836	121	1.0076	227	1.0128	335	0.9860
32	0.9853	135	1.0109	242	1.0092	349	0.9843
46	0.9878	152	1.0140	258	1.0057	365	0.9833
60	0.9909	166	1.0158	274	1.0011		
74	0.9945	182	1.0167	288	0.9972		
91	0.9993	196	1.0165	305	0.9925		

Table 3.10 ETM+ Solar Spectral Irradiances

Band	watts/(meter squared * µm)
1	1969.000
2	1840.000
3	1551.000
4	1044.000
5	225.700
7	82.07
8	1368.000

Therefore, the at-satellite reflectance images belonging to May, July, and August were generated according to the computation sequence given above. By applying the at-satellite reflectance based Tasselled Cap transformation to these generated at-satellite reflectance images, new six Tasselled Cap axes can be computed. The new axes are called "Brightness", "Greenness", "Wetness", "Fourth", "Fifth", and "Sixth" (Huang et. al., 2002). However, since the first three axes were enough for the study, only the "Brightness", "Greenness" and "Wetness" axes were created. The computation was performed using the TASSEL algorithm of PCI GEOMATICA software. The values were scaled to 0-255 range.

3.4.3 PER-PIXEL CLASSIFICATION

3.4.3.1 DECISION TREE CLASSIFICATION OF MULTI-TEMPORAL IMAGES

A decision tree is a layered classification procedure that recursively splits a data set into smaller groups on the basis of a set of tests defined at each branch in the tree. The tree is composed of a root node and a set of internal and terminal nodes. The output may be a terminal node (leaf) that refers to the class label or an internal node that indicates further separation on the classes.

After determining the leaf or internal nodes of the tree at each level, the scene corresponding to the selected class is masked out. This means that this part is excluded from further classification process. Therefore, this step by step classification prevents the classified pixels being used in the classification of other classes that show similar spectral signature values. When the output is an internal node, the group of classes that make up of this internal node is masked on the image and the classification process is carried out on the group of classes that are masked. Then, the classification procedure is continued on other branch(es) of the tree, until all the classes are separated or no class was able to be separated.

As can be observed on the coincidence spectral plots of the August image (Figure 3.14), it was not easy to discriminate the selected classes using this date of imagery. Therefore, the three dates of images (August, July, and May) were used together to perform the proposed decision tree classification procedure. Figure 3.14, Figure 3.15 and Figure 3.16 illustrate the coincidence spectral plots ($\pm 2\sigma$) of bands 1, 2, and 3 for the August, July, and May images, respectively. The remaining spectral plots are given in Appendix C.

After analyzing the coincidence spectral plots, 11, 14, and 8 level decision trees were designed for the August, July, and May images, respectively (Figure 3.17, Figure 3.18, and Figure 3.19). It should be noted that all decision trees are interrelated. The reason for this is that the three decision trees were designed together by utilizing the discernable classes across the images. That is when there was a difficulty in discriminating classes at an internal node of a decision tree, the class separation procedure was continued on the decision tree of another most proper image. This procedure was performed until all decision trees were generated. There were two ways for class separation used in designing the decision trees. One was the examination of the usual co-spectral plots, the other was the use of separated classes in the decision trees of the other images.

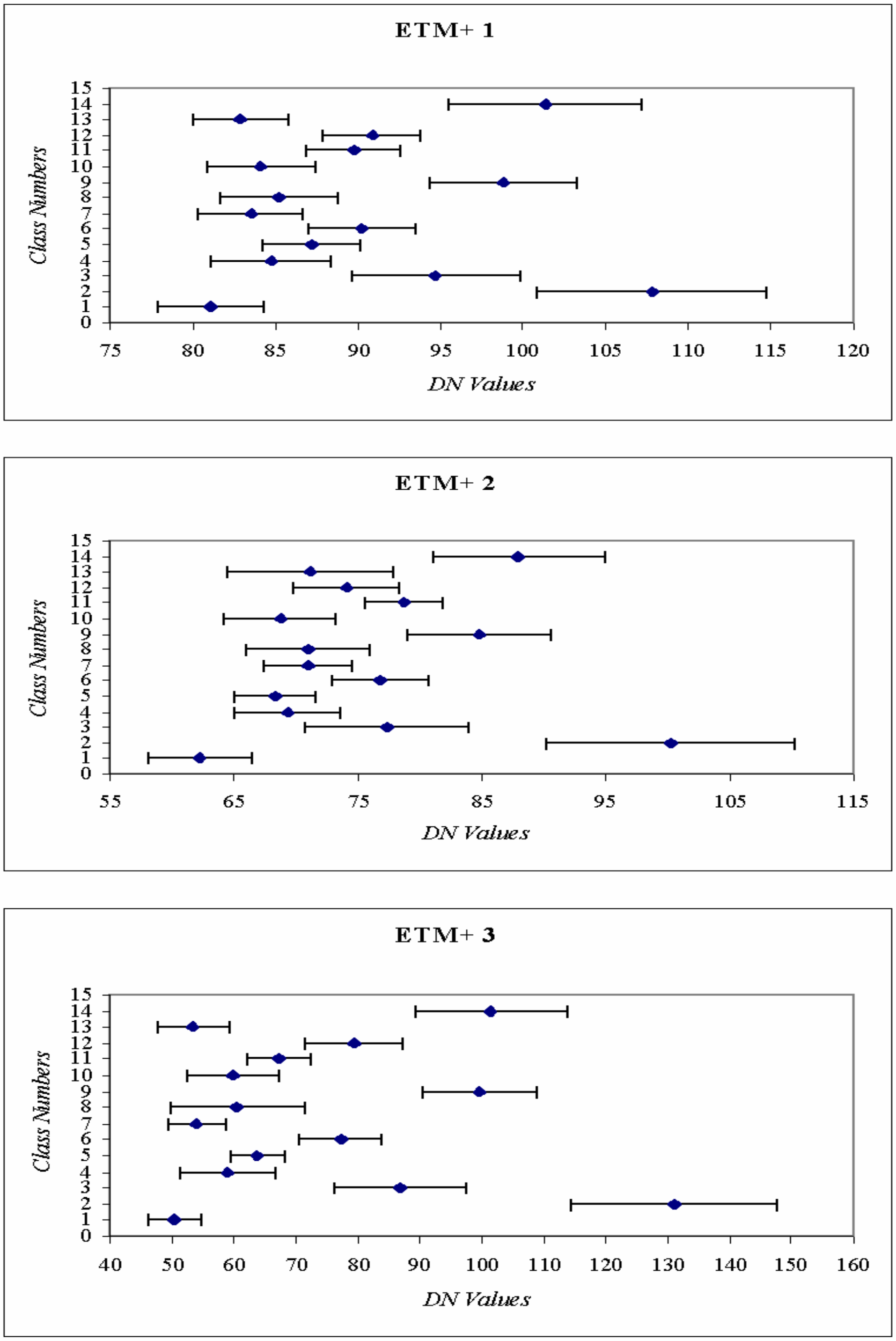

Figure 3.14 Coincidence spectral plots with ±2 standard deviations from the mean for August

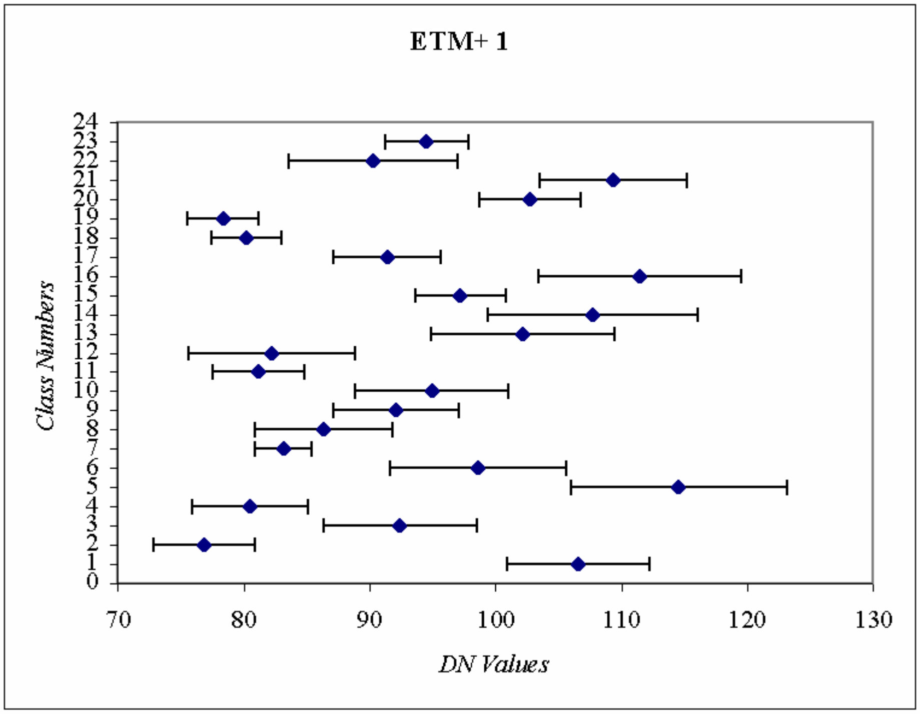

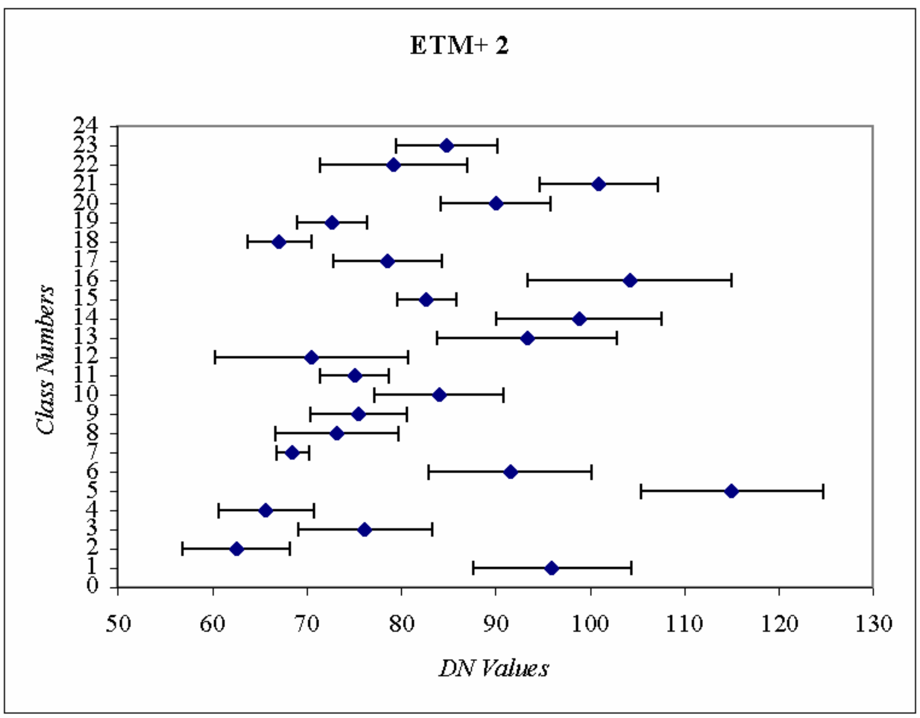

Figure 3.15 Coincidence spectral plots with ±2 standard deviations from the mean for July

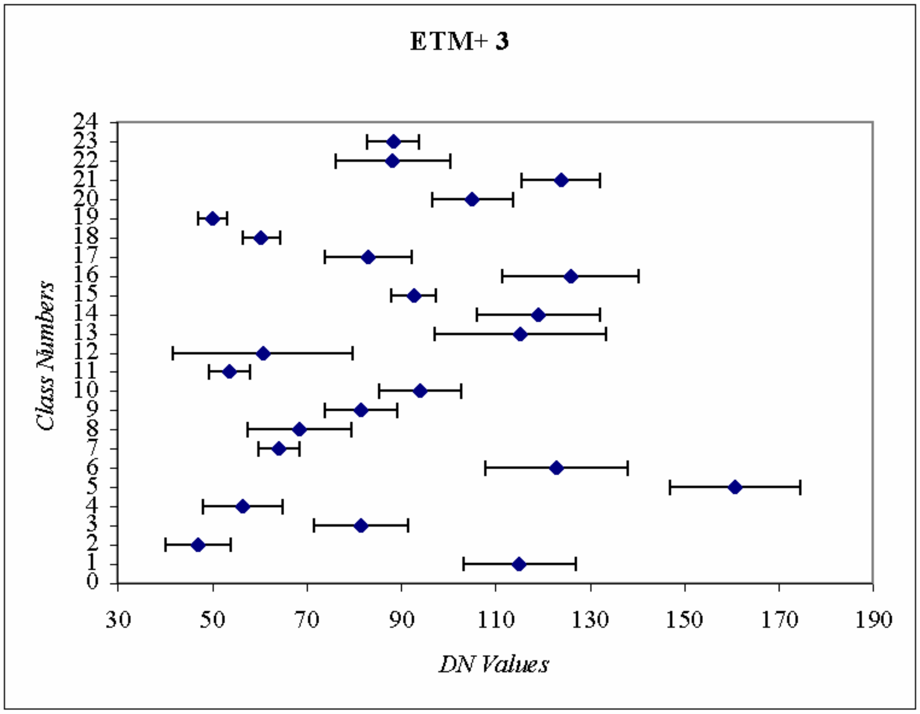

Figure 3.15 Coincidence spectral plots with ±2 standard deviations from the mean for July (cont'd)

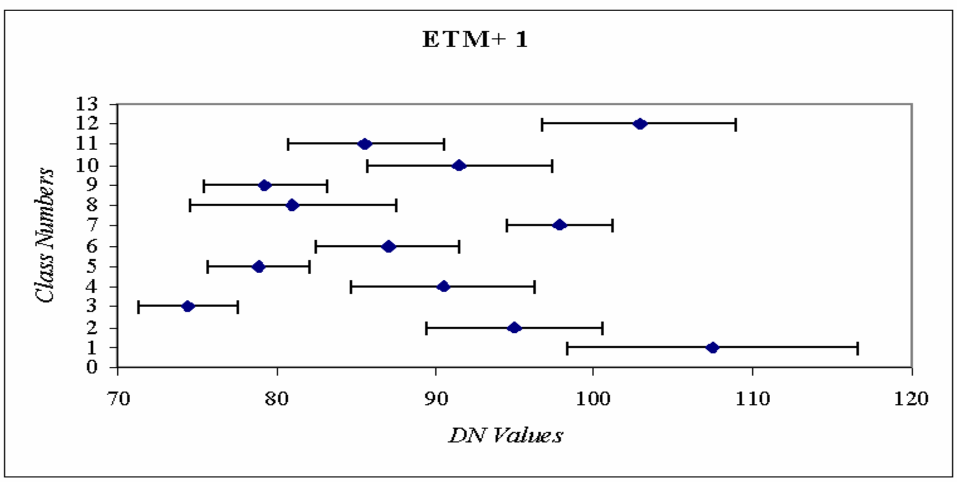

Figure 3.16 Coincidence spectral plots with ±2 standard deviations from the mean for May

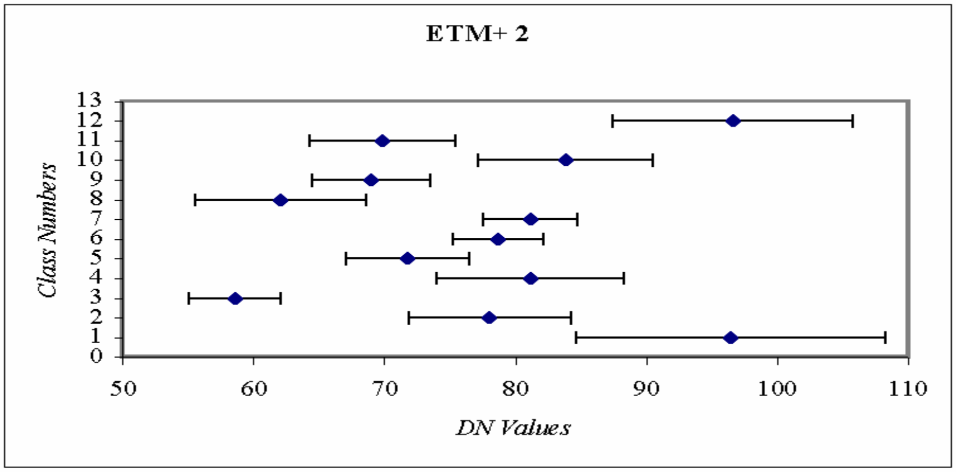

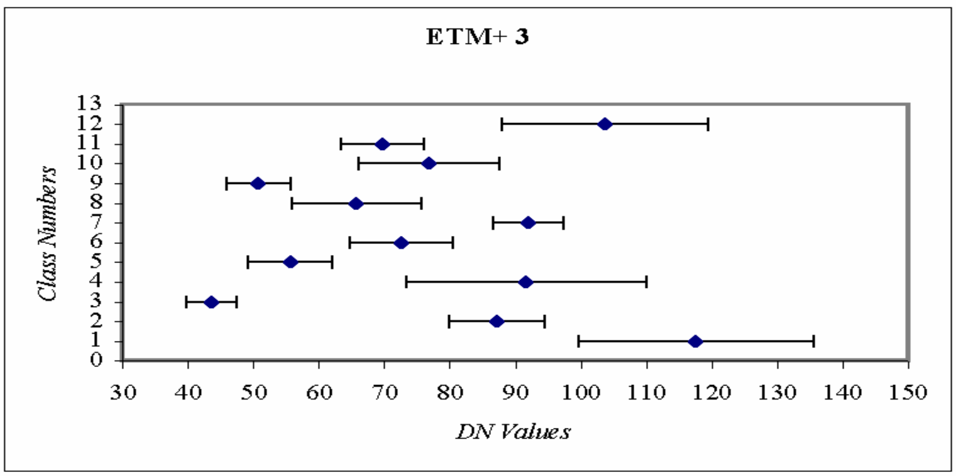

Figure 3.16 Coincidence spectral plots with ±2 standard deviations from the mean for May (cont'd)

In the initial decision tree, several classes were able to be separated using more than one band. The band or band combinations used to separate these classes were determined while performing the classification by visually checking their classification performance on the fields from which the training samples were taken. Therefore, the final forms of the decision trees were determined while classifying the images. For example, in the July co-spectral plots, sugar beet was observed to be easily separable using band 4, PCA-2, and Tasselled Wetness band of the July image. When classifying the July image, it was observed that the classified pixels except for a few were the same using either band 4 or PCA-2. However, several additional sugar beet pixels were able to be classified using Tasselled Wetness. Hence, PCA-2 and Tasselled Wetness band of the July image were selected to perform the separation of the sugar beet class. For such classes, only the band that classified most of the training fields was given either in the schematic diagrams of the decision trees or the tables that contain the lower and upper decision boundaries used to separate the land cover classes.

It was known from the ground truth data that which field contains what class at what date of image. Using this information for training samples, the same fields classified in different date images were checked visually to see if there would be any additional improvements in the classification. That is, if some of the pixels that were not able to be separated in one image could be separable in the other image. The residue class in the August image and the wheat class in the May image can be given as examples for this type of classification improvement. In May, the residue fields of the August image were planted with wheat. Therefore, the classified wheat pixels obtained from the May image was used as the mask and transferred onto the August image to see if they could increase the correctly classified residue pixels in the August image. The wheat pixels which increased the classification of residue in the August image was merged with the original residue mask obtained from the August image. The same procedure was applied for the May wheat fields. In this case, the classified residue pixels obtained from the August image was transferred onto the May image. During the classification process, this method was also utilized between the August and July images for the tomato and corn classes.

The decision tree classifiers designed for the classification of the August, July, and May images are illustrated in Figure 3.17, Figure 3.18, and Figure 3.19, respectively. In the diagrams, the ellipses represent the internal nodes and each rectangular box represents a leaf node. There are also grey-coloured rectangular boxes illustrating that the class is separated using the other date image. The information for the other date image is provided below the associated internal node. For example, at level 5 of the August decision tree “July (sugar beet=11)” indicates that the sugar beet class in the August image is classified using the sugar beet mask of the July image.

When classifying the images, the decision boundaries were defined as ±2σ (±2 standard deviations) since some of the classes or groups of classes were not distinctly separable at ±3σ range. However, where there was no spectral overlap between the classes the upper and/or lower extends of the classes were extended to ±3σ when performing the classification operation. The upper and lower decision boundaries used for separating individual classes or groups of classes are illustrated in Table 3.11, Table 3.12 and Table 3.13 for the August, July, and May images, respectively. For each class, the mean values and the standard deviations are given for each of the original and derived bands in Table B.1, Table B.2, and Table B.3 in Appendix B.

Table 3.11 The lower and upper decision boundaries used to separate the land cover classes on August image

Spectral Class	Level	Band	Lower Boundary	Upper Boundary
Residue-1	2	3	115	156
Residue-2	3	4	42	58
Pasture	4	5	130	167
Cauliflower	5	1	93	110
Tom-2_Uncultivated	7	PCA2	140	161
Clover	8	PCA3	138	149
Tom-2	8	PCA1	87	107
Uncultivated	8	PCA1	110	155
Tom-3	10	Tas-Greenness	122	156
Corn	11	2	56	64
Watermelon	11	2	75	83
Tom-1	12	2	64	75

Table 3.12 The lower and upper decision boundaries used to separate the land cover classes on July image

Spectral Class	Level	Band	Lower Boundary	Upper Boundary
Sugarbeet	2	PCA2	39	72
Rice-1	3	5	20	61
Corn-2_Rice-2	10	NDVI	175	195
Corn-2	11	2	57	68
Rice-2	11	2	69	76
Pepper-1	13	3	100	140
Tom-3_Pepper-2	14	4	46	69
Tom-1_Tom-2_Tom-4	15	4	70	127
Tom-3	15	PCA1	70	111
Pepper-2	15	PCA1	112	142

Table 3.13 The lower and upper decision boundaries used to separate the land cover classes on May image

Spectral Class	Level	Band	Lower Boundary	Upper Boundary
Rice-2	2	5	1	60
Wheat	3	2	54	62
Pea-1_Pea-2	5	Tas-Greenness	133	221
Onion-1	6	PCA1	81	117
Onion-2	7	4	95	114
Newlyseeded-1	9	7	109	163
Newlyseeded-2_Rice-1	9	7	58	108

The main objective of this study was to identify the summer (August) crops. Therefore, the decision tree of the August image is used to explain how the tree was designed based on the coincidence spectral plots and how the classes were separated from each other utilizing also the July and May images.

The whole data was defined at the first level of the decision tree. At the first level, the class residue-1 was easily separated from the other classes using band 3 of the August image. At the second level of the decision tree the scene corresponding to residue-1 was masked out and residue-2 was separated using band 4 of the masked August image. Similarly, the land cover class pasture was easily separated at level 3 from the class subset (1, 4, 5..8, 10..14) using band 5 and cauliflower was separated from the class subset (1, 4, 5..8, 10..13) at level 4 using band 1 of the August image.

At level 5 of the decision tree of the August image, the July image was started to be utilized for separating the classes. This was because there was not a separable class in the August co-spectral plots after level 5. Therefore, at the first level of the July decision tree, sugar beet was separated from the other classes using PCA-2 of the July image. At the second level, rice-1 was separated using band 5.

Residue-1 was able to be separated using band 3 at level 3 of the July decision tree. However, no further separation was succeeded for the next level. Then, the decision tree of the May image was started to be utilized for performing the class separation. At the first level of the May decision tree, rice-2 was separated from the class subset (1..7, 9..12) using band 5 and at the second level, the class wheat was separated using band 2. In the initial decision tree, the pasture-1 and pea-1 classes were able to be separated using PCA-1 at the third level of the tree. However, during the classification it was observed that classifying pea-1 in the first place would result in several pasture pixels to be incorrectly classified. Then, instead of pea-1, pasture-1 was classified first. Yet, the pasture pixels were incorrectly classified as pea. If pasture-2 was separable at this classification stage,

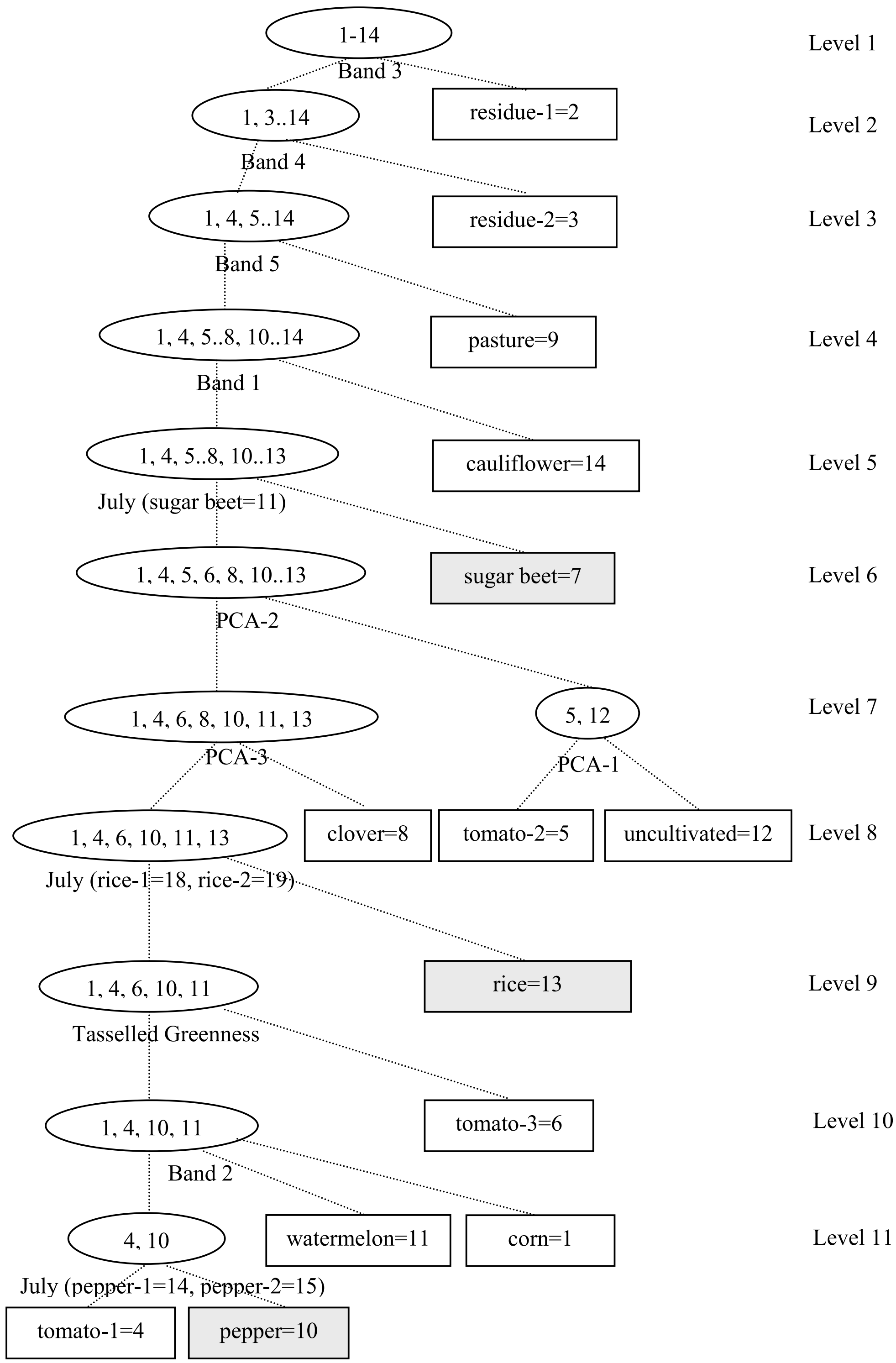

Figure 3.17 The decision tree designed for the August image

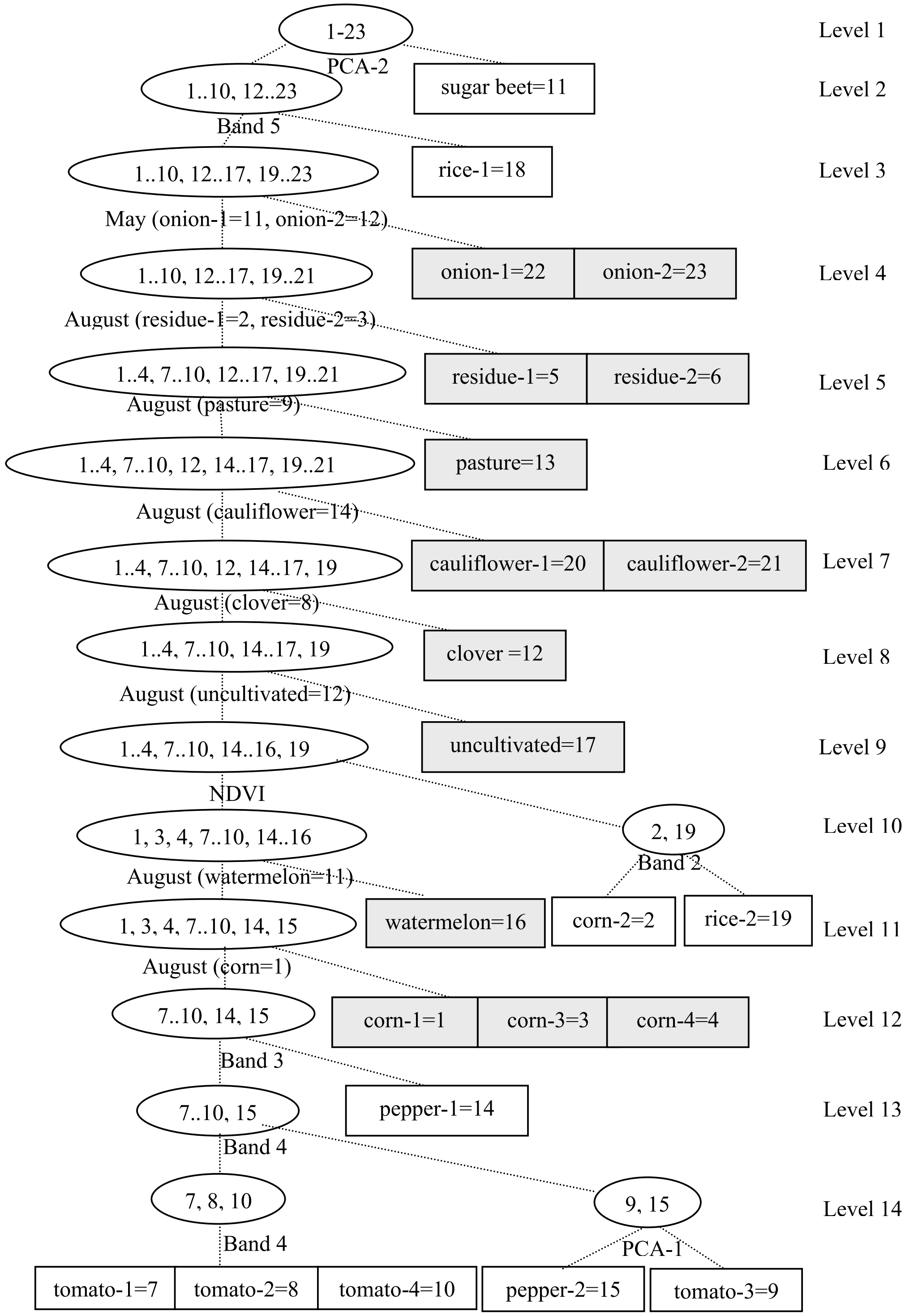

Figure 3.18 The decision tree designed for the July image

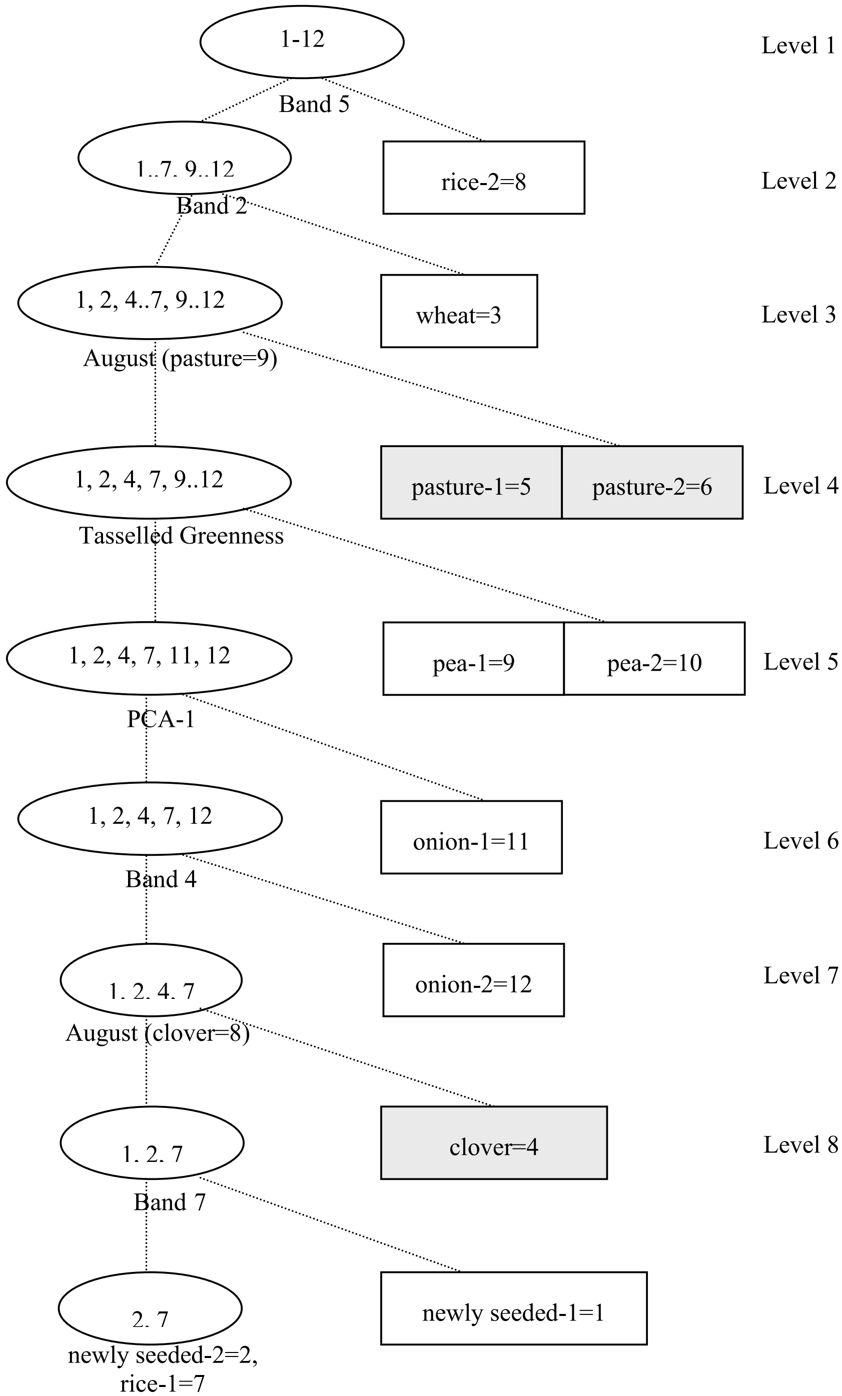

Figure 3.19 The decision tree designed for the May image

incorrectly classified pasture pixels might have been classified correctly. But, it was not possible to separate pasture-2 at this level. Therefore, at level 3 of the May decision tree, the pasture mask obtained in the August image was used to classify the pasture classes of the May image. At level 4, pea-1 and pea-2 classes were separated using Tasselled Greenness band. At level 5 and 6, onion-1 and onion-2 were separated using PCA-1 and the band 4, respectively. Although the clover class was able to be separated using the May image, the clover mask obtained in the August image was used at level 7. This is because it was observed that more clover pixels could be classified in the August image. At level 8, newly seeded-1 was separated from the class subset (2,7) using band 7. The classes newly seeded-2 and rice-1 were not able to be separated using the May image. Even though the rice mask generated in the July image was used to classify the rice-1 class in the May image, the result was observed to be unsuccessful after visually checking the associated training data.

Since these last two classes were not able to be separated in the May image any further, the process switched back to other decision trees. Although residue-1 was able to be separated at level 3 of the July decision tree using band 3, its selection as the leaf node was reevaluated. This was because it was observed that the classification of onion from the May image before the classification of residue-1 increased the classified onion pixels. Hence, at the third level of the July decision tree, the onion classes (onion-1and onion-2) of the July image were separated using the masks of the onion classes (onion-1and onion-2) in the May image. Since residue-1 was able to be separated using band 3 of the July image it was determined to be the leaf node at level 4. After level 4, the class separation was not able to be continued using the July image. On the other hand, the residue classes (residue-1 and residue-2) in the August image were able to be separated. Hence, the residue mask generated in the August image was utilized for the separation of residue at level 4 of the July decision tree. The pasture and cauliflower classes were separated using the masks of the August image at level 5 and 6, respectively. After the sixth level of the July decision tree, the classes in the image were not able to be separated any further. Then, the separation of classes was continued on the decision tree of the August image where it was left off before.

At level 5 of the August decision tree, sugar beet was not separable. It was however separable at level 1 of the July image using PCA-2 as mentioned in the previous steps. Therefore, at level 5 of the decision tree, sugar beet was separated from the class subset (1, 4, 5, 6, 8, 10..13) using the sugar beet mask produced in the July image. At level 6, two internal nodes were obtained using the PCA-2 of the August image. For each internal node of the tree, above described similar steps were carried out until the leaf nodes were reached. At level 7, the subset class (tomato-2 and uncultivated) was masked out and these two classes were separated from each other using PCA-1 of the August image. Similarly, clover was separated at level 7 from the class subset (1, 4, 6, 10, 11, 13) using PCA-3 of the August image. At level 8, since the classes in the image were not able to be classified further, the process was continued on the decision tree of the July image.

In the July decision tree, clover and uncultivated were able to be separated at level 7 and 8, respectively using the August image. At level 9, (corn-2 and rice-2) class subset was separable using the NDVI band. This class subset was further separated using band 2, at level 10. Since the other subset was not able to be separated any further the decision tree of the August image was continued from level 8.

The rice class was separated in the internal node of the August decision tree at level 8 using the rice masks (rice-1 and rice-2) of the July image. At level 9, tomato-3 was separated using Tasselled Greenness. Similarly, at level 10 watermelon and corn were separated from the subset class (tomato-1, pepper) using band 2 of the August image. At level 11, the subset class mentioned above was not able to be separated.

Therefore, from level 10 the class separation process was continued in the decision tree of the July image.

In July, watermelon at level 10 and corn-1, corn-2, and corn-3 at level 11 were separated utilizing the watermelon and corn masks of the August image. Then, band 3 was used to classify pepper-1 and band 4 was used to separate class subset (pepper-2 and tomato-3) from other class subset (tomato-1, tomato-2, and tomato-4). At level 14, pepper-2 was separated from tomato-3 using PCA-1 of the July image.

After finishing the July decision tree, finally, the class subset (tomato-1, pepper) was separated in the August decision tree using the pepper mask of the July image.

After the classification procedure was completed, for each information class, the corresponding spectral classes were merged. Figure 3.20 illustrates the classified August image performed through a decision tree classification of the multi-temporal images. The other per-pixel classified images using the decision tree classifier are given in Figure D.1 and Figure D.5 in Appendix D. In turn, the classified images were applied field-based analyses.

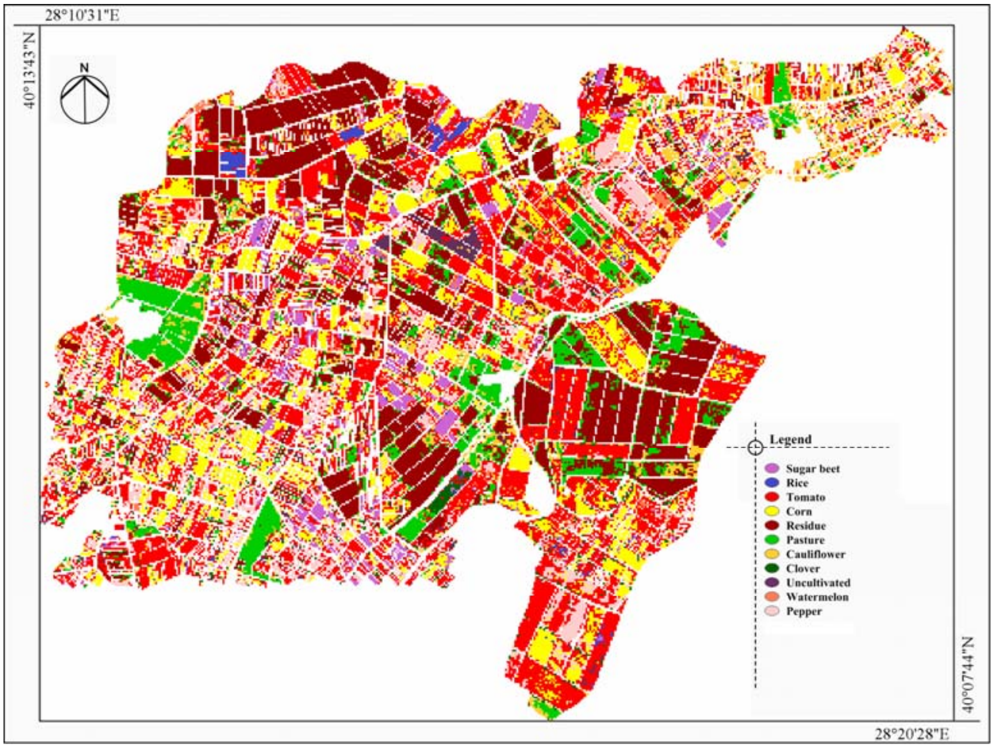

Figure 3.20 Per-pixel classified August image through decision tree classification of the multi-temporal images

3.4.3.2 MAXIMUM LIKELIHOOD CLASSIFICATION

To measure the performance of the proposed decision tree classification, the conventional maximum likelihood classification was carried out. The MLC is the most widely used per-pixel classification technique that was applied for classification of natural resource data.

The maximum likelihood classification was performed, for each date of imagery, using the ETM+ bands 1, 2, 3, 4, 5, and 7. Figure 3.21 shows the per-pixel classified August image performed through maximum likelihood classifier. As mentioned earlier, after performing the per-pixel classification for each image date, the spectral classes belonging to each information class were merged. The output of the per-pixel classified May and July images performed through maximum likelihood classifier are given in Figure D.3 and Figure D.7 in Appendix D.

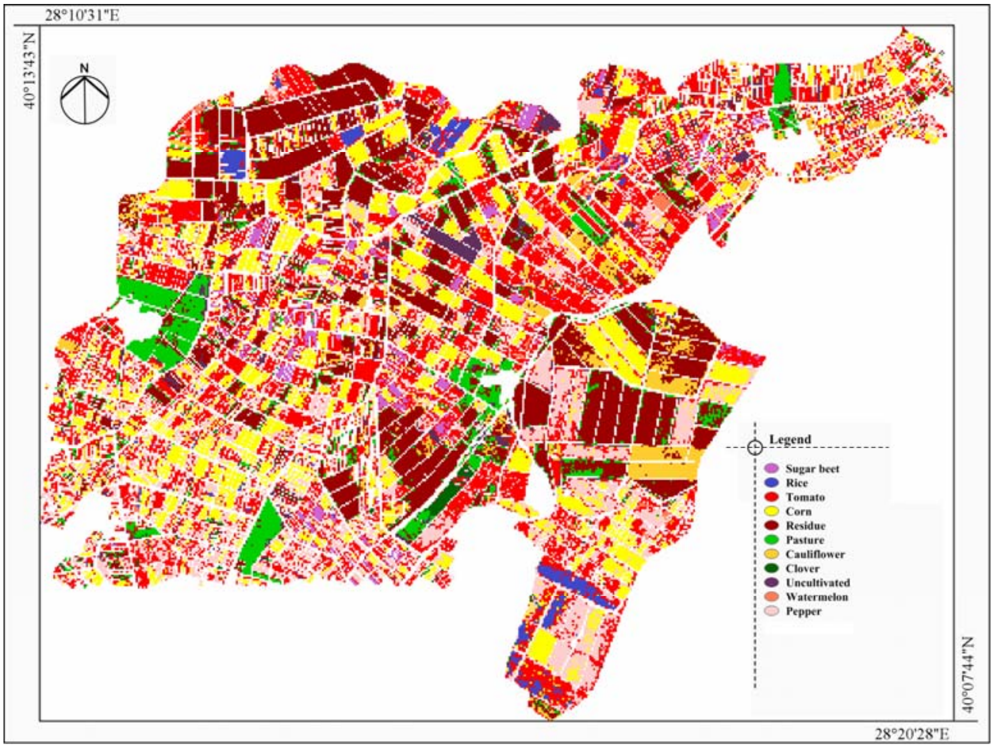

Figure 3.21 The per-pixel classified August image through maximum likelihood classification approach

3.4.4 FIELD-BASED ANALYSES

In per-pixel classification techniques, the class of a pixel is defined based on the spectral observations of the pixel. Although the per-pixel techniques are used extensively, the spectral variability of the pixels within agricultural fields may result in misclassification of the fields. To overcome such a problem, the contextual techniques have evolved which make use of the spatial context of the pixels before, during, and after classification.

The aim of a field-based analysis is to perform the classification procedure in a field-specific manner. The agricultural field boundary network integrated with remotely sensed data divides the image into spatial units which do not possess definite boundaries. The field geometry defines the contextual relationships between the image pixels. The decision by the analysis is taken, for each polygon, based on the coherent analysis of the pixels contained within. The boundary pixels can be eliminated by excluding them in the analysis of the field. Therefore, field-based classification techniques often generate less noisy and more reliable results than the per-pixel techniques.

In this study, the field-based analysis was applied to the outputs of both per-pixel decision tree and per-pixel maximum likelihood classification for each date of imagery. There were a total of 3240, 3245, and 3238 agricultural field polygons to be analyzed for the August, July, and May images, respectively. In order to represent the unclassified pixels, a new class called "unclassified" was defined.

Initially, for each field, the frequencies of classified pixels were computed using the Raster Aggregation function of SPANS GIS. The results were written to the additional columns in the GIS database. The names given to the columns were combined from the abbreviation of image date e.g. "aug", the sampling method used e.g. "hist", and the number given to the class e.g. "1" (Figure 3.22). Then, the vector layer with the appended database was imported into the SPANS environment. For each field, the number of pixels were calculated and written to a new column called "augcount". Thereafter, the percentages of the classes were calculated and appended as additional columns to the database. These columns were named with the first letter of the image date e.g. "a" and the abbreviation selected for the class e.g. "res" (Figure 3.22). Finally, the land cover class, which has the maximum percentage value, was assigned as the field's label and stored in the column called "majority". The "majority" field as well as the "aug_ref" referring to the classes in August were labeled with integer values in order to speed up the calculations. A part of the database with the appended columns for August is illustrated in Figure 3.22.

aughist1	aughist3	aughist4	aughist5	aughist6	aughist7	aughist2	aughist8	aughist9	aughis10	aughis11	augcount
0.0000000	0.0000000	0.0000000	20.0000000	0.0000000	9.0000000	0.0000000	0.0000000	10.0000000	0.0000000	1.0000000	40.00

ares	apas	aclf	asbt	aclv	atom	aunc	acorn	awmn	apep	arice	majority	aug_ref
0.00	0.00	0.00	0.50	0.00	0.23	0.00	0.00	0.25	0.00	0.03	1	1

Figure 3.22 A part of database with the appended columns for August

The per-field classification procedure can be illustrated with an example. If a field includes 50% sugar beet pixels, 23% tomato pixels, 25% classified watermelon pixels, and 3% rice pixels then, this field is assigned the label of sugar beet which has the highest percentage value (Figure 3.22). Figure 3.23 and Figure 3.24 illustrate the per-field classified August image performed through decision tree and maximum likelihood classifiers. The per-field classified July and May images are given in Appendix D.

3.4.5 THE ACCURACY ASSESSMENT

After finishing the classification procedure, the classified outputs should be assessed in order to measure their reliabilities. The classification accuracy is of great importance particularly if the classified outputs are stored in a GIS for performing further analysis operations by using the other relevant data.

There are various indices to estimate the accuracy of the classifications. These indices are mostly based on the analysis of a confusion (error) matrix, which is a square array of dimension nxn, where n is the number of classes. It represents the relationships between two sources of information that are (i) the reference test information collected through field observation, air photo interpretation, inspection of agricultural records, or other similar means and (ii) the remote-sensing-derived classification map.

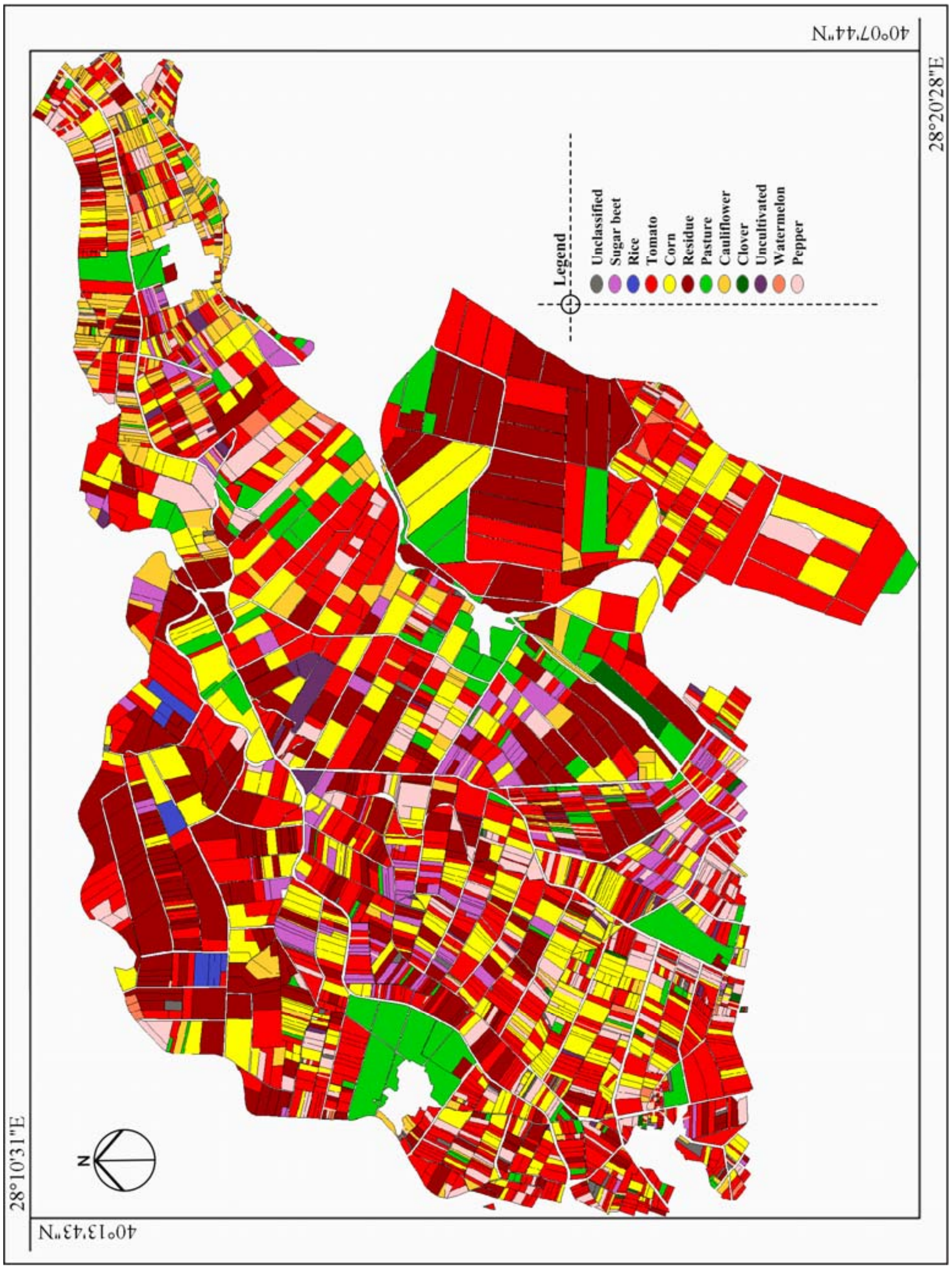

Figure 3.23 The per-field classified August image performed using the decision tree approach

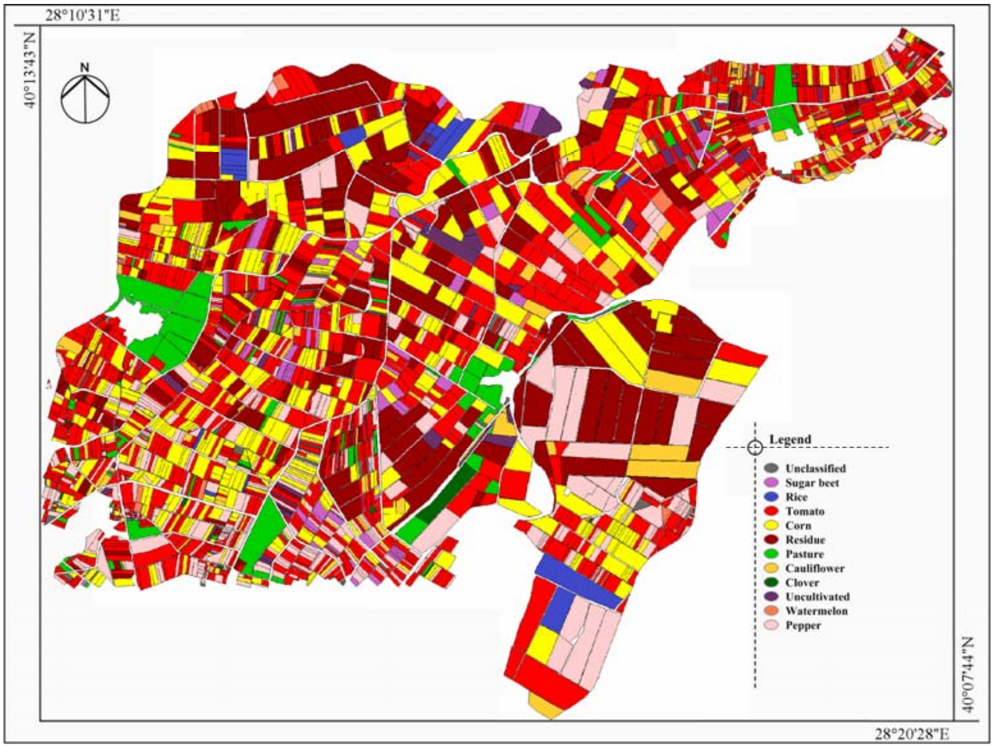

Figure 3.24 The per-field classified August image performed using the maximum likelihood classifier

In an error matrix, the columns represent the reference data, while the rows indicate the labels given by the classifier. The numbers laid out in each cell express the number of sample units (i.e., pixels, clusters of pixels, or polygons) assigned to a particular category relative to the actual category as verified in the field. In this study, the sample unit was taken as a field. Therefore, the accuracy assessment was carried out on a per-field basis.

The indices utilized to evaluate the information in error matrix can be simple descriptive statistics that are the overall, producer's, and user's accuracies. The overall accuracy is computed by dividing the sum of major diagonal entries in the matrix by the total number of samples. With this index, specific information about the accuracy of each individual class is not provided. In order to assess the accuracy of each information class individually, the producer's and user's accuracies can be used. The producer's accuracy indicates the probability of a reference pixel being correctly classified. It is calculated, for each class i in a confusion matrix, by dividing the entry (i,i) by the sum of column i. This statistic is a measure of omission error. The user's accuracy is an indicative of the proportion of classified pixels belonging to information class i that agree with the reference data. This is a measure of commission error and is obtained by dividing the entry (i,i) by the sum of row i.

In this study, approximately one third of the reference data were used for training area selection, while the rest of the reference data were utilized for the validation process. However, if a class had merely a few fields then, the training fields used to classify the images were not excluded from the accuracy assessment. For instance, the uncultivated class was represented by two fields only and therefore these two fields were utilized for both the training area selection and the accuracy assessment processes.

The results of the per-field classification belonging to August, July, and May images obtained through decision tree and maximum likelihood approaches were assessed to measure their accuracies. In order to quantify and identify the inaccuracies for the output thematic maps, the error matrices were constructed for each classified output. The error matrices and the computed statistics, i.e., the overall, producer's, and user's accuracies, are given, for each classified image, in the following chapter in Table 4.1, Table 4.2, Table 4.3, Table 4.4, Table 4.5, and Table 4.6.

As mentioned earlier, one of the aims of this study was to compare the results of the proposed decision tree classification with the results of conventional maximum likelihood classification. To make the comparison between the classification results of the two techniques, it is required that the same reference fields to be used. For each image date, in the resultant classified images obtained through decision tree and the maximum likelihood approaches, it was observed that some of the fields were not labeled due to containing equal percentage of classified pixels. Therefore, these fields containing equal percentage of classified pixels were reassessed. If a class had a similar percentage value with the other class that represents the reference test information then, this field was given the label of the reference test data. For example, if a classified field contains 50% residue and 50% pasture, then it is labeled residue since this field is known to contain residue from the reference data. On the other hand, if a classified field contains 25% residue, 38% cauliflower, and 38% uncultivated, then it is not labeled with any class, despite knowing from ground truth information that the field contains residue. Therefore, for both classifiers such fields were excluded from the test reference data.

CHAPTER 4

RESULTS AND DISCUSSION

4.1 RESULTS

4.1.1 DECISION TREE CLASSIFICATION

The producer's and user's accuracies and the overall accuracy for the decision tree classification of the August, July, and May images are provided in Table 4.1, Table 4.2, and Table 4.3. When compared the classification results of the three dates, the May image provided the highest overall accuracy (91.10 %). The overall accuracies for the July and August images were found to be 66.15% and 69.14%, respectively.

In August, the individual class accuracies ranged from 22.09% to 100% (Table 4.1). Sugar beet and rice provided 75.26% and 70.00% producer's accuracies and 82.95% and 100% user's accuracies. For tomato and corn, the producer's accuracies were computed as 72.95% and 63.49%, while the user's accuracies were computed as 64.94% and 91.43%, respectively. Residue, pasture, and cauliflower yielded 77.96%, 100%, and 65.52% producer's accuracies. The user's accuracies for these classes were 93.55%, 32.56%, and 34.55%. For clover both the producer's accuracy and the user's accuracy were 50.00%. The producer's accuracies of uncultivated and watermelon were achieved as to be 75.00% and 50.00% while the user's accuracies were computed as 37.50% and 77.78%, respectively. The pepper class exhibited the lowest producer's and user's accuracies in the classified August image that are 33.93% and 22.09%.

In July, the individiual class accuracies achieved through the decision tree approach are highly variable, ranging from 3.03% to 100% (Table 4.2). Sugar beet and rice yielded 71.57% and 70.00% producer's accuracies and 90.12% and 100% user's accuracies. For tomato and corn, the producer's accuracies were 69.52% and 57.31%, and the user's accuracies were 65.70% and 91.20%, respectively. The residue, pasture, and cauliflower provided 76.22%, 100%, and 57.69% producer's accuracies, while their user's accuracies were 91.56%, 34.15%, and 34.88%. The producer's accuracies of clover, uncultivated, and watermelon were computed as 50.00%, 60.00%, and 53.85%. The user's accuracies for these classes were computed 100%, 37.50%, and 70.00%, respectively. For pepper and onion the producer's accuracies were 50.00% and 14.29%, and the user's accuracies were 23.08% and 3.03%.

The remarkably high accuracy of the May image was due to the fact that the spectral classes were generally separable from each other (Table 4.3). In May, the cover of tomato, corn, pepper, and sugar beet was bare soil. Therefore, these classes were reduced to one class that is newly seeded. Due to its well spectral separability, newly seeded exhibited the highest producer's accuracy of 96.02% and a very good user's accuracy of 97.31%. The rice class had a producer's accuracy of 70% and a user's accuracy of 100%. The producer's and user's accuracies of wheat were computed as 84.50% and 98.83%, respectively. For pasture and pea, the producer's accuracies were obtained around 90%, and the user's accuracies were obtained around 60%. The onion class exhibited poor values for producer's and user's accuracies that are 30.00% and 16.67%, respectively. The clover class represented by only two fields and provided 50.00% producer's accuracy and 100% user's accuracy.

The error matrices and the computed statistics are shown in, for each classified output, from Table 4.1 to Table 4.6. The abbreviations used for the classes of interest and other relevant data in the tables hereafter are referred to as follows:

sgb: sugar beet, rce: rice, tom: tomato, crn: corn,
res: residue, pas: pasture, clf: cauliflower, clv: clover,
unc: uncultivated, wtm: watermelon, pep: pepper, onn: onion,
nsd: newly seeded, wht: wheat,
PA: Producer's Accuracy, UA: User's Accuracy.

Table 4.1 Error Matrix of classified data obtained with Decision Tree Classifier for August 2000

Classified Map Data	Reference Data: sgb 1	rce 2	tom 3	crn 4	res 5	pas 6	clf 7	clv 8	unc 9	wtm 10	pep 11	Total
sgb	73	0	6	7	0	0	0	1	0	0	1	88
rce	0	7	0	0	0	0	0	0	0	0	0	7
tom	21	3	213	56	4	0	4	0	1	2	24	328
crn	0	0	6	160	0	0	1	0	0	0	8	175
res	0	0	1	6	145	0	3	0	0	0	0	155
pas	0	0	2	1	26	14	0	0	0	0	0	43
clf	1	0	17	4	11	0	19	0	0	0	3	55
clv	0	0	0	0	0	0	0	1	0	0	1	2
unc	0	0	3	1	0	0	1	0	3	0	0	8
wtm	2	0	0	0	0	0	0	0	0	7	0	9
pep	0	0	44	17	0	0	1	0	0	5	19	86
Total	97	10	292	252	186	14	29	2	4	14	56	956

%	sgb	rce	tom	crn	res	pas	clf	clv	unc	wtm	pep
PA	75.26	70.00	72.95	63.49	77.96	100.00	65.52	50.00	75.00	50.00	33.93
UA	82.95	100.00	64.94	91.43	93.55	32.56	34.55	50.00	37.50	77.78	22.09

Overall Accuracy 69.14 %

Table 4.2 Error Matrix of classified data obtained with Decision Tree Classifier for July 2000

Reference Data

Classified Map Data	sgb 1	rce 2	tom 3	crn 4	res 5	pas 6	clf 7	clv 8	unc 9	wtm 10	pep 11	onn 12	Total
sgb	73	0	2	5	0	0	0	1	0	0	0	0	81
rce	0	7	0	0	0	0	0	0	0	0	0	0	7
tom	20	3	203	56	4	0	1	0	0	1	20	1	309
crn	0	0	7	145	0	0	0	0	0	0	7	0	159
res	0	0	1	6	141	0	5	0	0	0	0	1	154
pas	0	0	2	1	24	14	0	0	0	0	0	0	41
clf	0	0	13	2	10	0	15	0	0	0	0	3	43
clv	0	0	0	0	0	0	0	1	0	0	0	0	1
unc	0	0	3	1	0	0	1	0	3	0	0	0	8
wtm	3	0	0	0	0	0	0	0	0	7	0	0	10
pep	2	0	50	23	5	0	3	0	1	5	27	1	117
onn	4	0	11	14	1	0	1	0	1	0	0	1	33
Total	102	10	292	253	185	14	26	2	5	13	54	7	963

%	sgb	rce	tom	crn	res	pas	clf	clv	unc	wtm	pep	onn
PA	71.57	70.00	69.52	57.31	76.22	100.00	57.69	50.00	60.00	53.85	50.00	14.29
UA	90.12	100.00	65.70	91.20	91.56	34.15	34.88	100.00	37.50	70.00	23.08	3.03

Overall Accuracy 66.15 %

Table 4.3 Error Matrix of classified data obtained with Decision Tree Classifier for May 2000

Reference Data

Classified Map Data	rce 1	wht 2	pas 3	pea 4	onn 5	clv 6	nsd 7	Total
rce	7	0	0	0	0	0	0	7
wht	0	169	0	1	1	0	0	171
pas	0	7	11	0	0	0	0	18
pea	0	22	1	40	1	0	5	69
onn	0	1	0	1	3	0	13	18
clv	0	0	0	0	0	1	0	1
nsd	3	1	0	2	5	1	434	446
Total	10	200	12	44	10	2	452	730

%	rce	wht	pas	pea	onn	clv	nsd
PA	70.00	84.50	91.67	90.91	30.00	50.00	96.02
UA	100.00	98.83	61.11	57.97	16.67	100.00	97.31

Overall Accuracy 91.10 %

4.1.2 MAXIMUM LIKELIHOOD CLASSIFICATION

The producer's and user's accuracies and the overall accuracy for the maximum likelihood classification of the August, July, and May images are given in Table 4.4, Table 4.5, and Table 4.6. The overall accuracy for the August image was 70.82% while the accuracy for the July and May were 63.55% and 84.38%.

In August, the individual class accuracies were obtained in the range of 21.43% and 100% (Table 4.4). The producer's accuracy of sugar beet (42.27%) was nearly half of the user's accuracy that was computed as 95.35%. For rice the classification accuracies were found to be high (producer's accuracy of 90.00% and user's accuracy of 81.82%). The producer's accuracies of tomato and corn were computed as 85.62% and 68.65% while their user's accuracies were 66.49% and 90.10%, respectively. Residue, pasture, and cauliflower showed 74.19%, 100%, and 37.93% producer's accuracies. The user's accuracies for these classes were 97.87%, 41.18%, and 33.33%. For clover, both the producer's and the user's accuracies were achieved as 50.00%. The uncultivated class exhibited a relatively high producer's accuracy of 75.00% and the lowest user's accuracy of 21.43%. The watermelon and pepper classes yielded 50.00% and 53.57% producer's accuracies and 87.50% and 29.41% user's accuracies.

In July, the individual class accuracies ranged from 9.52% to 100% (Table 4.5). Sugar beet and rice showed 77.45% and 80.00% producer's accuracies and 94.05% and 100% user's accuracies. For tomato and corn, the producer's accuracies were 66.44% and 53.75%, and the user's accuracies were 68.07% and 75.56%, respectively. Residue, pasture, and cauliflower had 83.78%, 100%, and 30.77% producer's accuracies and 93.37%, 28.00%, and 25.00% user's accuracies. The producer's accuracies of clover and uncultivated were computed as 50.00% and 80.00%, respectively. While their user's accuracies were computed to be 100% and 66.67%, respectively. For watermelon, rather low classification accuracies were obtained. While the producer's accuracy of watermelon was 15.38% the user's accuracy was computed to be 9.52%. Pepper also exhibited lower classification accuracies that were 12.96% for producer's and 17.50% for user's. Onion had a higher producer's accuracy (57.14%) than the user's accuracy (11.11%).

In May, the producer's and user's accuracies for newly seeded reached 86.95% and 99.49%, respectively (Table 4.6). For rice and wheat the producer's accuracies were computed as 90.00% and 81.00% whereas the user's accuracies were computed as 31.03% and 100%. The pasture class showed a producer's accuracy of 91.67% and a user's accuracy of 57.89%. For pea both the producer's accuracy and the user's accuracy were computed to be 70.45%. The class onion showed a high producer's accuracy of 90.00%. Whereas the producer's accuracy, the user's accuracy of onion (11.25%) was quite low. For clover, the producer's and user's accuracies were computed as 50.00% and 100%, respectively.

Table 4.4 Error Matrix of classified data obtained with Maximum Likelihood Classifier for August 2000

Classified Map Data	Reference Data sgb 1	rce 2	tom 3	crn 4	res 5	pas 6	clf 7	clv 8	unc 9	wtm 10	pep 11	Total
sgb	41	0	1	0	0	0	0	0	0	1	0	43
rce	0	9	1	0	0	0	0	0	0	0	1	11
tom	51	0	250	36	8	0	11	0	1	5	14	376
crn	0	1	7	173	0	0	0	0	0	0	11	192
res	0	0	0	1	138	0	2	0	0	0	0	141
pas	0	0	0	1	17	14	2	0	0	0	0	34
clf	0	0	2	0	20	0	11	0	0	0	0	33
clv	0	0	0	1	0	0	0	1	0	0	0	2
unc	0	0	2	3	3	0	3	0	3	0	0	14
wtm	0	0	1	0	0	0	0	0	0	7	0	8
pep	5	0	28	37	0	0	0	1	0	1	30	102
Total	97	10	292	252	186	14	29	2	4	14	56	956

%	sgb	rce	tom	crn	res	pas	clf	clv	unc	wtm	pep
PA	42.27	90.00	85.62	68.65	74.19	100.00	37.93	50.00	75.00	50.00	53.57
UA	95.35	81.82	66.49	90.10	97.87	41.18	33.33	50.00	21.43	87.50	29.41

Overall Accuracy 70.82 %

Table 4.5 Error Matrix of classified data obtained with Maximum Likelihood Classifier for July 2000.

Classified Map Data	sgb 1	rce 2	tom 3	crn 4	res 5	pas 6	clf 7	clv 8	unc 9	wtm 10	pep 11	onn 12	Total
sgb	79	0	2	3	0	0	0	0	0	0	0	0	84
rce	0	8	0	0	0	0	0	0	0	0	0	0	8
tom	15	0	194	34	0	0	2	0	0	5	35	0	285
crn	1	1	25	136	3	0	5	1	0	0	8	0	180
res	0	0	1	7	155	0	3	0	0	0	0	0	166
pas	0	0	8	7	17	14	1	0	0	1	0	2	50
clf	0	0	10	9	1	0	8	0	0	2	1	1	32
clv	0	0	0	0	0	0	0	1	0	0	0	0	1
unc	1	1	27	21	2	0	0	0	4	1	3	0	60
wtm	0	0	1	18	0	0	0	0	0	2	0	0	21
pep	0	0	19	9	0	0	3	0	0	2	7	0	40
onn	6	0	5	9	7	0	4	0	1	0	0	4	36
Total	102	10	292	253	185	14	26	2	5	13	54	7	963

%	sgb	rce	tom	crn	res	pas	clf	clv	unc	wtm	pep	onn
PA	77.45	80.00	66.44	53.75	83.78	100.00	30.77	50.00	80.00	15.38	12.96	57.14
UA	94.05	100.00	68.07	75.56	93.37	28.00	25.00	100.00	66.67	9.52	17.50	11.11

Overall Accuracy 63.55 %

Table 4.6 Error Matrix of classified data obtained with Maximum Likelihood Classifier for May 2000

	Reference Data							
Classified Map Data	rce 1	wht 2	pas 3	pea 4	onn 5	clv 6	nsd 7	Total
rce	9	0	0	0	0	0	20	29
wht	0	162	0	0	0	0	0	162
pas	0	0	11	5	0	1	2	19
pea	0	9	1	31	0	0	3	44
onn	0	29	0	8	9	0	34	80
clv	0	0	0	0	0	1	0	1
nsd	1	0	0	0	1	0	393	395
Total	10	200	12	44	10	2	452	730

%	rce	wht	pas	pea	onn	clv	nsd
PA	90.00	81.00	91.67	70.45	90.00	50.00	86.95
UA	31.03	100.00	57.89	70.45	11.25	100.00	99.49

Overall Accuracy 84.38 %

4.1.3 COMPARISON OF THE RESULTS OF THE TWO CLASSIFICATION PROCEDURES

In May and July, the decision tree classifier produced higher overall classification accuracies that were 91.10% and 66.15 % than did the maximum likelihood classifier which were computed as 84.38% and 63.55%, respectively. In August, nearly similar overall accuracies were observed using the maximum likelihood and the decision tree approaches that were found to be 70.82% and 69.14%, respectively.

In May, the classes wheat, pea, and newly seeded provided higher producer's accuracies using the decision tree classifier than using the maximum likelihood classifier. Conversly, these classes showed higher user's accuracies using the maximum likelihood than using the decision tree classifier. For rice and onion, higher producer's accuracies were obtained using the maximum likelihood approach and higher user's accuracies were reached using the decision tree classifier. The producer's accuracy of pasture showed the same result using both classifiers. However, for this class, the user's accuracy was better using the decision tree classifier. For clover, both classifiers yielded the same producer's (50%) and the same user's (100%) accuracies.

In July, for cauliflower, watermelon, and pepper, much better producer's and user's accuracies were obtained using the decision tree classifier. For corn, the producer's and user's accuracies exhibited 3.56% and 15.64% higher values respectively using the decision tree approach. On the other hand, the producer's and user's accuracies of sugar beet, residue, uncultivated, and onion were found to be better using the maximum likelihood classifier than the decision tree approach. For rice, higher producer's accuracy was computed using the maximum likelihood classifier whereas the user's accuracy for this class was the same for both classifiers. Tomato had higher producer's accuracy using the decision tree approach and a higher user's accuracy using the maximum likelihood approach. The pasture class yielded the same producer's accuracy using the maximum likelihood and the decision tree classifiers whereas higher user’s accuracy was obtained using the decision tree approach. Clover exhibited the same producer’s (50%) and the same user’s (100%) accuracies for both classification approaches.

In August, cauliflower showed higher producer’s and user’s accuraciers using the decision tree approach. However, the producer’s and user’s accuracies of tomato and pepper were relatively higher using the maximum likelihood approach than using the decision tree classifier. Sugar beet and residue exhibited higher producer’s accuracies using the decision tree approach and higher user’s accuracies obtained through the maximum likelihood procedure. On the contrary, rice and corn produced higher producer’s accuracies using the maximum likelihood approach and higher user’s accuracies using the decision tree approach. For pasture and watermelon, the same producer’s accuracies, 100% and 50%, respectively were found using both classifiers. However, for these classes, the user’s accuracy were higher using the maximum likelihood than using the decision tree classifier. Clover had the same producer’s (50%) and the same user’s (50%) accuracies using both approaches. The uncultivated class also showed the same producer’s accuracy (75%) using both classifiers. However, for this class, the user’s accuracy was higher using the decision tree approach than using the maximum likelihood classifier.

4.2 DISCUSSION

It was observed that the use of additional bands of NDVI, PCA, and Tasselled Cap Transformations made the classification more effective for several classes. In the May image, PCA-1 was used for separating the class onion-1 whereas Tasselled Greenness was utilized for separating the classes pea-1 and pea-2. In the July image, PCA-1 was used for separating the classes pepper-2 and tomato-3, PCA-2 was used for separating the class sugar beet, and NDVI was used for separating the sub-class (corn-2 & rice-2). In the August image, the subclass (tomato-2 & uncultivated) was separated by PCA-2, the classes tomato-2 and uncultivated were separated by PCA-1, clover by PCA-3, and tomato-3 by Tasselled Greenness.

The Tasselled Greenness function is computed using a visible/near infrared contrast with very little contributions from bands 5 and 7 (Mather, 1989) whereas NDVI is calculated by dividing the differences of near infrared and red bands by the sum of these bands. Several research studies stated that many vegetation indices are not noticeably different and hence, when at least two of them are applied to the same dataset redundant information may be obtained (Jensen, 1996). This case was experienced in this study as can be deduced from the co-spectral plots of the NDVI and Tasselled Greenness bands (Figure C.1, Figure C.2, and Figure C.3). Figure 4.1, Figure 4.2, and Figure 4.3 depict the mean Tasselled Greenness and NDVI profiles for each class in the August, July, and May images, respectively. It can be noticed from these figures that some of the classes represent similar spectral reflectance characteristics for both bands. Thus, it can be said that these bands contain a certain level of duplication. However, it should be noted that although some similarity was observed between these two bands, a valuable information was obtained by using both for the analyses. For example, “pea-1” was able to be separated using NDVI band of the May image. However, “pea-2” and “pea-1” were able to be separated using the Tasselled Greenness band.

When classifying the images the masking procedure was used. During the masking procedure, the classified pixels were excluded from the proceeding classification process. Thus, a pixel once labeled with a class was not labeled again with a possible overlapping class down the hierarchy of the decision tree. The use of masking technique in the decision tree classification showed that the per-pixel classification sequences of the classes in the decision tree classifier affect the classification accuracy.

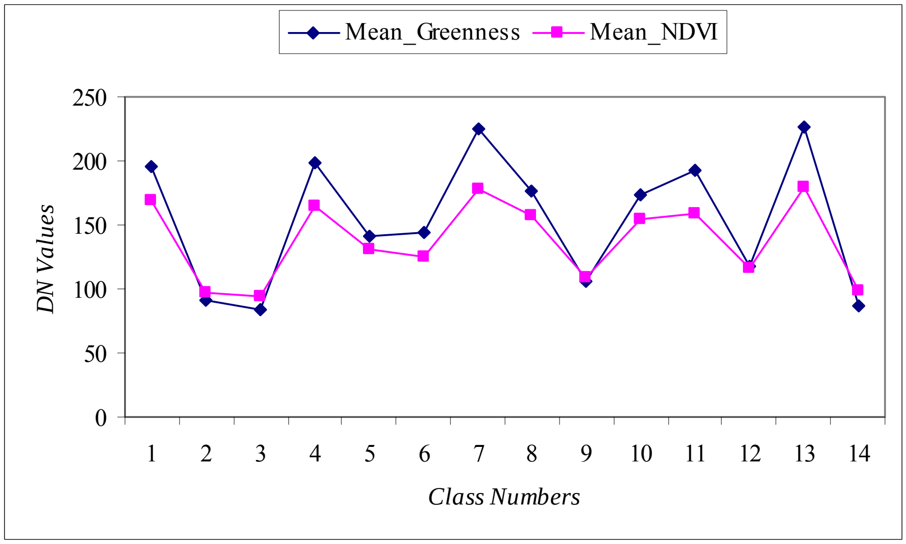

Figure 4.1 Mean Greenness and NDVI profile for each class in the August image

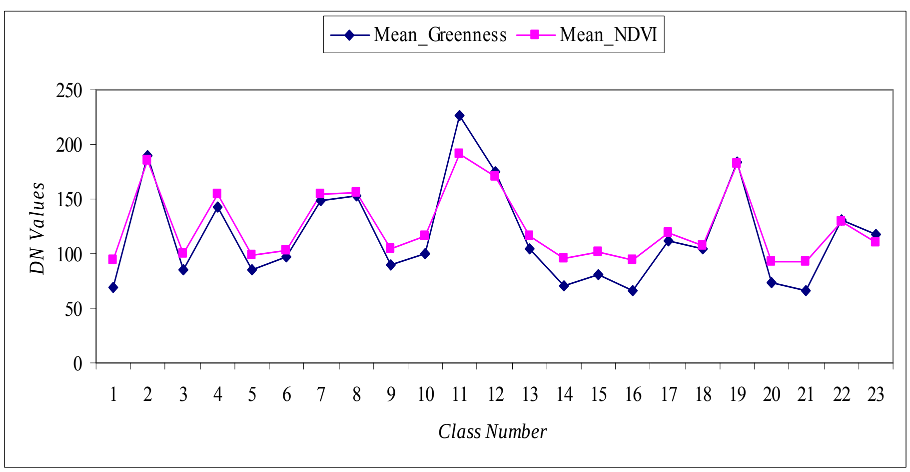

Figure 4.2 Mean Greenness and NDVI profile for each class in the July image

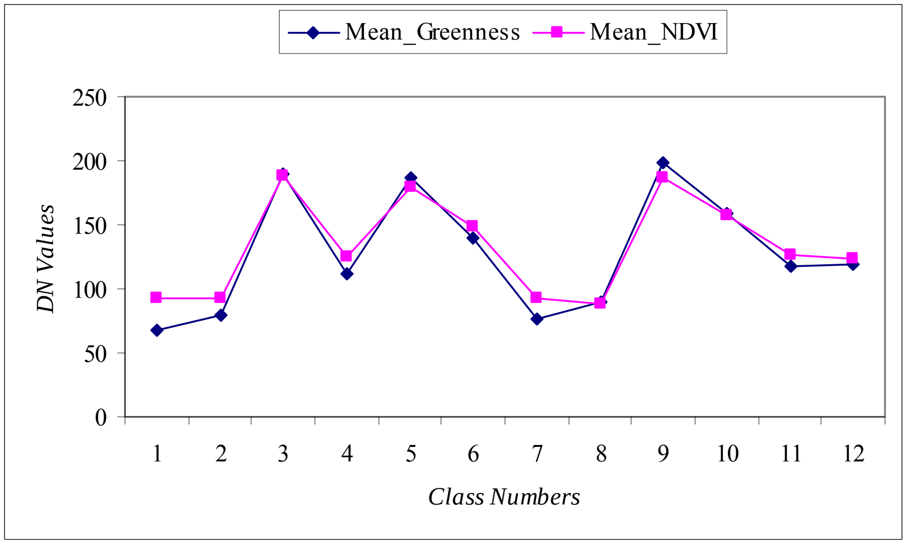

Figure 4.3 Mean Greenness and NDVI profile for each class in the May image

The classified output of a class obtained through one date of image (source) was used in classifying the same class in the other image (destination) whenever the relevant decision tree depicted as such. When the pixels that were classified in the source image did not exist in the destination image due to difference in the geometric corrections of two images, the classification accuracy of the destination image was affected negatively.

In general, it was observed that the per-pixel classification sequences of the classes in the decision tree classifier and the difference in the geometric corrections of the source and destination images highly affected the accuracy of, in particular, small sized fields negatively. An example for such small sized fields would be given from pepper fields. Half of the small sized pepper fields were correctly classified by the decision tree classifier in the July image (Table 4.2). However, although the same classified output of the pepper class was used in the August image, one third of the correctly classified fields in the July image were observed to be incorrectly classified in the August image (Table 4.1). For instance, field #28341, which is known to contain pepper on the ground, was correctly classified in the July image as it contains 19% clover, 29% tomato, and 52% pepper (Figure 4.4 (a)). However, the same field was incorrectly classified as tomato in the August image because it contains 24% clover, 43% tomato, and 33% pepper (Figure 4.4 (b)). The reason behind this is that due to the effect of geometric correction several correctly classified July pepper pixels were not included in the August image. Therefore, the decision for this field was not taken in the August imagery using the same pixels as in the July image.

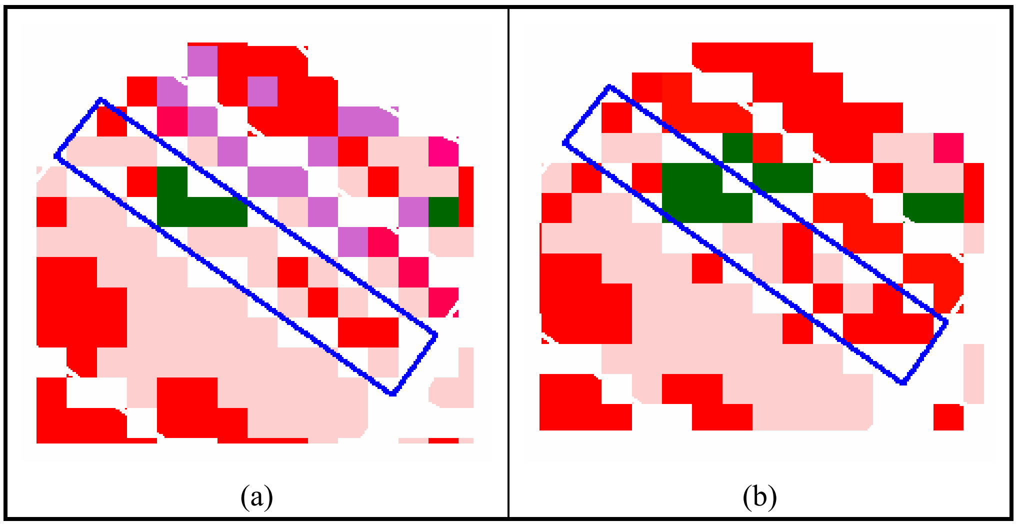

Figure 4.4 An image showing the pepper field in July and August

As another example, field #27960, which is known to contain pepper on the ground, was correctly classified in the July image as it contains 88% pepper and 13% tomato (Figure 4.5 (a)). However, the same field was incorrectly classified as tomato in the August image since it contains 88% tomato and 11% watermelon (Figure 4.5 (b)). This is because the pixels in the August image that correspond to the pixels correctly classified as pepper in the July image were already labeled with other classes and masked out in the previous classification stages. Hence, due to the decision of the tree design this unavoidable per-pixel classification sequence of pepper class in the classifier of the August image affected the classification accuracy.

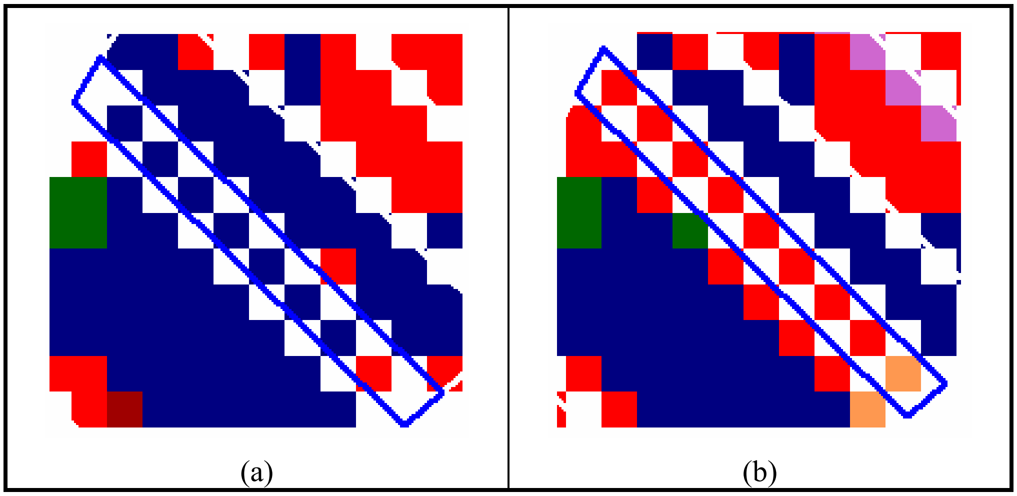

Figure 4.5 An image showing the pepper field in July and August

It is expected that better individiual class accuracies can be achieved using per-field multi-temporal classification results obtained by either decision tree or maximum likelihood classifiers. For example, if the field-based classified image for pepper class in the July image was used in the August image then, the producer's accuracy of pepper would increase by an amount of 16.07% in the August image classification. This means that instead of 33.93%, 50% of pepper fields on the ground would be correctly classified as pepper in the August image (Table 4.2 and Table 4.1). Besides, if the per-field maximum likelihood classified image for pepper class obtained in the August image is used then, the producer's accuracy of pepper becomes 53.57% (Table 4.4 and Table 4.1).

Similarly, field #18360, which is known to be pasture on the ground can be correctly classified in the May image using the per-field classified output obtained for this class in the August image. This class was classified in the May image using the per-pixel classified output for pasture class in the August image.

Figure 4.6 depicts this field. The field contains 42% pasture, 39% cauliflower, 6% clover, 9% tomato, 3% uncultivated, and 1% pepper. It was therefore, correctly classified as pasture in the August image (Figure 4.6 (a)). However, the same field including 41% pasture and 59% pea was incorrectly classified as pea in the May image (Figure 4.6 (b)).

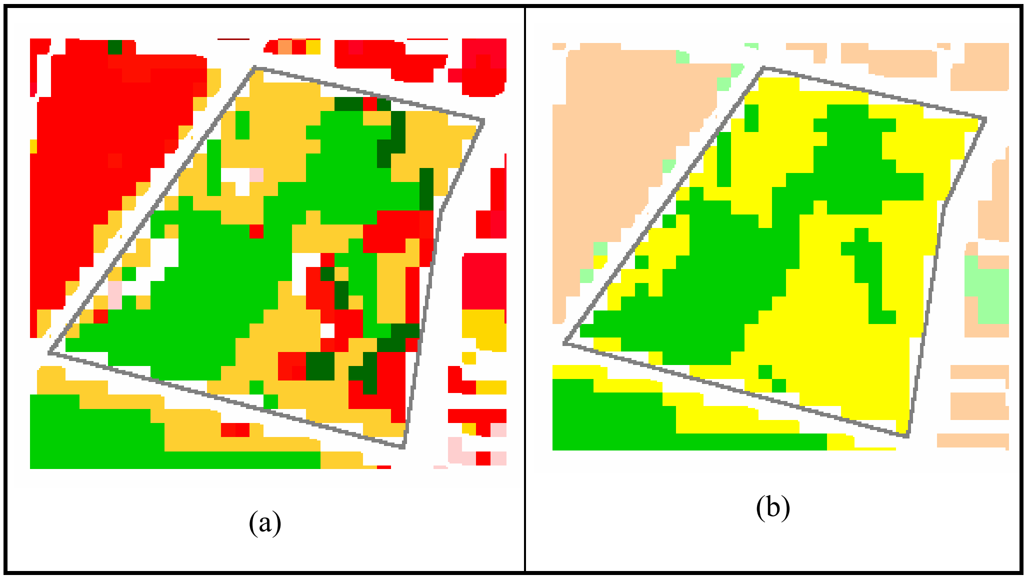

Figure 4.6 An image showing the pasture field in August and May

In the May image, newly seeded-2 and rice-1 were not separated from each other using the decision tree classifier. Therefore, it was not a surprise that three of ten rice fields were incorrectly classified as newly seeded using the decision tree classifier (Table 4.3). However, two of these fields were correctly classified using the maximum likelihood classifier as it took into account the probability function to assign the pixels a class label instead of using the strict boundaries of the decision tree classifier (Table 4.6).

Several newly seeded fields were incorrectly classified as rice using the maximum likelihood classifier while no newly seeded fields were classified as rice by the decision tree. This was also due to the same reason that the two rice fields were classified correctly using the maximum likelihood approach. For newly seeded class, the decision tree classification gave 9.07% better producer's accuracy when compared to the maximum likelihood classification (Table 4.3 and Table 4.6).

The class pea was succesfully discriminated using the Tasselled Cap Greenness band in the decision tree classification providing 90.91% producer's accuracy (Table 4.3) whereas the same class was correctly classified using the maximum likelihood approach with 70.45% producer's accuracy (Table 4.6).

Wheat also gave much better classification result using the decision tree (producer's accuracy 84.50%) (Table 4.3). However, when compared to the maximum likelihood classification almost twice number of wheat fields were incorrectly classified as pea by decision tree classifier. The confusion between these two classes was attributed to the classification improvement process used for the wheat class. That is the classified residue pixels obtained from the August image was used as the mask and transferred onto the May image. When the error matrix of August image was examined, several residue fields were observed to be incorrectly classified as cauliflower. In addition, it is known from the farmer cropping traditions in the study area that cauliflower is planted in place of several crop types, one of which is pea. Hence, it was concluded that at the expense of the improvement of the wheat class accuracy, the mask of the residue pixels, which were incorrectly classified as cauliflower, was also transferred onto the fields that were known to contain pea in the May image.

Among the May land cover classes, onion displayed the lowest classification accuracy in the decision tree classifier (producer's accuracy 30.00% and user's accuracy 16.67%) (Table 4.3). This was attributed to the heterogeneity observed in most of the fields and having several small sized fields. The reasons behind the heterogeneity might have been the plantation of onion at different times in the same field, the farming traditions of onion growing and harvesting within the field such as leaving some for seed and harvesting only some for marketing needs and/or the growing conditions such as irrigation. Through the maximum likelihood approach only one onion field was incorrectly classified. However, compared to the decision tree classifier, several wheat, pea, and newly seeded fields were classified as onion using the maximum likelihood classifier (Table 4.6). In the May image, the pasture and clover classes were classified using the masks obtained from the August image for these classes.

In July, several crop types (eight of twelve) were classified using the other date images. Therefore, the inaccuracies of these classes in the source images affected the overall and the individual classification accuracies of the classes. Onion, residue, pasture, cauliflower, clover, uncultivated, watermelon, and corn were the classes discriminated using the May and August images (Figure 3.18). As illustrated with the pepper class, the sequence of class separation through decision tree procedure and the drawback encountered while utilizing the classified images as the masks from the other images also affected the accuracies. This drawback is the loss of pixels within the fields due to the difference in the geometric corrections of images and the geometric distortion occurred during the rasterization of vector boundaries for the masks.

The greatest amount of confusion observed between tomato and pepper, corn and pepper, and corn and tomato using the decision tree approach in comparison to the maximum likelihood classification (Table 4.2 and Table 4.5). On the other hand, the number of correctly classified tomato, corn, and pepper fields is respectively higher when compared to the maximum likelihood approach. The confusion between tomato and corn might be partially because of the applied classification improvement process. Another reason was attributed to the fact that pepper, several tomato and corn fields are small sized fields that include a large number of mixed pixels causing misclassification of these fields. Besides, it is important to note that for tomato, corn, and pepper there were additional spectral classes for which no representative training samples were able to be gathered due to the insufficient field representation for these classes. On the other hand, some spectral classes of corn displayed heterogeneity. Sugar beet also displayed the greatest amount of confusion with tomato (Table 4.2). This is another class that has several small sized fields.

In the decision tree classification of the August image, sugar beet, rice, and pepper were classified using the classified output of the July image corresponding to these classes. Tomato and corn exhibited a confusion with most of the other crop classes except rice, clover, and watermelon. These two classes were particularly highly confused with pepper. On the other hand, a number of corn fields were incorrectly classified as tomato. The reasons discussed for tomato, corn, and pepper in the classification of the July image also apply for this case. In August, some spectral classes of tomato and corn displayed heterogeneity. This was attributed to the partly harvesting of these crops within the field.

In general, it was seen that nearly the similar overall accuracies were obtained for the maximum likelihood (70.82 %) and decision tree (69.14 %) approaches in August. The classification accuracy for sugar beet and cauliflower classes in August using DT were 56% and 58% higher respectively than using MLC. This suggests that the decision tree classifier for August produced better discrimination features for these classes. In particular, it should be stressed that sugar beet in August was separated using the sugar beet mask obtained from the July image. However, since sugar beet and cauliflower classes only covered a small portion of the fields, these high accuracies were remained ineffective. Although the aim of the study was to discriminate the August crop types, it was observed from the by-products of the applied process that the proposed method gave higher classification accuracy for the July and May images instead of the August image in comparison with the conventional MLC. Since the performance of the decision tree classification is highly affected by the tree structure and the choice of feature subsets (Tso and Mather, 2001) the classification results for July and May images are promising for decision tree classification of multi-temporal images for field-based crop mapping in the calculation of the overall accuracy.

The accuracy results for the July image, in particular, suggest that even with relatively large number of highly overlapping spectral classes and manual construction of the decision tree if a discriminant feature can be obtained from other images the decision tree classification might well outperform the conventional MLC. The accuracy results for the May image demonstrate that the decision tree with a relatively low number of classes and less heterogeneity gives higher accuracy results as well as less confusion among classes than MLC. The comparison of the classification results for the August image suggests that only a few of the spectral classes could be separated using other date images whereas there were a number of spectral classes highly contributing to the accuracy by occupying a larger area that could be utilized from the discriminant features of another image.

In the overall, it is believed that aside from the inherent mapping inaccuracies and the lack of detailed knowledge about the study area, the use of decision trees with well-distinguished features for classes in multi-temporal images give satisfactory classification results.

CHAPTER 5

CONCLUSIONS AND RECOMMENDATIONS

5.1 CONCLUSIONS

The conclusions drawn from the study are as follows:

- Using only one date of imagery (August), the sugar beet, rice, and pepper classes were not able to be discriminated using the decision tree classifier approach. However, with the use of multi-temporal masking technique together with the decision tree approach, these classes were discriminated succesfully.
- The use of NDVI, PCA, and Tasselled Cap Transformations made the classification more effective for several classes.
- By utilizing a per-field analysis approach, it was easy to deal with the misclassification problem which is the result of internal spectral variability within the fields.
- For the May image, the overall classification accuracies of the decision tree approach was found to be higher than the maximum likelihood approach. While the overall classification accuracy of the decision tree was computed as 91.10%, the maximum likelihood approach provided an accuracy of 84.38%.
- Similarly, the overall classification accuracy of the July image using the decision tree approach was found to be higher than the maximum likelihood classifier. The accuracies for the decision tree and the maximum likelihood approaches were computed to be 66.15 % and 63.55%, respectively.

- For the August image, unlike the May and July images, the overall accuracies of the decision tree approach (70.82%) and the maximum likelihood approach (69.14%) were nearly the same.
- The developed classification methodology gave much better overall accuracy for the May image where the number of determined classes are less in comparison to the other dates.
- Though significant spectral overlaps were observed in the July co-spectral plots when compared to either May or August, the proposed multi-temporal decision tree method was successful to classify the July image providing higher classification accuracy than the traditional MLC approach.
- In general, the differences in geometric correction during the registration process of the images and inaccuracies caused by the rasterization of vector boundaries for the masks, the small sized and irregular shaped fields, the fields displaying phenological variations for the same crop type and the selection of features during the decision tree design affected the individual class accuracies.
- It was concluded that individiual class accuracies can be improved by using per-field multi-temporal classification results obtained with either decision tree or maximum likelihood classifiers.
- It took a considerable amount of time to design a decision tree and perform the separation of the classes using the decision tree classifier of the multi-temporal images. This was particularly valid for the July and August images for which the number of classes is considerably higher than the May image. Hence, the manual design process is not suitable for decision tree classification and it may also lead inaccurate results if there are features in the data that could not be distinguishable by human capabilities.

5.2 RECOMMENDATIONS

For further studies, the followings are recommended:

- Objective decisions should be made for the number and timing of the images by analyzing the annual NDVI profiles. In this way, sufficient and suitable image data can be selected by taking into account the spectral characteristics of the classes of interest.
- Collection of more detailed and realistic ground truth data during each satellite overpass makes the interpretation of spectral classes more reliable. For example, information about sowing and harvesting time, irrigation, soil condition, signs of evolution or degradation of the vegetation (Miguel-Ayanz, J. S., 1997), differences in productivity, crop varieties used, duration of vegetative, reproductive and maturity periods (Granados-Ramirez, R., 2004).
- Instead of visual observations, the band or combinations of bands should be selected by using a statistical method that achieve the best discrimination of the class subsets. This process will be resulted in the separation of the class subsets more accurately as well as the decreased computation time for the analyses when compared to visual inspection of the optimum bands.
- In the decision tree, different classification algorithms should be utilized to discriminate some class subsets. Using such an approach, which is called "hybrid decision tree classifier", the class subsets or a data set (or both) can be more accurately classified (Friedl and Brodley, 2001).
- The sub-pixel scale classification for subsequent per-field classification approach (Aplin and Atkinson, 2001) can be used to cope with the classification problems particularly encountered with the small sized fields. Even, the use of fine spatial resolution images (e.g. the IKONOS multispectral sensor with the 4 m spatial resolution) can improve the

classification accuracy of small sized fields. In particularly, using this approach can be useful for fields that include pixels in the form of a straight line such as pepper fields in the study area.

- Prior probabilities should be incorporated into the analyses in order to improve the classification accuracy of inseparable classes.
- To increase the amount of interclass variation in small sized fields, high resolution images (higher than 15 m.) should be used.
- Automated signature extraction and classification procedures should be used to decrease the time spent for the analyses.

REFERENCES

1. Aplin, P., P. M. Atkinson, and P. J. Curran, 1999. Fine Spatial Resolution Simulated Satellite Sensor Imagery for Land Cover Mapping in the United Kingdom, *Remote Sensing of the Environmen*t, 68:206-216.

2. Aplin, P., and P. M. Atkinson, 2001. Sub-pixel Land Cover Mapping for Per-field Classification, *International Journal of Remote Sensing*, Vol.22, No.14, 2853-2858.

3. Archibald, P. D., 1987. GIS and Remote Sensing Data Integration, *Geocarto International*, Vol.3, 67-73.

4. Arıkan, M., 2003. A Multi-Temporal Masking Classification Method For Field-Based Agricultural Crop Mapping, Unpublished M.Sc. Thesis in Geodesy and Geographic Information Technologies, Middle East Technical University, Ankara, Turkey.

5. Aronoff, S., 1995. Geographic Information Systems: A Management Perspective, WDL Publications, Ottawa, Canada.

6. Bailey, K. D., R. C. Frohn, R. A. Beck, and M. W. Price, 2001. Remote Sensing Analysis of Wild Rice Production Using Landsat 7 for the Leech Lake Band of Chippewa in Minnesota, *Photogrammetric Engineering & Remote Sensin*g, 67(2):189-192.

7. Beltrán, C. M., and A. C. Belmonte, 2001. Irrigated Crop Area Estimation Using Landsat TM Imagery in La Mancha, Spain, *Photogrammetric Engineering & Remote Sensin*g, 67(10):1177-1184.

8. Bruzzone, L., and S.B. Serpico, 2000. A Technique for Feature Selection in Multiclass Problems, *International Journal of Remote Sensing*, Vol.21, No.3, 549-563.

9. Congalton, R. G., M. Balogh, C. Bell, K. Green, J. A. Milliken, and R. Ottman, 1998. Mapping and Monitoring Agricultural Crops and Other Land Cover in the Lower Colorado River Basin, *Photogrammetric Engineering & Remote Sensin*g, 64(11):1107-1113.

10. Chalifoux, S., F. Cavayas, and J. T. Gray, 1998. Map-Guided Approach for the Automatic Detection on Landsat TM Images of Forest Stands Damaged by the Spruce Budworm, *Photogrammetric Engineering & Remote Sensin*g, 64(6):629-635.

11. Chan, J. C.-W., K.-P. Chan, and A. G.-O. Yeh, 2001. Detecting the Nature of Change in an Urban Environment: A Comparison of Machine Learning Algorithms, *Photogrammetric Engineering & Remote Sensing*, 67(2):213-225.

12. Chavez, P. S. Jr., and A. Y. Kwarteng, 1989. Extracting Spectral Contrast in Landsat Thematic Mapper Image Data Using Selective Principal Component Analysis, *Photogrammetric Engineering & Remote Sensing*, 55(3):339-348.

13. Ehlers, M., G. Edwards, and Y. Bedard, 1989. Integration of Remote Sensing with Geographic Information Systems: A Necessary Evolution, *Photogrammetric Engineering & Remote Sensing*, 55(11):1619-1627.

14. Ehlers, M., D. Greenlee, T. Smith, and J. Star, 1991. Integration of Remote Sensing and GIS: Data and Data Access, *Photogrammetric Engineering & Remote Sensing*, 57(6):669-675.

15. Friedl, M. A., and C. E. Brodley, 1997. Decision Tree Classification of Land Cover from Remotely Sensed Data, *Remote Sensing of Environment,* 61:399-409.

16. Granados-Ramirez, R., T. Reyna-Trujillo, G. Gomez-Rodriguez, and J. Soria-Ruiz, 2004. Analysis of NOAA-AVHRR-NDVI Images for Crops Monitoring, *International Journal of Remote Sensing*, Vol.25, No.9, 1615-1627.

17. Guerschman, J. P., J. M. Paruelo, C. D. Bella, M. C. Giallorenz, and F. Pacin, 2003. Land Cover Classification in the Argentine Pampas Using Multi-temporal Landsat TM Data, *International Journal of Remote Sensing*, Vol.24, No.17, 3381-3402.

18. Huang, C., B. Wylie, L.Yang, C. Homer, and G. Zylstra, 2002. Derivation of a Tasselled Cap Transformation Based on Landsat 7 at-satellite reflectance, *International Journal of Remote Sensing*, Vol.23, No.8, 1741-1748.

19. Hutchinson, C. F., 1982. Techniques for Combining Landsat and Ancillary Data for Digital Classification Improvement, *Photogrammetric Engineering & Remote Sensing*, 48(1):123-130.

20. Janssen, L. L. F., J. D. van Amsterdam, 1991. An Object Based Approach to the Classification of Remotely Sensed Images, *Proceedings International Geoscience and Remote Sensing Symposium*, 4:2191-2195.

21. Jensen, J. R., 1996, Introductory Digital Image Processing, 2nd edition, Prentice Hall Inc., U.S.A.

22. Lanjeri, S., J. Meliá, and D. Segarra, 2001. A Multitemporal Masking Classification Method for Vineyard Monitoring in Central Spain, *International Journal of Remote Sensing*, Vol.22, No.16, 3167-3186.

23. Lauver, C. L., and J. L. Whistler, 1993. A Hierarchical Classification of Landsat TM Imagery to Identify Natural Grassland Areas and Rare Species Habitat, *Photogrammetric Engineering & Remote Sensing*, 59(5):627-634.

24. Lawrence, R. L., and A. Wright, 2001. Rule-Based Classification Systems Using Classification and Regression Tree (CART) Analysis, *Photogrammetric Engineering & Remote Sensing*, 67(10):1137-1142.

25. Lillesand, M., and R. W. Kiefer, 1994. Remote Sensing & Image Interpretation, 3rd edition, John Wiley & Sons, Inc., U.S.A.

26. Ma, Z., M. M. Hart, and R. L. Redmond, 2001. Mapping Vegetation Across Large Geographic Areas: Integration of Remote Sensing and GIS to Classify Multisource Data, *Photogrammetric Engineering & Remote Sensin*g, 67(3):295-307.

27. Mather, P. M., 1989. Computer Processing of Remotely-Sensed Images: An Introduction, John Wiley & Sons, Great Britain.

28. McCauley, S., and S. J. Goetz, 2004. Mapping Residential Density Patterns Using Multi-temporal Landsat Data and a Decision-tree Classifier, *International Journal of Remote Sensing*, Vol. 25, No.6, 1077-1094.

29. McIver, D. K., and M. A. Friedl, 2002. Using Prior Probabilities in Decision-tree Classification of Remotely Sensed Data, *Remote Sensing of Environment,* 81:253-261.

30. Miguel-Ayanz, J. S., and G. S. Biging, 1997. Comparison of Single-Stage and Multi-Stage Classification Approaches for Cover Type Mapping with TM and SPOT Data, *Remote Sensing of Environment,* 59:92-104.

31. Murakami, T., S. Ogawa, N. Ishitsuka, K. Kumagai, and G. Saito, 2001. Crop Discrimination with Multitemporal SPOT/HRV Data in the Saga Plains, Japan, *International Journal of Remote Sensing*, Vol. 22, No.7, 1335-1348.

32. Oetter, D. R., W. B. Cohen, M. Berterretche, T. K. Maiersperger, and R. E. Kennedy, 2000. Land Cover Mapping in an Agricultural Setting Using Multiseasonal Thematic Mapper Data, *Remote Sensing of Environment,* 76:139-155.

33. Özen, H., 2000. Per Field Image Classification for Agricultural Lands in the Integration of Remote Sensing and GIS, Unpublished M.Sc. Thesis in Geodesy and Geographic Information Technologies, Middle East Technical University, Ankara, Turkey.

34. PCI Geomatica, 1997, ImageWorks manual, Canada.

35. Ricotta, C., G. C. Avena, and F. Volpe, 1999. The Influence of Principal Component Analysis on the Spatial Structure of a Multispectral Dataset, *International Journal of Remote Sensing*, Vol. 20, No.17, 3367-3376.

36. Schriever, J. R., and R. G. Congalton, 1995. Evaluating Seasonal Variability as an Aid to Cover-Type Mapping from Landsat Thematic Mapper Data in the Northeast, *Photogrammetric Engineering & Remote Sensing*, 61(3):321-327.

37. Seong, J. C., and E. L. Usery, 2001. Fuzzy Image Classification for Continental-Scale Multitemporal NDVI Series Images Using Invariant Pixels and an Image Stratification Method, *Photogrammetric Engineering & Remote Sensing*, 67(3):287-294.

38. Todd, S. W., and R. M. Hoffer, 1998. Responses of Spectral Indices to Variations in Vegetation Cover and Soil Background, *Photogrammetric Engineering & Remote Sensing*, 64(9):915-921.

39. Tso, B., and P. M. Mather, 2001. Classification Methods for Remotely Sensed Data, Taylor & Francis, London.

40. Walsh, S. J., J. W. Cooper, I. E. V. Essen, and K. R. Gallager, 1990. Image Enhancement of Landsat Thematic Mapper Data and GIS Data Integration for Evaluation of Resource Characteristics, *Photogrammetric Engineering & Remote Sensing*, 56(8):1135-1141.

41. Wayman, J. P., R. H. Wynne, J. A. Scrivani, and G. A. Reams, 2001. Landsat TM-Based Forest Area Estimation Using Iterative Guided Spectral Class Rejection, *Photogrammetric Engineering & Remote Sensing*, 67(10):1155-1166.

42. White, J. D., G. C. Kroh, and J. E. Pinder III, 1995. Forest Mapping at Lassen Volcanic National Park, California, Using Landsat TM Data and a Geographical Information System, *Photogrammetric Engineering & Remote Sensing*, 61(3):299-305.

43. Wolter, P. T., D. J. Miadenoff, G. E. Host, and T. R. Crow, 1995. Improved Forest Classification in the Northern Lake States Using Multi-Temporal Landsat Imagery, *Photogrammetric Engineering & Remote Sensing*, 61(9):1129-1143.

44. Landsat 7 Science Data Users Handbook, http://ltpwww.gsfc.nasa.gov/IAS/handbook/handbook_htmls/chapter11, 25/7/2003.

45. Chesapeake Bay & Mid-Atlantic from Space, Digital Image Processing, http://chesapeake.towson.edu/data/ndvi.asp, 1/7/2003.

46. Canada Centre for Remote Sensing (CCRS), Fundamentals of Remote Sensing, http://www.ccrs.nrcan.gc.ca, 29/9/2003.

47. University of Idaho, Remote Sensing Lecture Notes, http://www.cnr.uidaho.edu/remotesensing/rs_courses/for472/lectures/process2.pdf, 23/7/2003.

APPENDIX A

Table A.1 J-M distance values computed for training data sets using six original ETM+ bands of August image

	unc	clf	clv	crn	pas	pep	res-1	rce	sgb	tom-1	tom-2	tom-3	wtm
clf	2.000												
clv	2.000	2.000											
crn	2.000	2.000	2.000										
pas	1.997	2.000	2.000	2.000									
pep	2.000	2.000	2.000	1.883	2.000								
res-1	2.000	2.000	2.000	2.000	1.981	2.000							
rce	2.000	2.000	2.000	1.994	2.000	2.000	2.000						
sgb	2.000	2.000	2.000	1.998	2.000	2.000	2.000	1.997					
tom-1	2.000	2.000	2.000	1.837	2.000	1.814	2.000	1.968	1.856				
tom-2	1.997	2.000	2.000	2.000	2.000	1.981	2.000	2.000	2.000	1.982			
tom-3	1.998	2.000	1.996	2.000	2.000	1.976	2.000	2.000	2.000	1.996	2.000		
wtm	2.000	2.000	2.000	2.000	2.000	1.994	2.000	2.000	2.000	1.999	2.000	2.000	
res-2	2.000	1.891	2.000	2.000	2.000	2.000	2.000	2.000	2.000	2.000	2.000	2.000	2.000

Table A.2 J-M distance values computed for training data sets using six original ETM+ bands of July image

	clv	sgb	pas	wtm	rce-1	rce-2	clf-1	clf-2	onn-1	pep-1	pep-2	res-1	res-2	crn-1	crn-2	crn-3	crn-4	tom-1	tom-2	tom-3	tom-4	unc
sgb	2.000																					
pas	1.997	2.000																				
wtm	2.000	2.000	2.000																			
rce-1	2.000	2.000	2.000	2.000																		
rce-2	1.989	2.000	2.000	2.000	2.000																	
clf-1	2.000	2.000	2.000	2.000	2.000	2.000																
clf-2	2.000	2.000	2.000	1.041	2.000	2.000	1.985															
onn-1	1.949	2.000	1.951	2.000	2.000	2.000	2.000	2.000														
pep-1	2.000	2.000	1.999	1.496	2.000	2.000	1.999	0.798	2.000													
pep-2	2.000	2.000	2.000	2.000	2.000	2.000	1.931	2.000	2.000	2.000												
res-1	2.000	2.000	1.998	2.000	2.000	2.000	2.000	2.000	2.000	2.000	2.000											
res-2	2.000	2.000	2.000	2.000	2.000	2.000	2.000	2.000	2.000	2.000	2.000	2.000										
crn-1	2.000	2.000	1.999	1.412	2.000	2.000	1.980	1.239	2.000	1.264	1.988	2.000	2.000									
crn-2	1.987	2.000	2.000	2.000	2.000	1.984	2.000	2.000	2.000	2.000	2.000	2.000	2.000	2.000								
crn-3	2.000	2.000	2.000	2.000	2.000	2.000	1.979	2.000	2.000	2.000	1.982	2.000	2.000	2.000	2.000							
crn-4	2.000	2.000	2.000	2.000	2.000	2.000	2.000	2.000	2.000	2.000	2.000	2.000	2.000	2.000	1.977	1.999						
tom-1	2.000	2.000	2.000	2.000	2.000	2.000	2.000	2.000	2.000	2.000	2.000	2.000	2.000	2.000	2.000	2.000	1.940					
tom-2	2.000	2.000	2.000	2.000	2.000	2.000	2.000	2.000	2.000	2.000	2.000	2.000	2.000	2.000	1.992	2.000	1.971	1.686				
tom-3	2.000	2.000	2.000	2.000	2.000	2.000	1.992	2.000	2.000	2.000	1.954	2.000	2.000	2.000	2.000	1.204	2.000	2.000	2.000			
tom-4	2.000	2.000	1.999	2.000	2.000	2.000	2.000	1.999	2.000	1.939	1.987	2.000	2.000	1.987	2.000	2.000	2.000	2.000	2.000	2.000		
unc	2.000	2.000	1.993	2.000	2.000	2.000	2.000	2.000	1.978	2.000	2.000	2.000	2.000	2.000	2.000	1.997	1.992	2.000	1.997	1.995	1.996	
onn-2	2.000	2.000	2.000	2.000	2.000	2.000	2.000	2.000	2.000	2.000	2.000	2.000	2.000	2.000	2.000	2.000	2.000	2.000	1.989	2.000	1.998	2.000

Table A.3 J-M distance values computed for training data sets using six original ETM+ bands of May image

	wht	clv	pea-1	pea-2	rce-1	rce-2	onn-1	onn-2	pas-1	pas-2	nsd-1
clv	2.000										
pea-1	1.999	2.000									
pea-2	2.000	2.000	1.995								
rce-1	2.000	2.000	2.000	2.000							
rce-2	2.000	2.000	2.000	2.000	2.000						
onn-1	2.000	2.000	2.000	2.000	2.000	2.000					
onn-2	2.000	2.000	2.000	1.988	2.000	2.000	2.000				
pas-1	2.000	2.000	1.984	1.989	2.000	2.000	2.000	2.000			
pas-2	2.000	2.000	2.000	2.000	2.000	2.000	2.000	2.000	2.000		
nsd-1	2.000	2.000	2.000	2.000	1.950	2.000	2.000	2.000	2.000	2.000	
nsd-2	2.000	2.000	2.000	2.000	1.347	1.995	2.000	2.000	2.000	2.000	1.992

APPENDIX B

Table B.1 The mean and standard deviation values of the spectral classes determined for August image

	TM1		TM2		TM3		TM4		TM5		TM7		NDVI	
	Mean	Std.dev.	Mean	Std.dev.	Mean	Std.dev.	Mean	Std.dev.	Mean	Std.dev.	Mean	Std.dev.	Mean	Std.dev.
crn	81.14	1.62	62.23	2.08	50.48	2.16	100.77	6.72	73.75	3.23	34.23	2.05	169.39	4.73
res-1	107.82	3.47	100.26	5.01	131.10	8.32	82.09	4.43	156.67	8.45	104.56	6.51	97.60	1.61
res-2	94.74	2.53	77.36	3.32	86.86	5.37	51.77	3.40	105.28	9.28	90.47	8.47	94.58	1.72
tom-1	84.75	1.83	69.38	2.12	59.01	3.92	108.89	8.69	78.61	2.94	40.92	3.83	164.85	7.66
tom-2	87.23	1.48	68.42	1.63	63.85	2.18	71.24	4.73	73.22	2.19	47.38	2.40	130.98	21.17
tom-3	90.25	1.60	76.82	1.93	77.34	3.33	84.53	3.68	101.44	5.23	65.86	4.94	124.96	32.16
sgb	83.56	1.59	71.05	1.80	54.08	2.29	124.44	5.53	71.22	2.87	31.84	2.17	177.37	4.21
clv	85.25	1.77	71.02	2.48	60.54	5.44	98.88	6.45	110.92	5.75	59.08	7.63	157.73	9.17
pas	98.83	2.22	84.81	2.90	99.76	4.57	75.26	5.02	146.34	6.93	93.28	6.68	109.05	5.39
pep	84.18	1.62	68.77	2.26	59.95	3.76	93.19	6.08	85.64	5.84	48.74	5.18	154.78	4.96
wtm	89.77	1.43	78.77	1.57	67.37	2.48	113.05	3.78	98.01	3.14	50.98	3.73	159.41	3.51
unc	90.88	1.50	74.13	2.11	79.38	3.94	66.55	2.77	100.96	7.43	64.50	4.90	115.84	3.70
rce	82.95	1.45	71.22	3.32	53.46	2.90	127.68	3.72	86.34	1.67	40.24	1.42	179.47	2.55
clf	101.36	2.94	88.02	3.45	101.58	6.15	64.45	2.90	120.27	4.38	102.20	4.53	98.43	3.40

Table B.1 The mean and standard deviation values of the spectral classes determined for August image (cont'd)

	PCA1		PCA2		PCA3		PCA4		TasBrightness		TasGreenness		TasWetness	
	Mean	Std.dev.	Mean	Std.dev.	Mean	Std.dev.	Mean	Std.dev.	Mean	Std.dev.	Mean	Std.dev.	Mean	Std.dev.
crn	74.89	3.74	123.93	6.70	128.91	2.07	125.03	2.09	140.08	6.04	195.54	9.74	215.64	3.19
res-1	218.36	11.78	113.59	6.73	117.26	6.84	123.70	2.34	175.99	8.50	91.77	3.03	124.88	8.74
res-2	157.26	11.85	161.88	5.71	134.19	5.58	131.40	2.72	123.41	6.97	83.91	2.17	161.37	11.09
tom-1	86.29	6.53	114.69	8.02	124.08	2.53	130.72	2.18	152.55	6.44	197.83	14.44	211.41	4.23
tom-2	96.73	3.57	151.91	4.76	122.87	1.67	126.04	1.27	121.93	3.98	140.47	7.95	208.63	2.36
tom-3	129.59	6.70	130.50	4.54	128.32	2.82	127.34	2.52	145.05	3.78	143.41	7.14	179.95	6.08
sgb	71.74	4.21	102.09	4.89	119.67	2.38	134.47	1.84	162.62	4.05	224.87	9.51	224.05	3.27
clv	117.96	11.53	113.94	4.81	143.16	3.07	121.10	1.60	152.34	2.73	175.96	14.46	174.47	8.52
pas	186.77	10.17	124.43	5.48	137.77	3.16	117.80	2.19	155.74	5.47	106.41	9.03	131.87	8.19
pep	97.92	7.60	127.47	6.85	130.61	2.60	126.55	1.83	141.86	6.67	174.15	8.74	199.55	6.54
wtm	109.33	4.96	103.95	3.79	125.49	2.11	129.59	1.53	165.06	3.47	192.20	6.91	193.97	4.26
unc	132.64	7.73	147.09	3.56	127.70	5.36	120.30	2.03	129.67	3.41	118.05	4.92	178.52	8.11
rce	84.02	2.57	94.53	3.80	129.54	3.31	132.33	1.96	168.63	4.23	227.01	4.52	207.43	1.97
clf	180.79	7.84	144.86	3.72	129.11	4.80	136.80	2.09	144.78	5.12	86.37	4.71	148.24	4.89

Table B.2 The mean and standard deviation values of the spectral classes determined for July image

	TM1		TM2		TM3		TM4		TM5		TM7		NDVI	
	Mean	Std.dev.	Mean	Std.dev.	Mean	Std.dev.	Mean	Std.dev.	Mean	Std.dev.	Mean	Std.dev.	Mean	Std.dev.
crn-1	106.57	2.84	95.99	4.18	115.13	5.93	68.26	6.07	137.75	8.56	120.06	9.33	94.16	4.56
crn-2	76.92	2.01	62.61	2.84	47.02	3.45	124.42	7.59	89.65	4.86	42.10	3.66	184.69	5.16
crn-3	92.44	3.04	76.23	3.57	81.62	4.98	53.47	5.18	86.72	4.87	67.15	5.21	100.21	6.65
crn-4	80.49	2.31	65.74	2.51	56.53	4.18	87.65	5.73	86.12	4.40	48.73	5.64	154.56	7.90
res-1	114.57	4.28	115.08	4.83	160.87	6.90	102.84	4.42	180.31	7.78	119.72	5.97	98.84	1.70
res-2	98.65	3.51	91.57	4.30	122.91	7.55	83.04	4.40	126.86	4.76	78.82	3.09	102.25	2.38
tom-1	83.19	1.12	68.55	0.88	64.25	2.16	98.38	4.68	90.38	3.02	55.80	2.65	153.83	2.87
tom-2	86.35	2.74	73.20	3.25	68.45	5.51	108.13	6.56	98.08	5.77	65.37	6.91	155.77	6.55
tom-3	92.08	2.49	75.48	2.56	81.61	3.85	57.21	4.05	90.21	4.11	71.17	4.93	104.47	6.00
tom-4	94.98	3.05	84.07	3.43	94.08	4.34	80.18	3.95	123.06	5.50	101.04	6.65	116.79	4.56
sgb	81.19	1.81	75.09	1.81	53.72	2.12	162.38	8.37	81.13	3.18	35.92	2.57	191.22	3.94
clv	82.27	3.30	70.50	5.12	60.75	9.54	123.01	8.16	117.24	6.99	60.82	8.29	170.50	12.34

Table B.2 The mean and standard deviation values of the spectral classes determined for July image (cont'd)

	TM1		TM2		TM3		TM4		TM5		TM7		NDVI	
	Mean	Std.dev.	Mean	Std.dev.	Mean	Std.dev.	Mean	Std.dev.	Mean	Std.dev.	Mean	Std.dev.	Mean	Std.dev.
pas	102.20	3.65	93.38	4.76	115.34	9.05	96.18	5.08	162.77	10.73	105.87	11.10	115.56	6.37
pep-1	107.75	4.18	98.87	4.39	119.23	6.51	72.90	4.78	139.35	4.00	123.85	5.50	96.17	6.59
pep-2	97.23	1.79	82.71	1.56	92.69	2.34	61.46	2.59	110.49	5.05	94.61	5.46	101.07	3.01
wtm	111.47	4.03	104.22	5.41	126.02	7.22	75.18	5.42	150.46	7.31	136.82	6.48	94.59	2.49
unc	91.41	2.13	78.60	2.88	83.04	4.62	79.87	3.86	110.82	8.26	74.27	6.04	119.23	25.26
rce-1	80.26	1.40	67.14	1.68	60.42	2.00	49.72	5.41	40.51	7.09	25.26	3.71	107.56	26.32
rce-2	78.37	1.41	72.68	1.85	50.22	1.53	125.93	6.53	107.78	4.35	53.51	2.19	181.88	3.44
clf-1	102.75	2.03	90.05	2.89	105.20	4.26	60.26	4.96	108.36	6.06	92.61	4.22	92.14	4.09
clf-2	109.38	2.93	100.95	3.15	123.94	4.17	72.10	3.29	142.77	6.98	129.89	10.03	93.12	3.45
onn-1	90.28	3.35	79.26	3.91	88.34	6.10	98.44	6.44	123.76	6.96	76.69	7.18	129.28	26.07
onn-2	94.56	1.64	84.83	2.67	88.36	2.79	90.58	1.92	106.89	3.81	83.47	4.57	111.00	44.69

Table B.2 The mean and standard deviation values of the spectral classes determined for July image (cont'd)

	PCA1		PCA2		PCA3		PCA4		TasBrightness		TasGreenness		TasWetness	
	Mean	Std.dev.	Mean	Std.dev.	Mean	Std.dev.	Mean	Std.dev.	Mean	Std.dev.	Mean	Std.dev.	Mean	Std.dev.
crn-1	169.81	13.03	149.53	6.42	114.52	5.83	134.14	2.66	120.70	6.92	69.27	5.03	123.74	9.49
crn-2	49.49	6.78	90.32	7.59	122.49	2.32	122.91	1.97	123.59	5.22	189.35	9.30	190.70	4.62
crn-3	88.29	8.85	165.06	5.60	134.87	2.33	129.10	2.52	89.53	5.00	85.85	6.17	179.87	4.55
crn-4	58.58	7.11	127.87	6.16	126.83	4.26	121.45	1.98	102.51	3.21	142.01	8.90	187.86	5.46
res-1	226.20	10.22	108.66	4.88	138.96	6.82	125.19	4.76	159.90	5.64	85.65	3.47	103.04	8.10
res-2	145.25	7.98	131.40	4.47	148.10	6.16	123.34	3.74	124.65	5.21	96.61	3.25	153.05	4.67
tom-1	69.94	3.70	118.39	4.74	126.87	2.44	126.49	1.20	112.68	3.57	148.36	4.89	183.67	3.12
tom-2	82.96	10.60	109.12	6.41	122.45	3.00	130.92	2.50	122.63	5.10	153.52	8.96	175.57	6.60
tom-3	91.84	7.36	161.38	4.06	131.12	2.77	128.93	1.83	92.54	3.21	89.27	6.08	175.31	4.76
tom-4	134.42	9.70	137.15	4.02	113.13	3.36	129.76	1.72	117.88	3.29	100.07	6.86	140.42	6.43
sgb	48.91	3.89	55.40	8.35	135.39	2.05	142.42	2.27	150.25	5.33	227.09	9.99	207.74	3.30
clv	85.25	15.29	88.86	8.08	114.51	2.32	117.05	1.70	132.05	2.33	174.88	15.89	163.30	8.29

Table B.2 The mean and standard deviation values of the spectral classes determined for July image (cont'd)

	PCA1		PCA2		PCA3		PCA4		TasBrightness		TasGreenness		TasWetness	
	Mean	Std.dev.	Mean	Std.dev.	Mean	Std.dev.	Mean	Std.dev.	Mean	Std.dev.	Mean	Std.dev.	Mean	Std.dev.
pas	175.13	17.14	114.33	5.70	116.69	4.68	115.66	5.26	139.61	5.58	104.99	9.67	113.86	11.40
pep-1	175.82	8.68	145.54	5.33	114.95	4.94	137.46	3.74	125.46	2.86	71.18	9.19	122.07	4.81
pep-2	123.87	6.08	157.01	2.78	119.75	4.90	131.08	1.67	103.58	2.60	81.20	3.12	151.25	6.22
wtm	194.43	11.70	143.30	5.78	109.50	6.20	139.57	2.69	131.92	6.78	65.87	3.65	109.25	7.16
unc	106.02	10.01	135.23	4.60	125.18	4.79	123.01	2.52	110.71	4.50	112.20	4.26	161.05	8.28
rce-1	24.95	5.58	171.23	6.16	157.07	4.72	133.33	2.50	71.09	4.66	104.81	5.16	230.70	6.68
rce-2	70.09	3.54	86.15	6.77	114.70	2.53	120.29	2.28	130.25	4.73	183.80	7.10	173.42	3.89
clf-1	132.02	8.10	159.13	5.45	131.88	3.04	136.55	1.57	106.32	5.13	73.29	4.12	156.85	5.42
clf-2	184.32	11.16	146.83	3.67	113.78	6.75	138.96	2.75	127.27	3.68	66.27	6.05	117.24	9.45
onn-1	117.15	11.22	115.09	6.85	123.71	4.51	119.95	2.64	125.32	5.12	130.54	9.36	152.30	7.76
onn-2	113.28	6.04	127.89	1.95	124.92	2.84	136.03	1.85	120.22	1.16	117.94	4.48	162.44	4.75

Table B.3 The mean and standard deviation values of the spectral classes determined for May image

	TM1		TM2		TM3		TM4		TM5		TM7		NDVI	
	Mean	Std.dev.	Mean	Std.dev.	Mean	Std.dev.	Mean	Std.dev.	Mean	Std.dev.	Mean	Std.dev.	Mean	Std.dev.
nsd-1	107.49	4.57	96.46	5.92	117.67	8.95	67.59	4.82	142.12	11.36	130.33	11.05	92.40	1.61
nsd-2	95.00	2.80	78.06	3.10	87.20	3.65	50.89	3.78	91.26	5.58	77.43	6.17	93.25	3.28
wht	74.48	1.55	58.61	1.75	43.52	1.93	125.52	8.99	69.78	2.71	34.57	1.93	188.88	5.02
clv	90.51	2.88	81.17	3.58	91.68	9.18	89.47	2.47	149.63	7.07	99.52	8.19	124.88	13.16
pas-1	78.96	1.61	71.79	2.33	55.62	3.22	133.76	4.53	102.94	5.81	50.68	2.51	179.82	3.43
pas-2	87.02	2.28	78.74	1.73	72.60	3.98	102.02	3.71	114.29	4.81	71.12	4.41	148.57	5.27
rce-1	97.88	1.68	81.18	1.81	92.05	2.71	52.66	1.92	99.68	7.14	85.00	7.72	92.11	1.28
rce-2	81.06	3.25	62.08	3.28	65.78	4.97	35.26	4.72	30.39	14.26	24.18	11.44	88.07	5.02
pea-1	79.31	1.95	69.04	2.26	50.80	2.49	140.72	5.80	82.19	3.70	39.51	2.68	187.05	4.25
pea-2	91.50	2.91	83.84	3.35	76.85	5.36	123.68	4.83	108.08	5.57	69.55	7.29	156.95	5.60
onn-1	85.64	2.44	69.86	2.78	69.71	3.21	73.36	6.94	78.93	4.80	54.76	5.27	126.89	21.02
onn-2	102.89	3.07	96.64	4.59	103.68	7.90	104.72	3.34	128.54	9.34	99.03	7.27	123.60	23.52

Table B.3 The mean and standard deviation values of the spectral classes determined for May image (cont'd)

	PCA1		PCA2		PCA3		Tas-Brightness		Tas-Greenness		Tas-Wetness	
	Mean	Std.dev.	Mean	Std.dev.	Mean	Std.dev.	Mean	Std.dev.	Mean	Std.dev.	Mean	Std.dev.
nsd-1	206.52	15.55	140.90	11.80	126.53	4.50	132.38	8.86	66.94	3.44	113.57	10.95
nsd-2	138.81	6.59	91.16	6.79	131.23	4.19	98.40	4.78	78.93	2.60	166.67	6.21
wht	46.09	4.94	135.06	8.18	125.51	1.45	129.46	6.08	189.86	10.13	200.90	2.33
clv	163.85	13.93	154.60	3.69	111.10	3.19	136.06	3.06	112.01	8.22	118.33	7.63
pas-1	76.18	4.12	161.65	3.92	123.89	5.52	146.44	3.07	186.28	5.08	173.92	5.69
pas-2	116.74	7.12	144.14	3.74	122.86	3.14	133.15	2.17	139.46	6.10	156.35	5.05
rce-1	149.79	8.29	98.35	6.00	130.98	4.25	103.32	3.50	76.04	1.63	158.44	8.35
rce-2	70.55	14.12	38.38	11.72	145.73	7.20	65.51	7.25	89.35	3.40	227.78	14.47
pea-1	55.12	6.26	156.21	4.08	132.63	1.89	146.14	3.11	198.65	7.71	194.13	3.49
pea-2	108.73	10.68	160.90	4.49	135.67	3.93	149.53	3.35	159.24	8.14	165.51	6.71
onn-1	99.33	6.18	99.58	8.27	130.60	3.12	104.37	6.34	117.22	6.36	184.65	4.90
onn-2	160.06	12.81	161.16	5.69	139.78	5.41	150.50	4.29	118.46	7.03	140.45	8.84

APPENDIX C

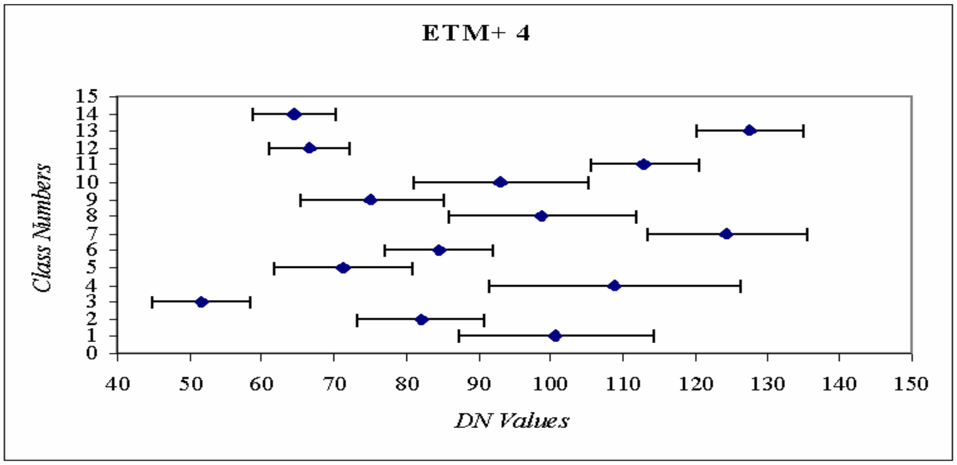

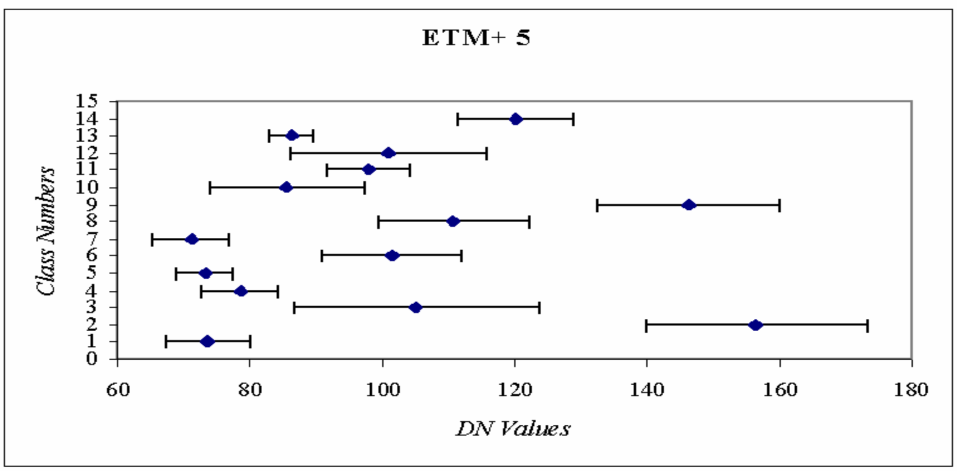

Figure C.1 Coincidence spectral plots with ±2 standard deviations from the mean for August

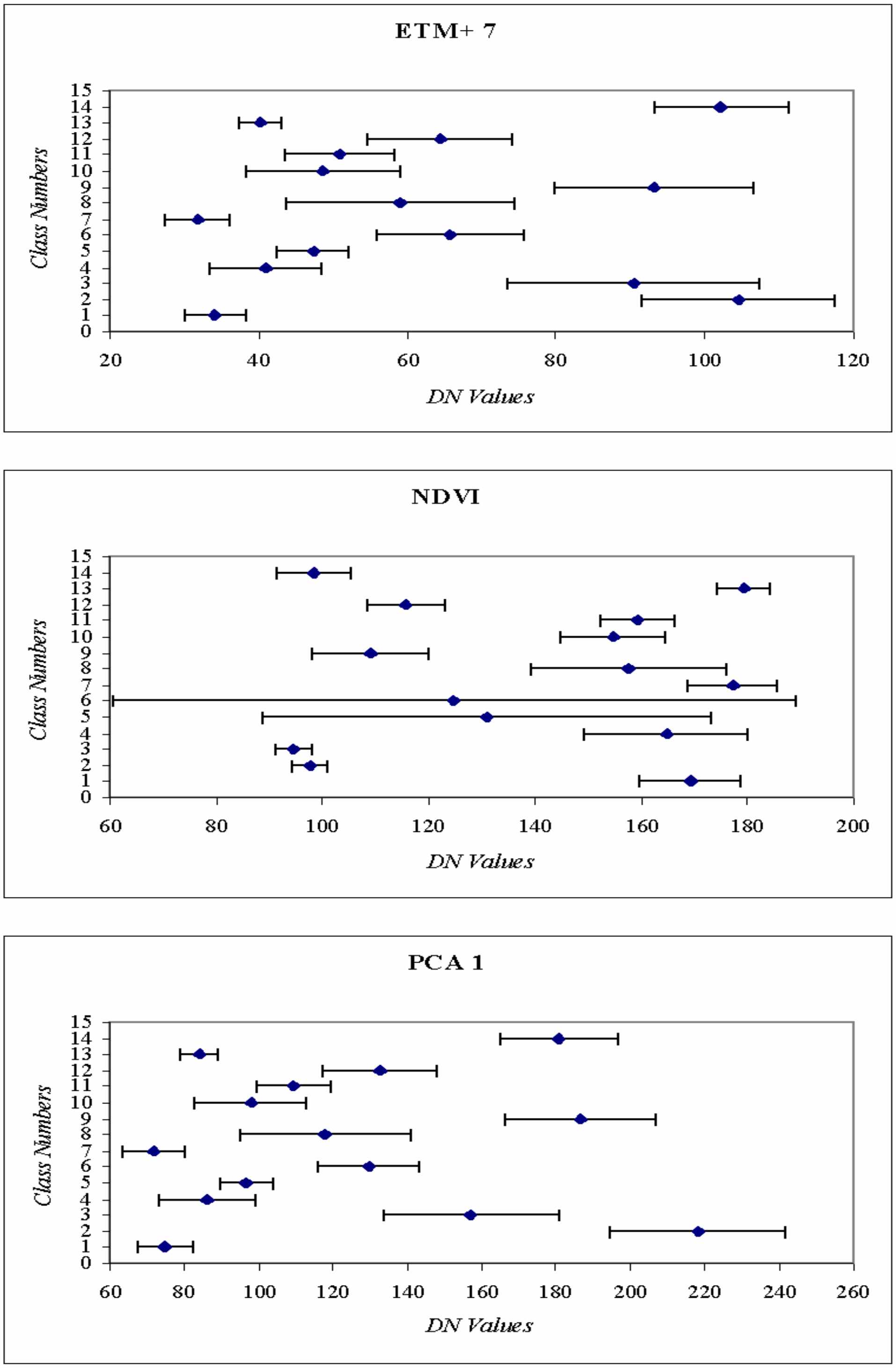

Figure C.1 Coincidence spectral plots with ±2 standard deviations from the mean for August (cont'd)

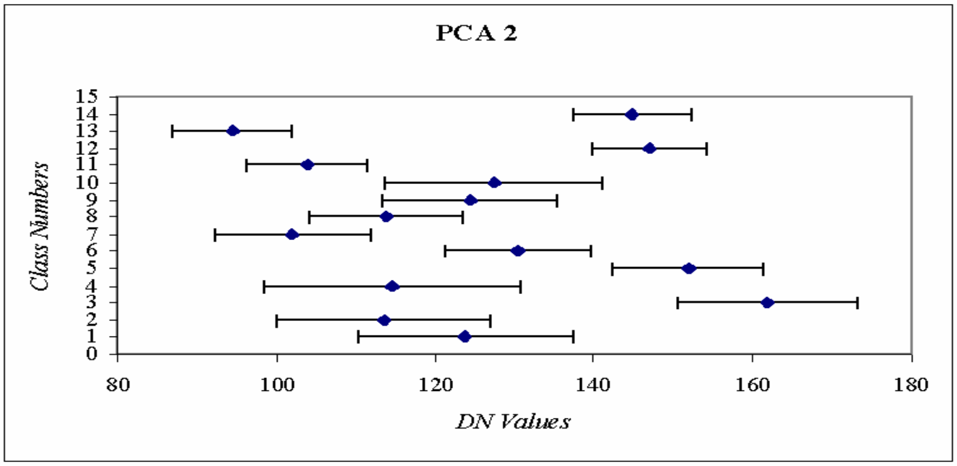

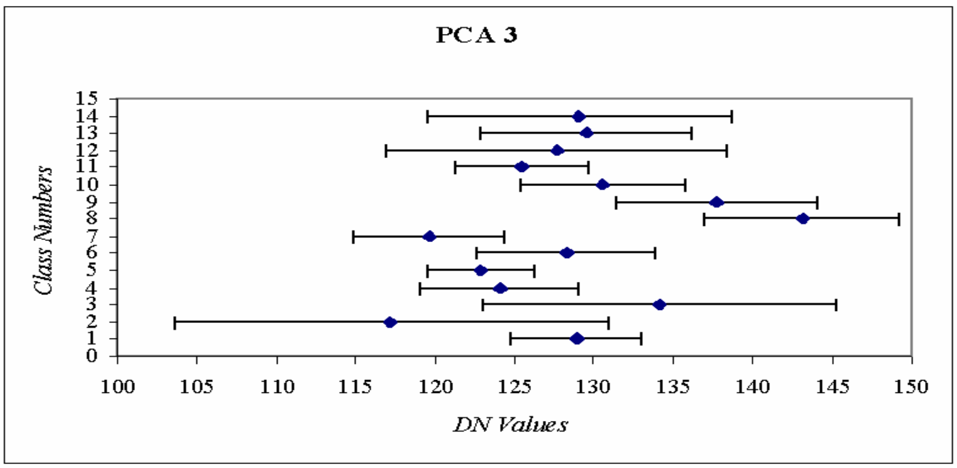

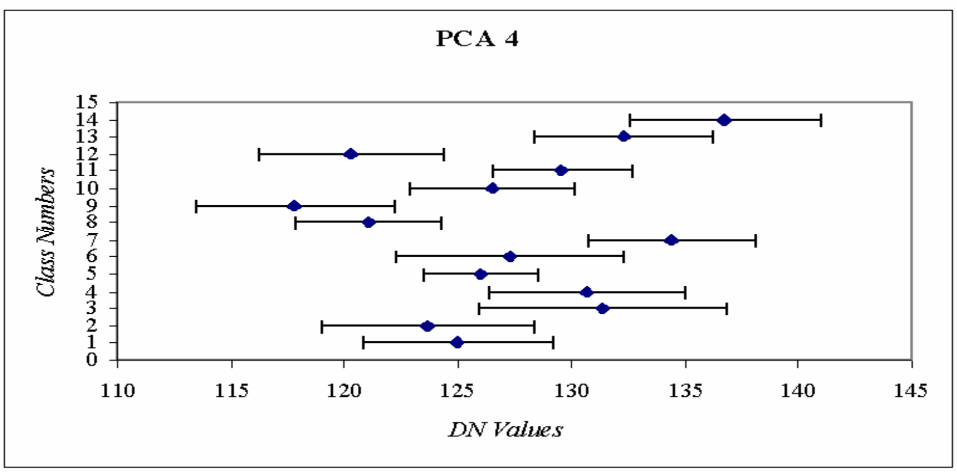

Figure C.1 Coincidence spectral plots with ±2 standard deviations from the mean for August (cont'd)

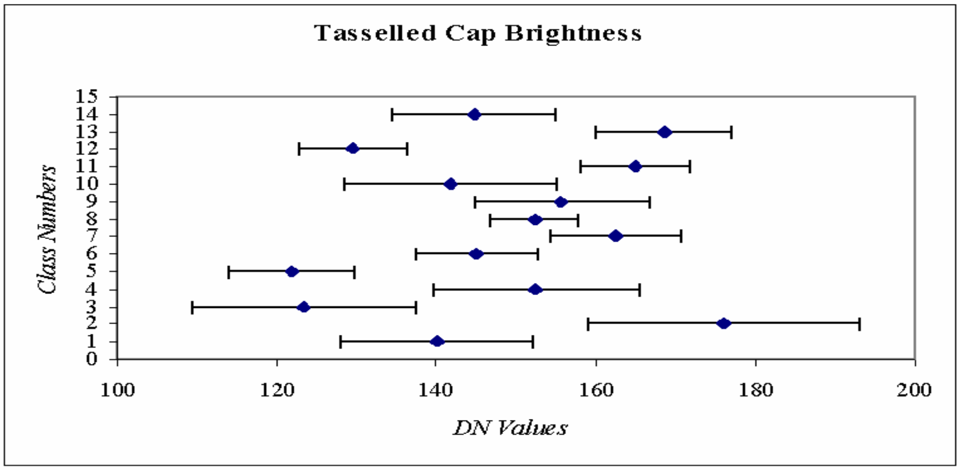

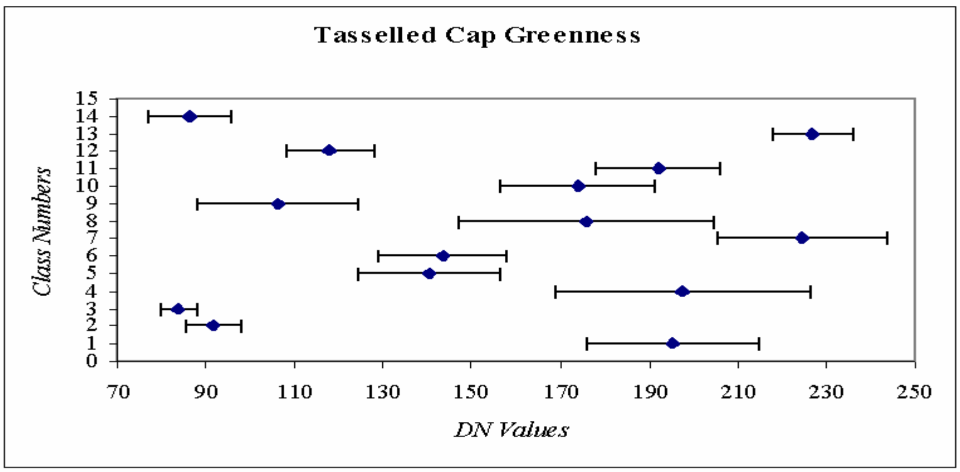

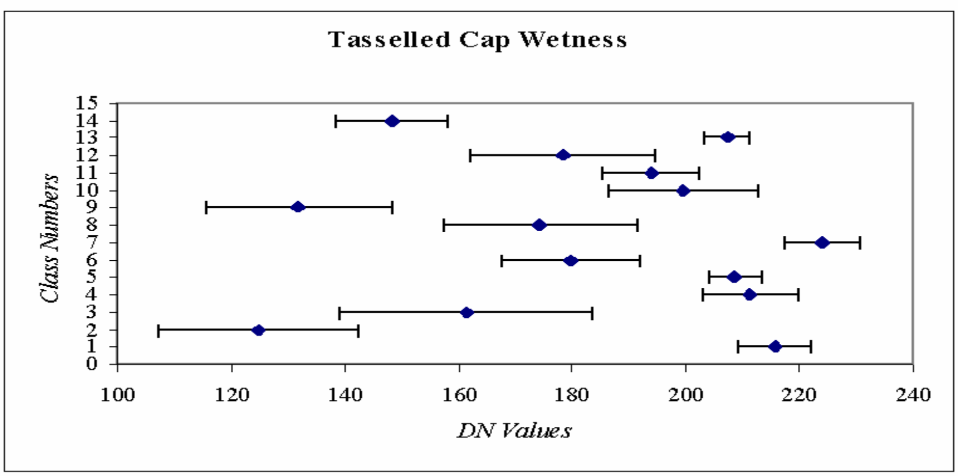

Figure C.1 Coincidence spectral plots with ±2 standard deviations from the mean for August (cont'd)

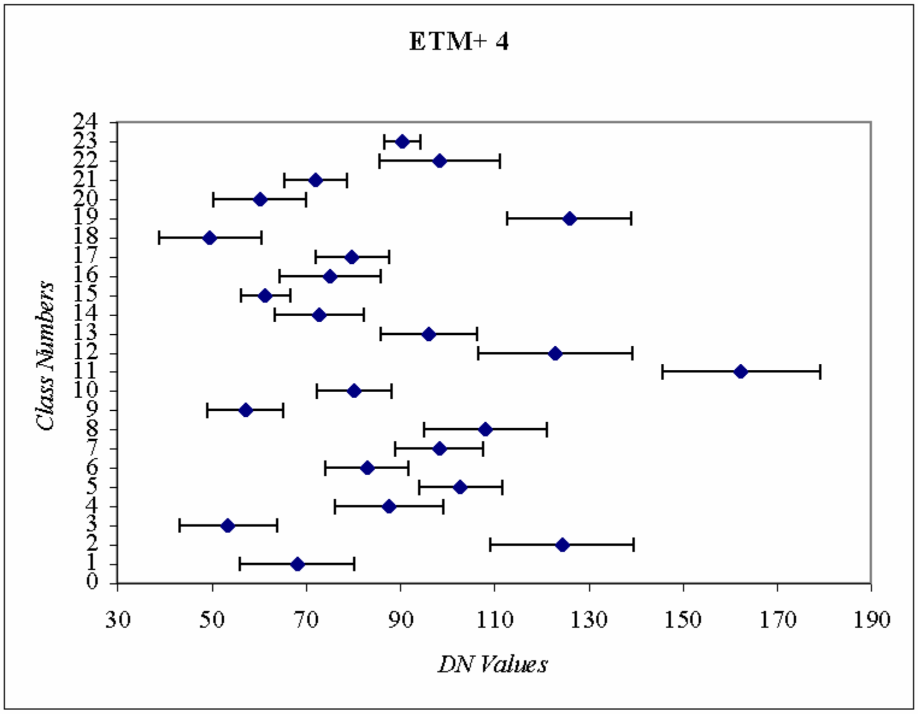

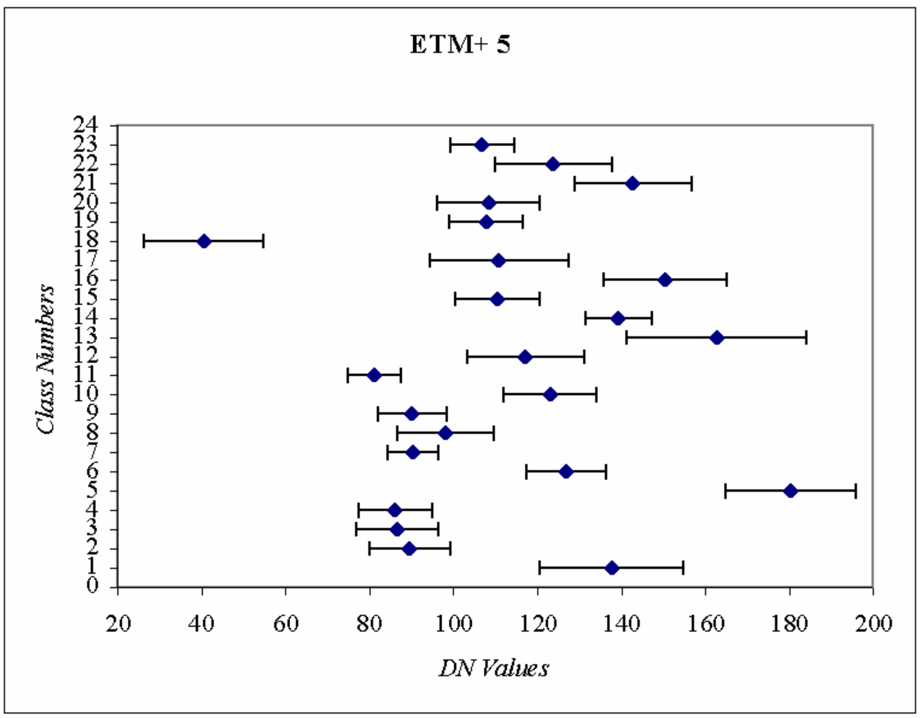

Figure C.2 Coincidence spectral plots with ±2 standard deviations from the mean for July

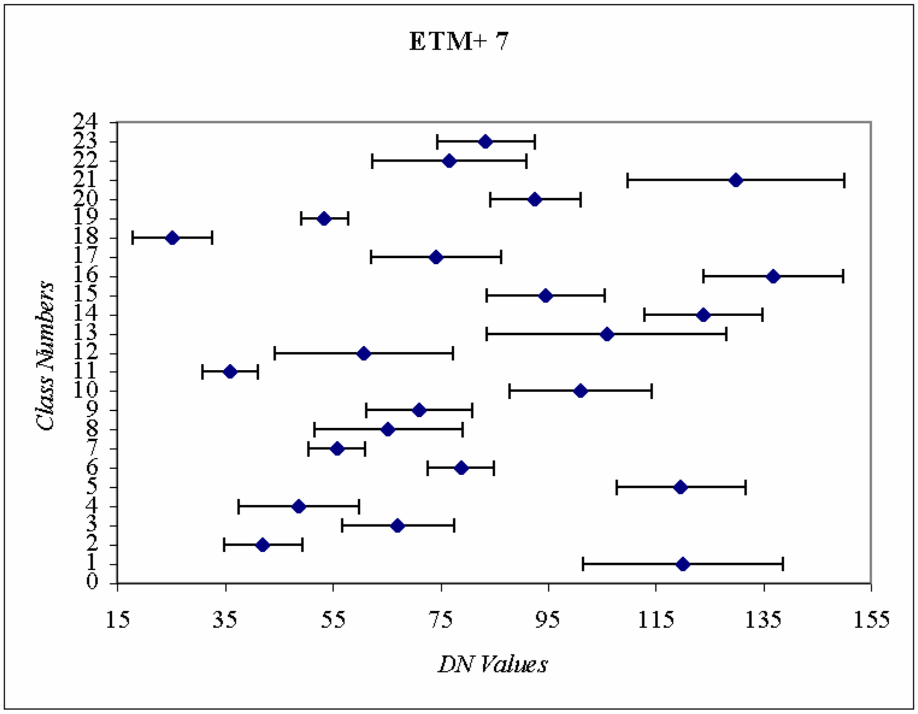

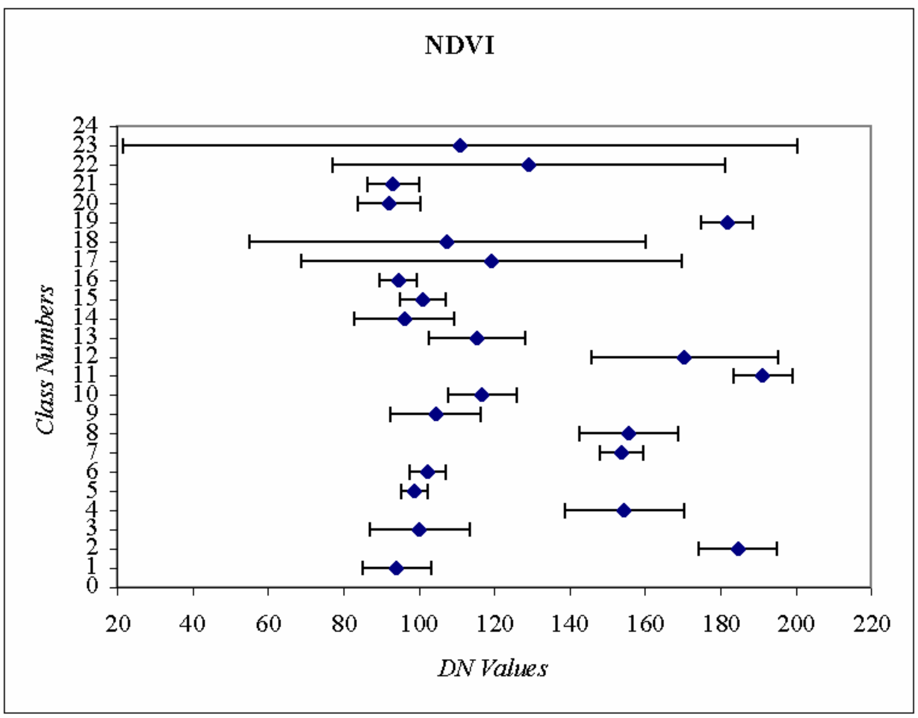

Figure C.2 Coincidence spectral plots with ±2 standard deviations from the mean for July (cont’d)

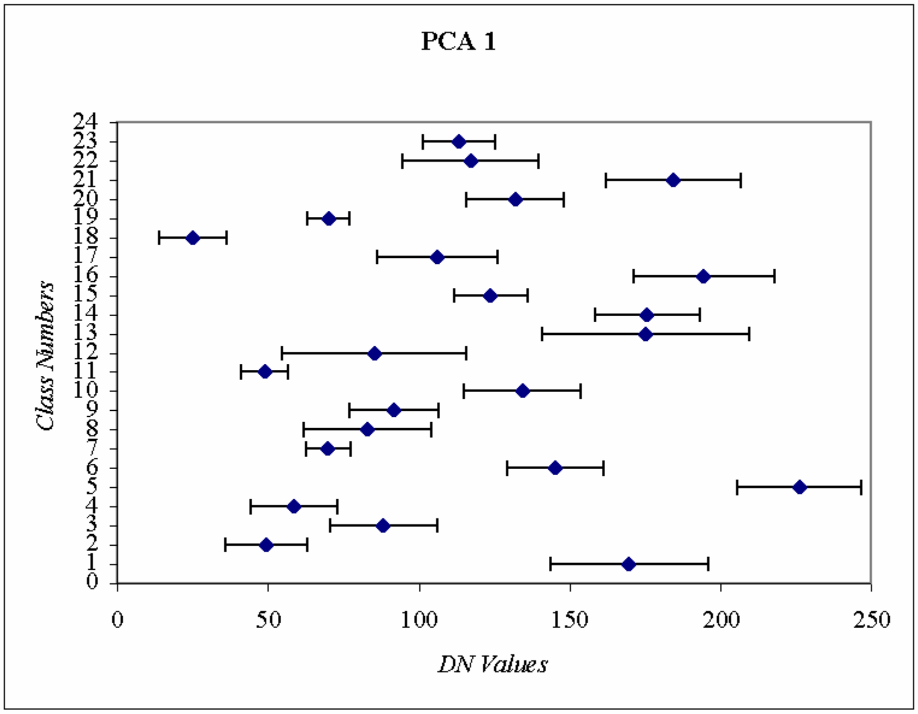

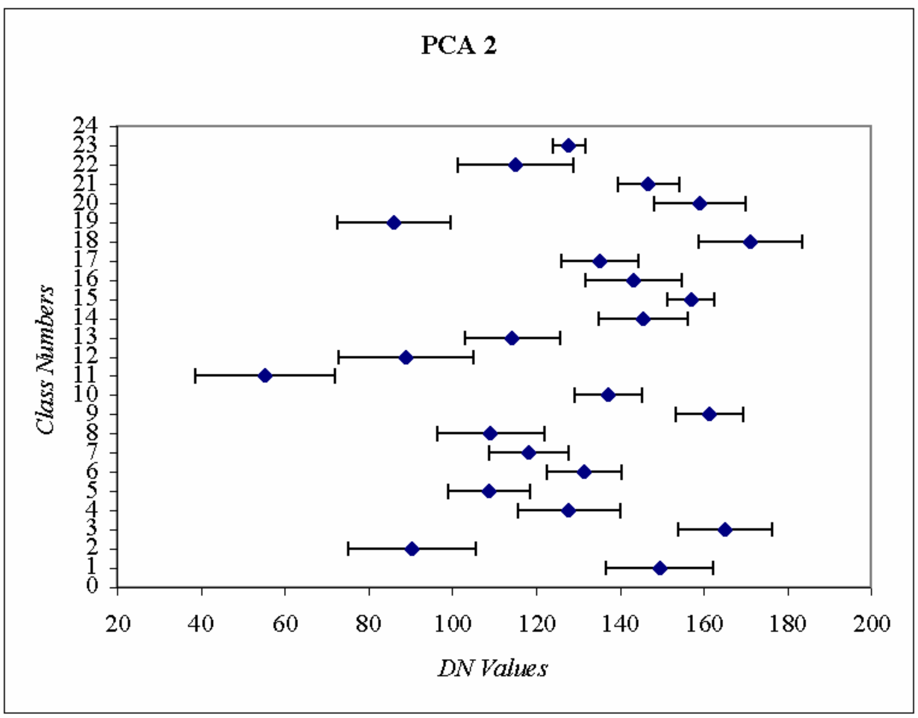

Figure C.2 Coincidence spectral plots with ±2 standard deviations from the mean for July (cont'd)

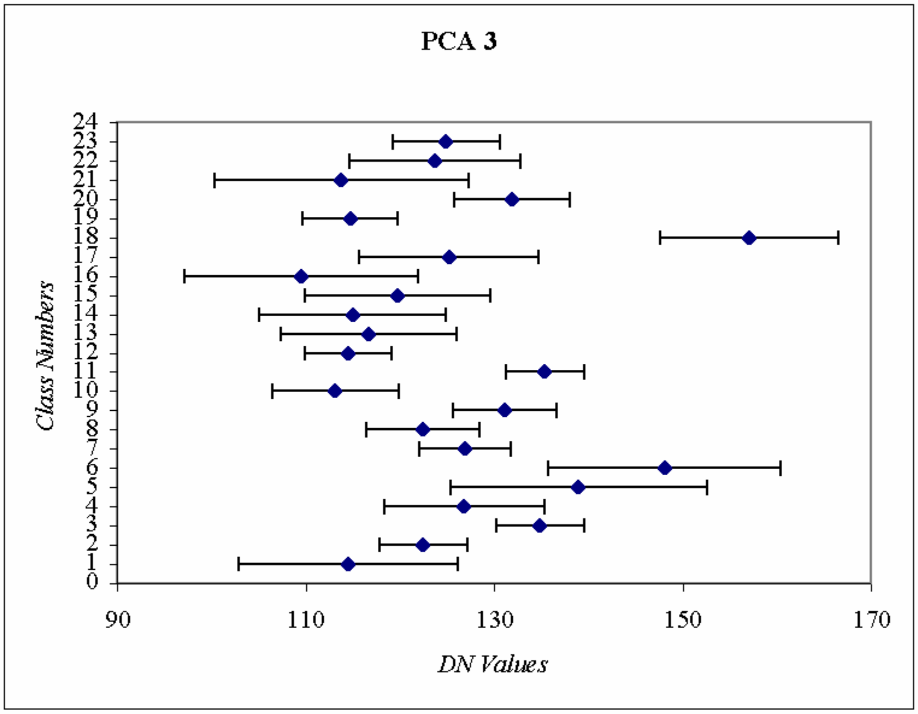

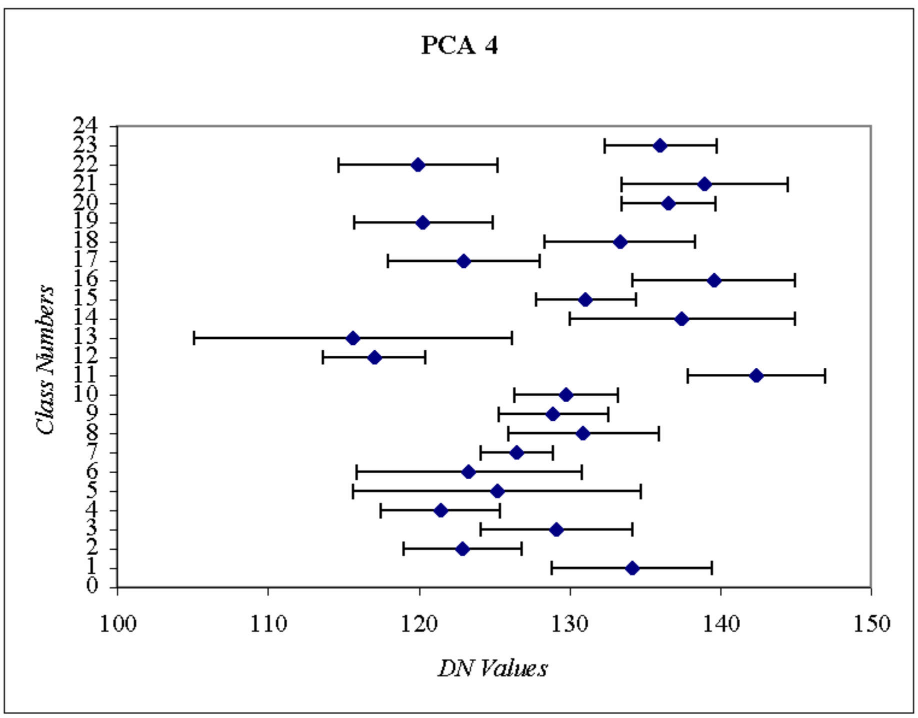

Figure C.2 Coincidence spectral plots with ±2 standard deviations from the mean for July (cont'd)

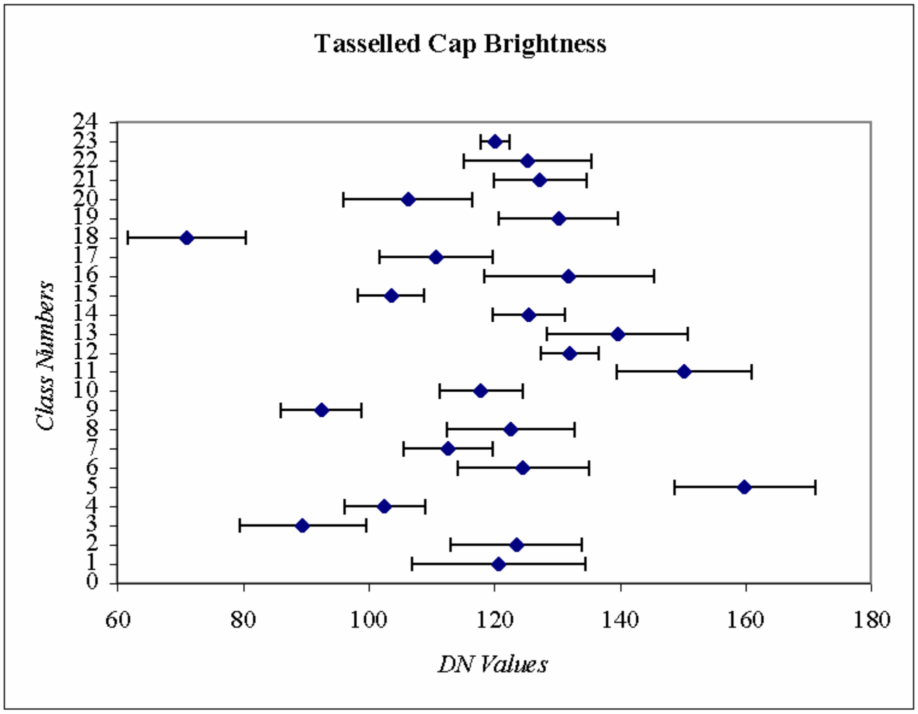

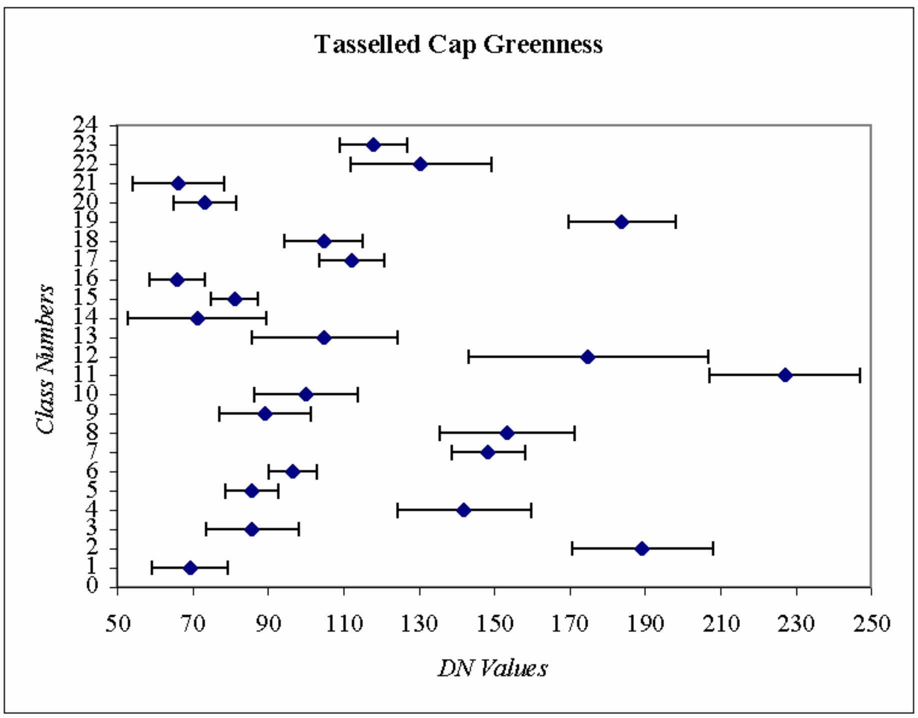

Figure C.2 Coincidence spectral plots with ±2 standard deviations from the mean for July (cont'd)

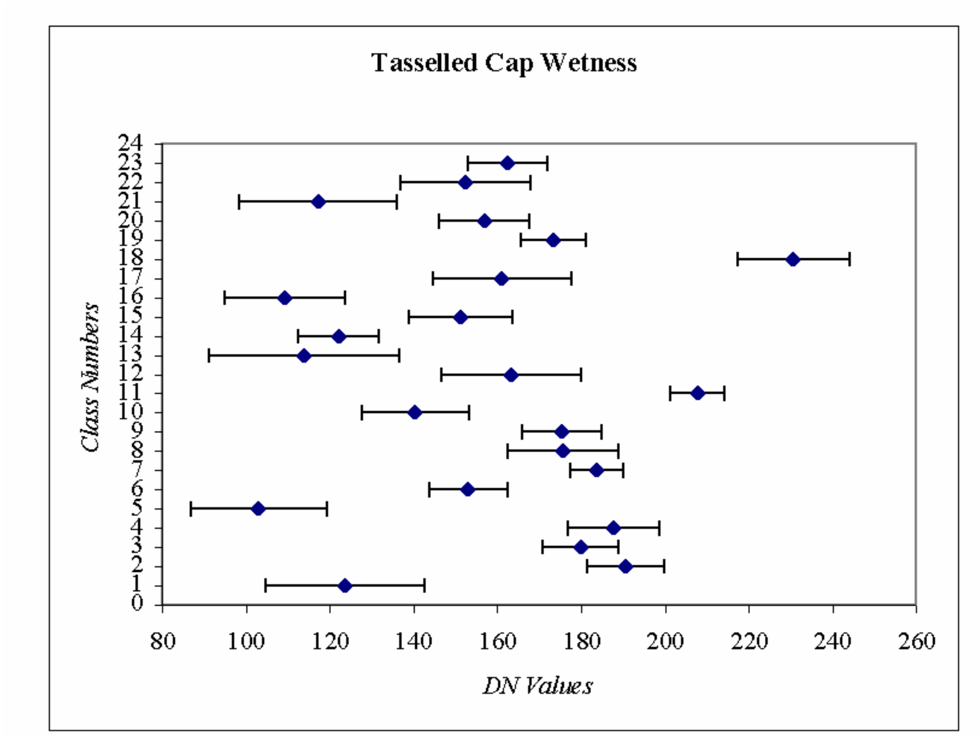

Figure C.2 Coincidence spectral plots with ±2 standard deviations from the mean for July (cont'd)

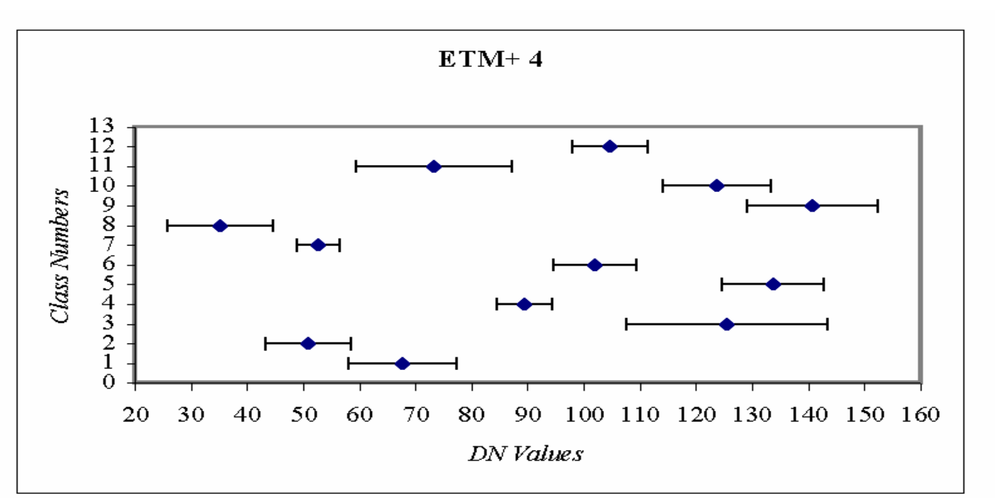

Figure C.3 Coincidence spectral plots with ±2 standard deviations from the mean for May

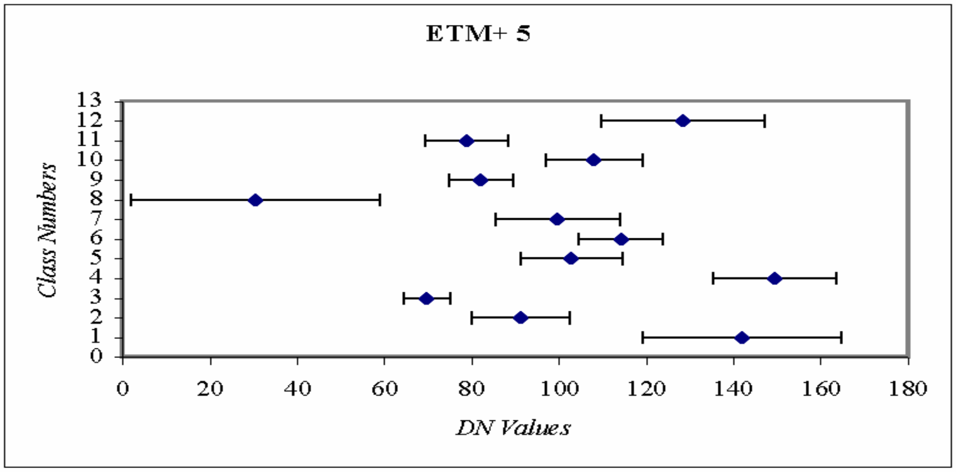

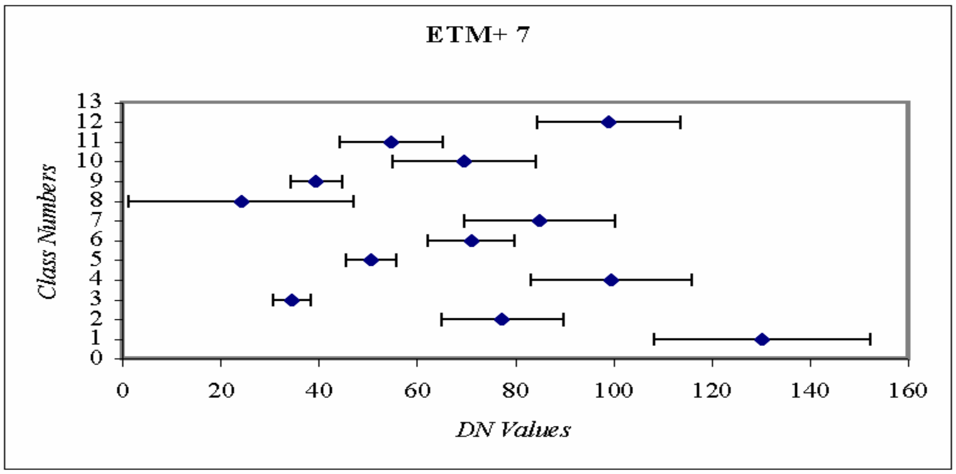

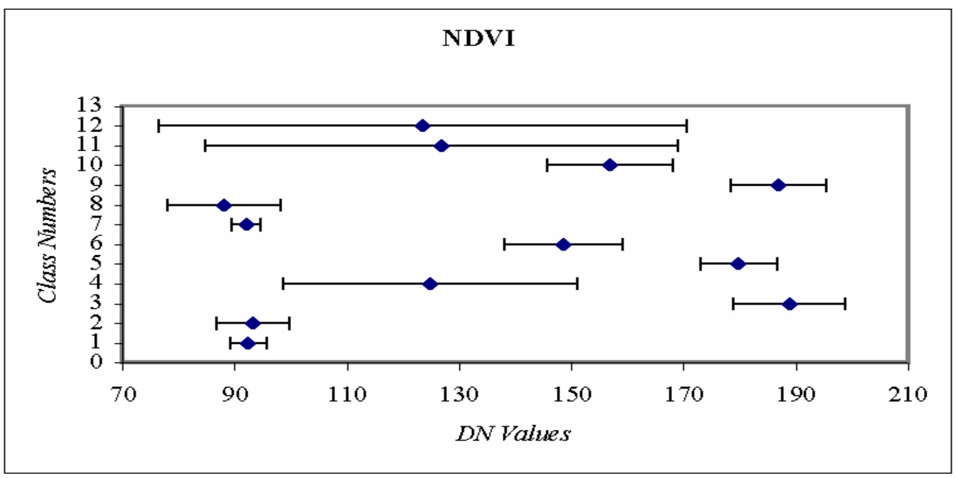

Figure C.3 Coincidence spectral plots with ±2 standard deviations from the mean for May (cont'd)

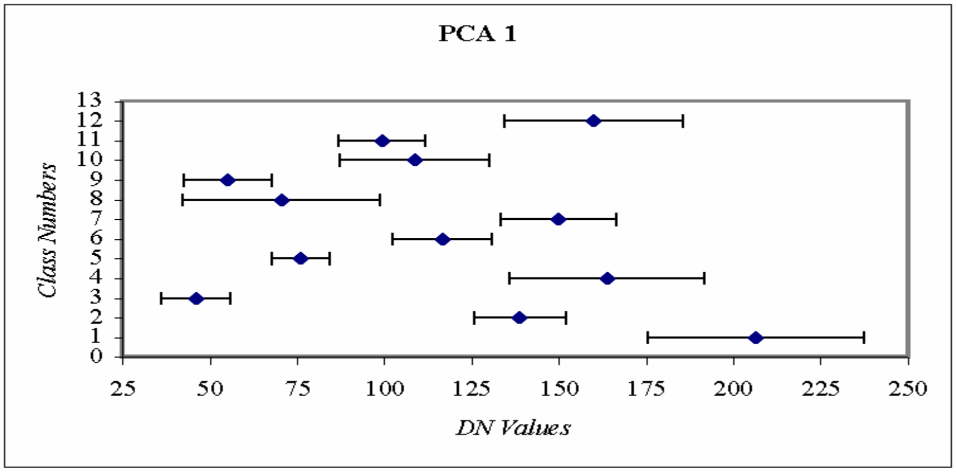

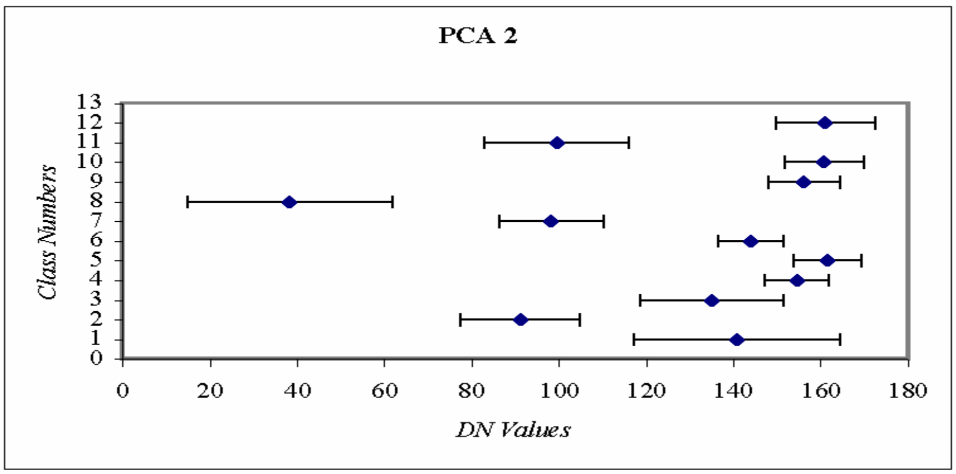

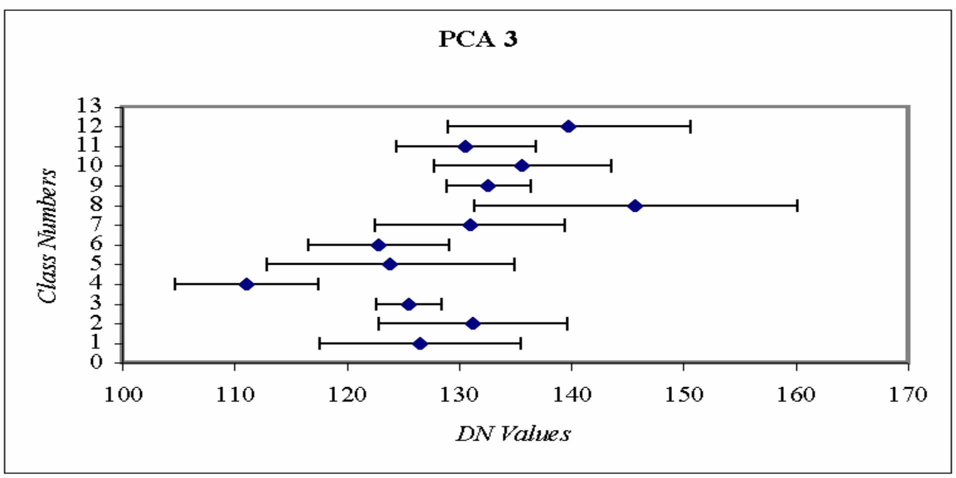

Figure C.3 Coincidence spectral plots with ±2 standard deviations from the mean for May (cont'd)

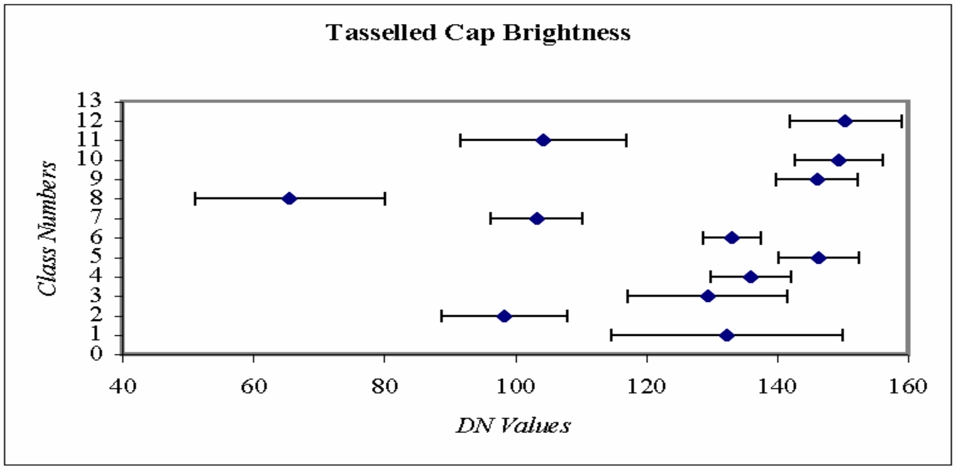

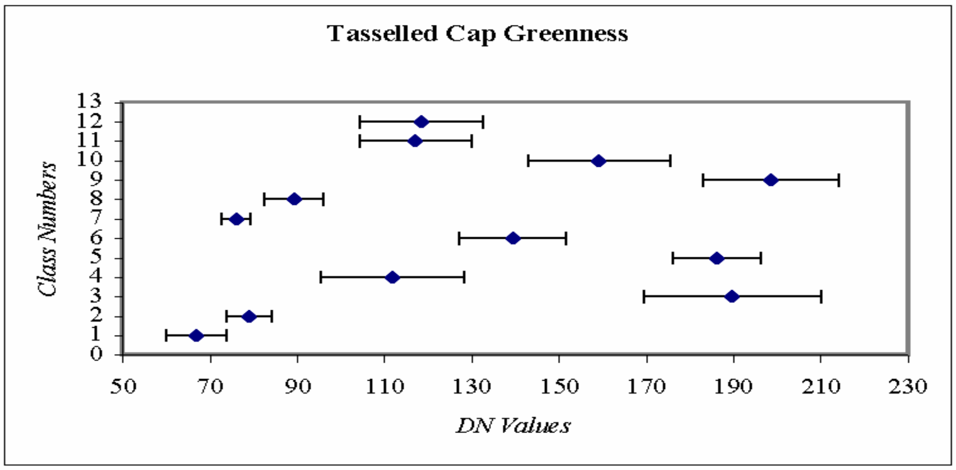

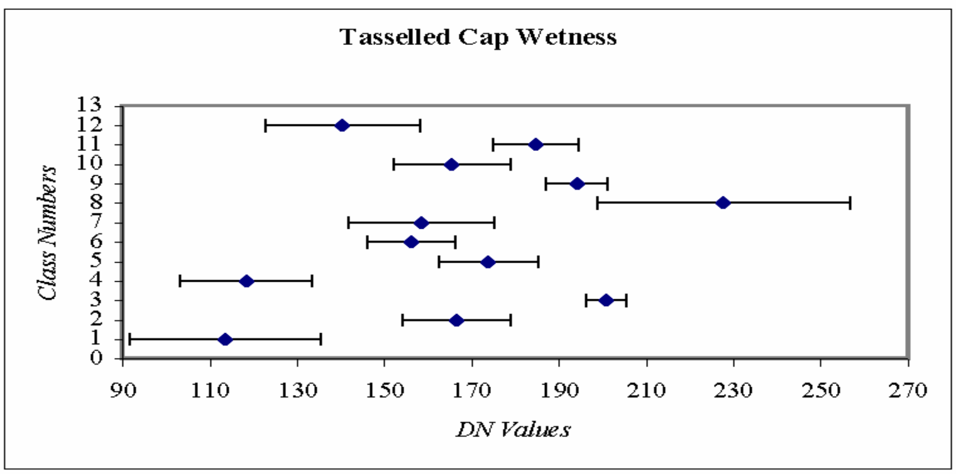

Figure C.3 Coincidence spectral plots with ±2 standard deviations from the mean for May (cont'd)

APPENDIX D

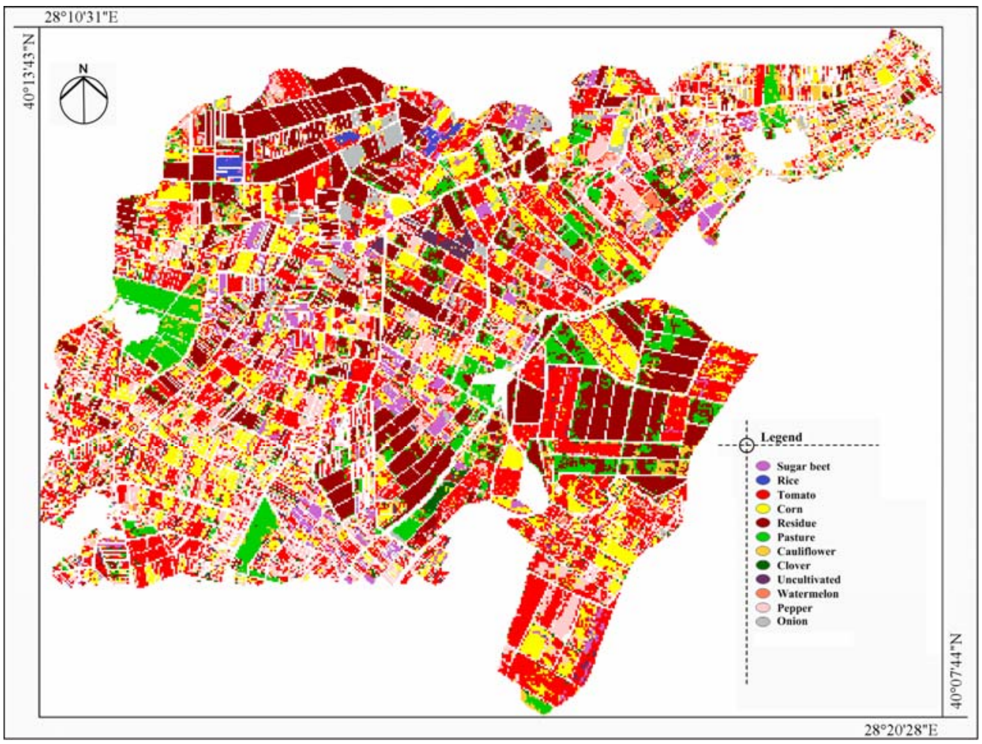

Figure D.1 Per-pixel classified July image using decision tree classifier with multi-temporal images

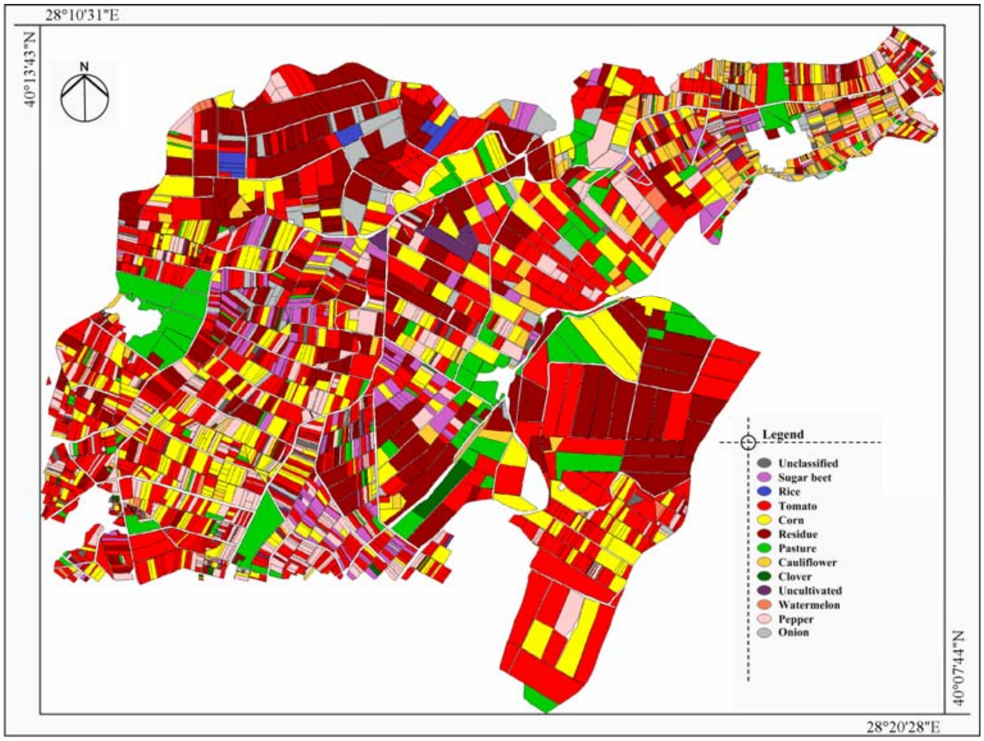

Figure D.2 Per-field classified July image using decision tree classifier

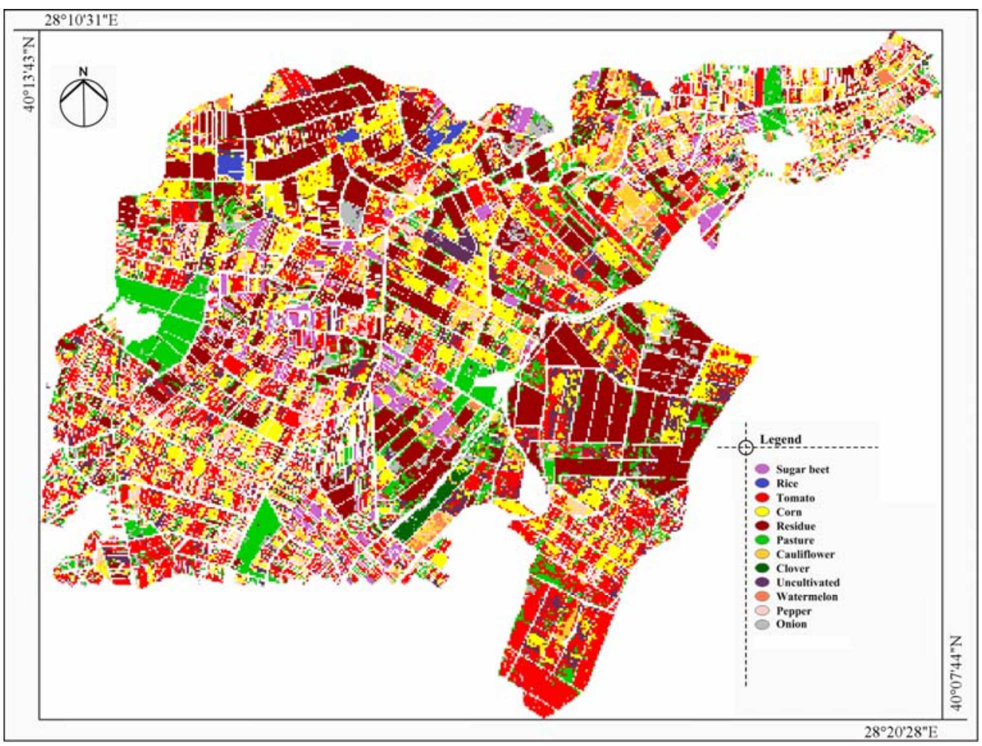

Figure D.3 Per-pixel classified July image using maximum likelihood classifier

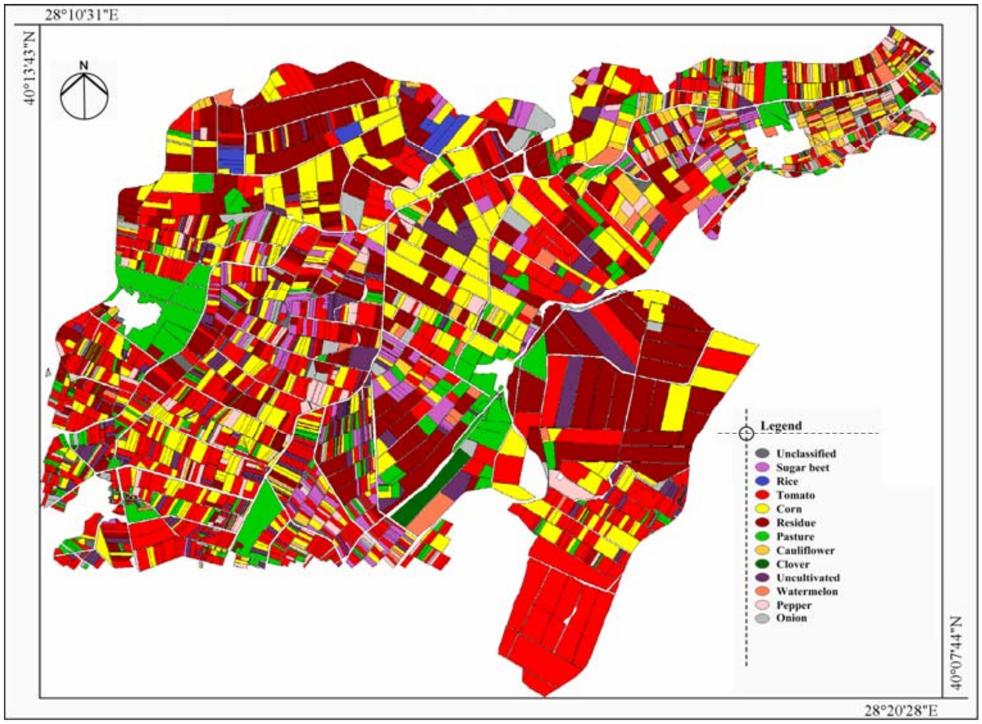

Figure D.4 Per-field classified July image using maximum likelihood classifier

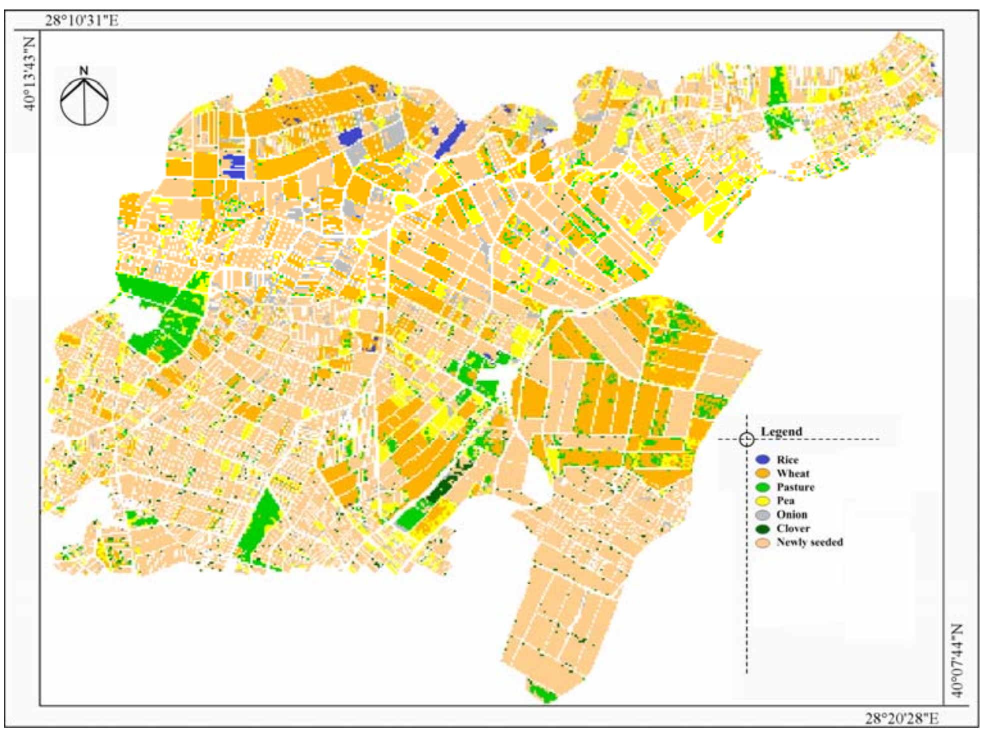

Figure D.5 Per-pixel classified May image using decision tree classifier with multi-temporal images

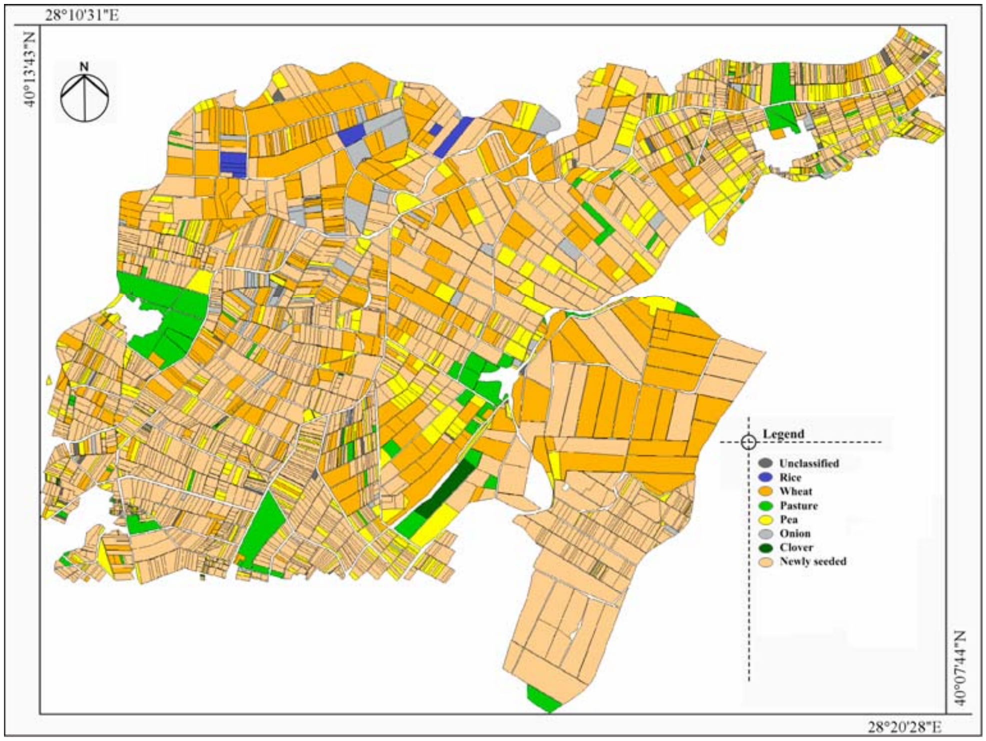

Figure D.6 Per-field classified May image using decision tree classifier

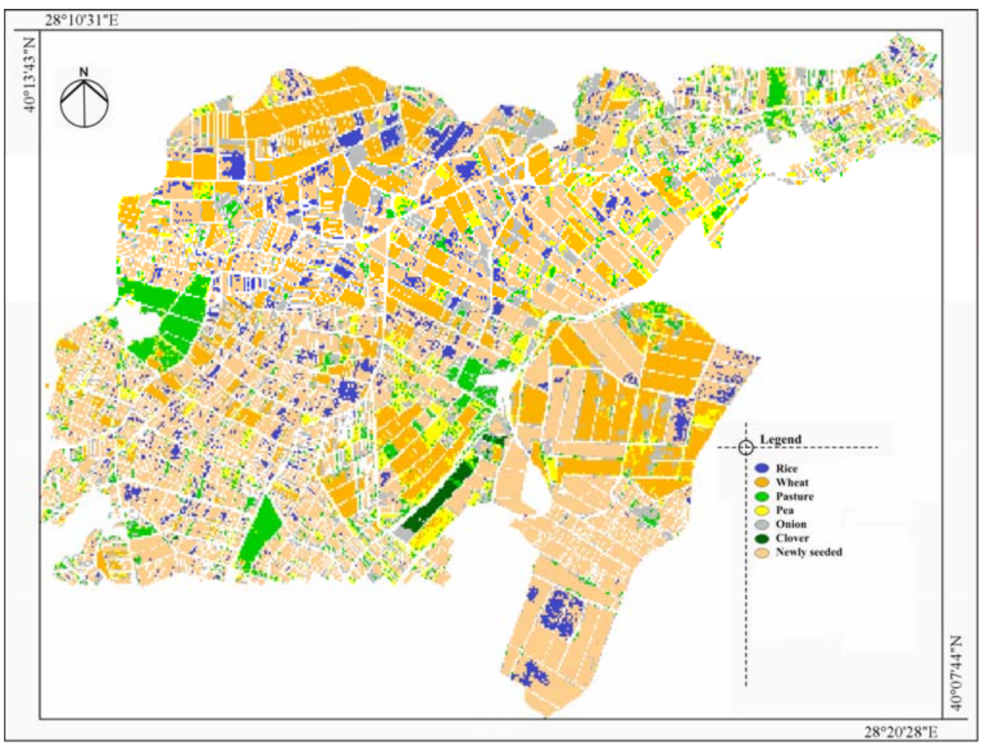

Figure D.7 Per-pixel classified May image using maximum likelihood classifier

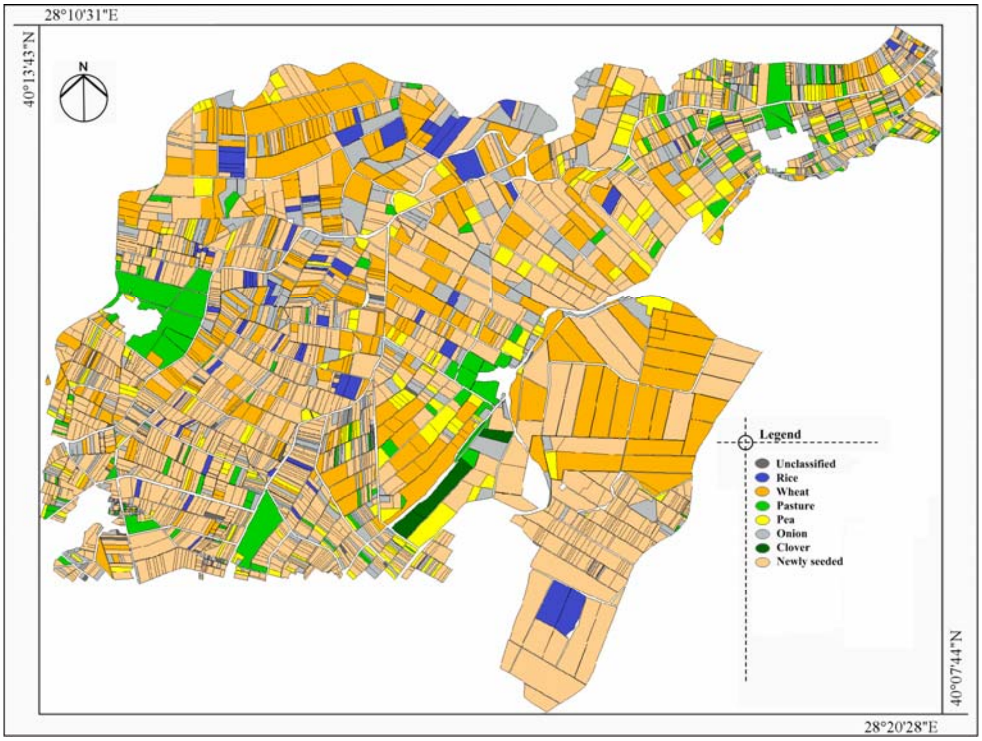

Figure D.8 Per-field classified May image using maximum likelihood classifier